NSF-RA-E-75-273

PB 284 348

DECEMBER 1974

Report to the
National Science Foundation
Project GI 38521

EARTHQUAKE INDUCED PERMANENT DEFORMATIONS OF EMBANKMENTS

Principal Investigator: Kenneth L. Lee

UCLA • SCHOOL OF ENGINEERING AND APPLIED SCIENCE

50272-101

REPORT DOCUMENTATION PAGE	1. REPORT NO. NSF-RA-E-75-273	2.	3. Recipient's Accession No. PB 284 548

4. Title and Subtitle Earthquake Induced Permanent Deformations of Embankments	5. Report Date December 1974
	6.
7. Author(s) K.L. Lee	8. Performing Organization Rept. No. UCLA-ENG-7498
9. Performing Organization Name and Address University of California School of Engineering and Applied Science Mechanics and Structures Department Los Angeles, California	10. Project/Task/Work Unit No.
	11. Contract(C) or Grant(G) No. (C) (G) GI38521
12. Sponsoring Organization Name and Address Applied Science and Research Applications (ASRA) National Science Foundation 1800 G Street, N.W. Washington, D.C. 20550	13. Type of Report & Period Covered
	14.

15. Supplementary Notes

16. Abstract (Limit: 200 words)

A method is proposed for calculating the permanent deformations at all points within an earth dam due to the effect of an earthquake. The method uses a seismic response analysis to calculate seismic stresses caused by a given time history of base accelerations. Data from laboratory cyclic triaxial tests are used to estimate the permanent strains caused by the induced cyclic stresses. These permanent strains are combined with the cyclic stresses to give a pseudo secant modulus. Sufficient data are obtained to define this pseudo modulus at all locations in the embankment. A finite element computer program is then used to calculate the permanent deformation resulting from this seismic disturbance. This new method was used to calculate the permanent deformations in five older dams, for which actual measurements and other data were available. In all cases the calculated results gave reasonable comparison with observed movements. In addition, several parametric studies were performed to investigate the relative importance of many of the parameters which enter into the analysis. The results of this study suggest that the proposed method, when used with currently obtainable input data, should lead to a useful supplemental or alternative method of assessing the effects likely to result from a strong earthquake near the site of an earth dam, embankment, or slope.

17. Document Analysis a. Descriptors

Earthquakes
Embankments
Dams
Earth dams
Slopes
Deformation
Earthquake resistant structures

b. Identifiers/Open-Ended Terms

c. COSATI Field/Group

18. Availability Statement	19. Security Class (This Report)	21. No. of Pages
NTIS.		192
	20. Security Class (This Page)	22. Price

(See ANSI-Z39.18) See *Instructions on Reverse* **OPTIONAL FORM 272** (4-77)
(Formerly NTIS-35)
Department of Commerce

CAPITAL SYSTEMS GROUP, INC.
6110 EXECUTIVE BOULEVARD
SUITE 250
ROCKVILLE, MARYLAND 20852

UCLA-ENG-7498
JANUARY 1975

Earthquake Induced Permanent Deformations of Embankments

by

Kenneth L. Lee

Report to the
National Science Foundation
Project GI 38521

Principal Investigator: Kenneth L. Lee

Mechanics and Structures Department
School of Engineering and Applied Science
University of California
Los Angeles, California

December 1974

TABLE OF CONTENTS

EARTHQUAKE INDUCED PERMANENT DEFORMATIONS

OF EMBANKMENTS

by Kenneth L. Lee

Synopsis

Analytical methods of seismic stability analysis of earth embankments currently in use (1974) are based on a limiting equilibrium concept that if the calculated stresses are less than the strength the dam is safe and if the stresses exceed the strength the embankment is unsafe. Observed performance of many embankments during earthquakes suggest that a more appropriate analysis should lead to an estimate of the amount of permanent deformation likely to occur in an embankment as a result of an earthquake. Large deformations would suggest an unsatisfactory structure whereas small calculated deformations may be tolerable.

A method is proposed herein for calculating the permanent deformations at all points within an earth dam due to the effect of an earthquake. The method uses a seismic response analysis to calculate seismic stresses caused by a given time history of base accelerations. Data from laboratory cyclic triaxial tests are used to estimate the permanent strains caused by the induced cyclic stresses. These permanent strains are combined with the cyclic stresses to give a pseudo secant modulus. Sufficient data are obtained to define this pseudo modulus at all locations in the embankment. A finite element computer program is then used to calculate the permanent deformation resulting from this seismic disturbance.

An analogy of the method may be envisioned by assuming that the embankment behaves during an earthquake, much as one would expect a

pile of material containing zones of tar to behave on a hot day. Just as the earthquake will soften the soil and lead to strains in a test specimen or deformation in the embankment, so will a temperature increase soften the tar and cause a test specimen or the pile to strain or slump to a new position which is in equilibrium with the overall static gravity stresses and the reduced modulus of the sample.

This new method was used to calculate the permanent deformations in five older dams, for which actual measurements and other data was available. In all cases the calculated results gave reasonable comparison with observed movements. Very good agreement was not obtained nor should be expected in some cases, especially where the actual dam movements involved shearing, cracking or breaking up. Such catastrophic behavior is not within the scope of the present method of analysis.

Several parametric studies were performed to investigate the relative importance of many of the parameters which enter into the analysis. The most important single parameter appeared to be the input base acceleration. Within the range of confident knowledge of the input base accelerations for a particular case, the calculated permanent deformations varied over wider limits than for any other single parameter.

This report is intended to be preliminary, indicating an alternative approach to the safe/unsafe concept inherent in the existing limiting equilibrium methods. More work is required to refine many of the aspects of this proposed method, especially to better account for the zones of soil above the water table which are not saturated, and for which very little cyclic loading data is presently available. More analytical and experimental studies by currently available techniques will be helpful in these areas. There is also a great need for a better definition of the input base motion for a particular case and this can probably only be obtained through continuing recording of strong motion earthquakes. Nevertheless, in spite of need for improvement and more data, the results of this study suggest that the method proposed herein, when used with currently obtainable input data, should lead to a useful supplemental or alternative method of assessing the effects likely to result from a strong earthquake near the site of an earth dam, embankment or slope.

EARTHQUAKE INDUCED PERMANENT DEFORMATIONS

OF EMBANKMENTS

by

Kenneth L. Lee

Introduction

Current (1974) methods of seismic stability analysis for earth embankments and slopes are based on a limiting equilibrium concept that if the calculated stresses exceed the strength, the embankment is unsafe and vice versa. There is no rational analytical way of handling the intermediate problem of measurable but tolerable permanent deformations caused by seismic forces. As Hardy Cross defined this for structural analyses, "a structure breaks if it does not hold together". Observed performance of earth dams subjected to earthquake loading indicates that this limiting concept in not necessarily always true. A dam or slope may suffer permanent deformation which, depending on the magnitude, may or may not be considered to constitute failure.

The objective of this study was to investigate a method for predicting the amount of permanent deformation in an earth embankment or dam which might be produced by the effect of an earthquake. Being a first step in this regard, the selected method was rather simple in concept, and clearly avoided many known complications. The method was used to analyze four different dams which had been subjected to strong earthquaking in the past, which lead to varying amounts of permanent deformation. The suggested method did predict the correct sense and order of magnitude of movement in each case, although agreement between the actual numerical values was not particularly good.

Several variations in assumed input data were used to illustrate the relative importance of many of the parameters. Unfortunately, some of the input data had to be based on extrapolations and estimations so that in no case was there complete knowledge of all the necessary input parameters.

Because there was reasonable agreement between the predicted and observed permanent deformations considering the limitations in the input data, and because the suggested method was a first step in solving this complicated problem, it seemed appropriate to summarize the studies conducted thus far into a progress report.

There is much remaining which can be done both in the way of more sophisticated analytical formulations, and in obtaining better input data for soil properties. However, it is hoped that the description of the method used, and the summary of the results obtained thus far will be a useful step toward the goal of obtaining a reliable method for predicting earthquake induced permanent deformations in earth dams, embankments, slopes or soil foundations.

Brief Review of Seismic Stability Analysis Methods

Seismic stability analyses of embankments, dams, slopes and retaining walls have been performed for many decades. Following the 1923 Tokyo earthquake, Japanese engineers Mononabe and Okabe and others proposed a pseudo static method of calculating earthquake induced earth pressures behind retaining walls. After extensive investigations by Jacobsen and the TVA, this method has enjoyed considerable popularity in the United States. A recent review of the Mononabe-Okabe pseudo static method and other related recent data on calculating seismic earth pressures on walls has been given by Seed and Whitman (1).

Essentially the same pseudo static approach may also be used for seismic stability analyses of earth embankments and slopes (2,3,4). The method follows the same procedure as used for static slope stability analysis which equates the resisting and driving forces along some assumed sliding surface. However, in addition to the usual static forces, the earthquake effects are represented by a single additional static force defined by a seismic coefficient K multiplied by the total weight of the potential sliding mass. This seismic force is assumed to act in an arbitrarily assigned direction, usually horizontal. Some writers suggest that the seismic coefficient should be equal to the maximum ground acceleration/gravity ratio caused by the earthquake (2,3). However, there is no rational basis for this, and other than following previous traditional trends or intuition, selection of a value for K is completely arbitrary.

The pseudo static method of slope stability analysis has been critically examined by Seed (5) who points out that besides the arbitrary selection of direction and magnitude, there are a great many other arbitrary choices which must be made in applying this method to an actual problem. There is no doubt but that with any of the assumptions the method will lead to a lower computed factor of safety than for static loading alone. However, the reliability of the method to adequately predict the actual performance of a slope during an earthquake has been shown in recent analyses to be unsatisfactory (6,7). This was realized many years ago by Terzaghi who wrote in his classical paper on mechanism of landslides "...the (pseudo static) equation is based on the simplifying assumptions that the horizontal acceleration acts permanently on the slope material and in one direction only. Therefore, the concept it conveys of earthquake affects on slopes is very inaccurate to say the least. Theoretically, a factor of safety

FS = 1.0 would mean a slide, but in reality a slope may remain stable in spite of FS being smaller than unity and it may fail at a value of FS greater than 1, depending on the character of the slope forming material".

As mentioned above, one of the serious problems with the pseudo static approach is the arbitrary method of assigning a value for seismic coefficient. Based on analytical response analyses work by Ambraseys (8), Seed and Martin have suggested a method by which the seismic coefficient can be calculated for a given earthquake motion (10). An additional problem with using a pseudo static approach is the definition of the soil strength under seismic loading conditions. However, much progress has been made in this regard in recent years, and cyclic loading test methods have been developed from which appropriate strength values can be obtained (12,13,14,15). Several years ago, Seed (9) proposed a slip surface method of seismic stability analysis similar to the Lowe-Karafiath method(11) but using a value of seismic coefficient calculated from a seismic response analysis and soil strength measured from cyclic loading tests. This method was applied with some satisfaction in a back figuring stability analysis of the Dry Canyon Dam (16,17) which suffered some damage during the 1952 Kern County Earthquake.

Recent studies of the behavior of soil under simulated earthquake loading have shown that the strength of soil under cyclic loading depends on the density and on the effective static normal and shear stresses acting on the potential failure plane. For loose, saturated, sandy soils carrying very low static shear stresses, several pulses of cyclic can be applied with only little resulting deformation. Then, after reaching a critical number of stress cycles, the sample suddenly loses much of its strength or liquefies, and will undergo large deformations if the cyclic loading is continued (13). On the other hand, dense soils and soils subjected to a significant static shear stress on the potential failure plane, will typically undergo a small amount of permanent deformation under each cyclic load pulse, and never lose strength to the point of collapse or liquefaction (13,14,15). It is therefore, difficult to define failure in these cases and some arbitrary definition must be selected. The Dry Canyon Dam studies (16,17) indicated that failure in cyclic loading triaxial tests defined by 5 percent axial strain would lead to a computed factor of safety of about 1.0 for field conditions of apparent near instability. It has also been observed that for isotropically consolidated triaxial samples (no shear stress on the failure plane) usually undergo less than 5 percent axial strain prior to liquefaction.

One of the serious problems with the slip surface type of analyses described above is that they do not correctly predict the position of the failure surface. In fact, all the soil is assumed to remain uneffected by the earthquake except along the thin assumed position of sliding. Finite element analyses methods have made possible the calculation of stresses at all locations within an embankment and thus greatly enlarged the scope of seismic stability analyses.

Finite element methods currently in use proceed similar to the seismic slip surface method previously mentioned except that the stability of each element in the embankment is evaluated separately rather than to obtain a single factor of safety for one potential sliding surface which cuts through the entire embankment. A static finite element analysis is performed to evaluate the pre-earthquake static consolidation stresses in each element. Sufficient cyclic load tests are performed in the laboratory to permit the pulsating loading strength of the soil to be evaluated for each element.

Failure in the laboratory test is defined by some arbitrarily selected strain, commonly 5 percent axial strain in a cyclic triaxial test. A seismic response analysis is also performed by a finite element method to obtain the seismic shear stresses induced in each element due to the input base motion. Comparison is then made between the calculated seismic stresses and the laboratory measured cyclic loading strength to determine a factor of safety for each element. The stability of the entire embankment is evaluated on the basis of the relative number of elements which are overstressed during the earthquake.

This method has been successfully used to back figure the stability of the Sheffield and Upper and Lower San Fernando dams which were seriously damaged or failed during earthquakes (6,7).

A major limitation of this finite element method and the previously described slip surface methods is that they are all based on limiting equilibrium theory. That is, the element or the slip surface is either understressed (safe) or overstressed (failed). There is no indication of the consequences of an overstress condition in terms of the deformation which may result therefrom. There is at present no rational way of analytically relating the failure criterion of say 5 percent permanent axial strain in a cyclic load triaxial test with permanent deformations of the entire embankment.

Use of limiting equilibrium theory is justified for static loading conditions because the applied loads remain constant for a long time, provided the deformations are not so large as to change the geometry significantly. However, under seismic conditions each load pulse is transiently applied for only a fraction of a second. Even if the soil at a particular element were temporarily overstressed during this instant, the seismic stress would have changed and probably revised several times before the affected mass of soil could undergo a large permanent deformation.

Newmark recognized this problem some years ago and proposed a method of seismic slope stability analysis which would take this into account (18). He proposed a progressive type of analysis whereby the soil strength and the seismic stress were compared on a continuing time basis. By a double integration method over intervals of time when the seismic stress exceeded the soil strength it is theoretically possible to keep a running tally of the permanent deformations which develop throughout the entire time history of the earthquake. For simplicity, Newmark suggested at that time (1965) that the soil strength would remain constant and equal to the static strength throughout the earthquake. Later, Seed and Goodman (19) applied the method in analyzing permanent deformations on a slope of uniformly graded dry sand on a laboratory shaking table. They found that even with dry sand the strength varied with the strain developed, and only by including this variation in strength were they able to successfully reproduce analytically the permanent deformations induced from the shaking table tests.

Unfortunately, the strength of saturated soils under cyclic loading conditions is considerably more complicated than the strength of dry sands. Current knowledge on this subject is not yet sufficiently refined to permit a step by step progressive evaluation of the strength of saturated soils under earthquake loading conditions. The best that can be found at present (1973) is the number of cycles of stress required to cause failure as defined by any preselected strain.

Furthermore, the storage and computation time required for a step by step seismic finite element analysis in which both the stress and the strength vary with each time step of say 0.01 to 0.05 seconds throughout a 20 to 40 second long earthquake would be economically unacceptable on todays computers. Thus, although it is conceptically possible to perform a Newmark type of permanent deformation analysis, practically speaking, this must wait until new advances are made both in soil testing and computer capacity.

In the meantime, however, it is possible to use current technology and build on presently used methods to improve the procedures for stability analyses of embankments and slopes to include an estimation of the permanent deformations resulting from an earthquake loading condition. Such a method is described in the following section.

Equilibrium Method of Seismic Stability Analysis of Earth Embankments

The suggested method of calculating permanent deformations in earth embankments due to earthquakes utilizes many of the principles of the currently used method of seismic stability analysis of earth dams (6,7), including static and dynamic stress analyses and cyclic loading triaxial tests to find the response of representative samples of soil to pulsating loads. For this reason it is useful to review briefly the essential concepts involved in the current methods of seismic stability analysis of earth embankments. Some of these essential features are illustrated schematically for a typical dam cross section shown on Fig. 1a.

The static stresses on a typical element before the earthquake are indicated by σ_{fc} and τ_{fc}. These are respectively the equilibrium effective normal and the shear stress on a horizontal plane after complete consolidation under the static gravity and steady state seepage conditions during normal operation conditions. At the time of the earthquake the base of the dam is subjected to shaking from upward propogating shear waves caused

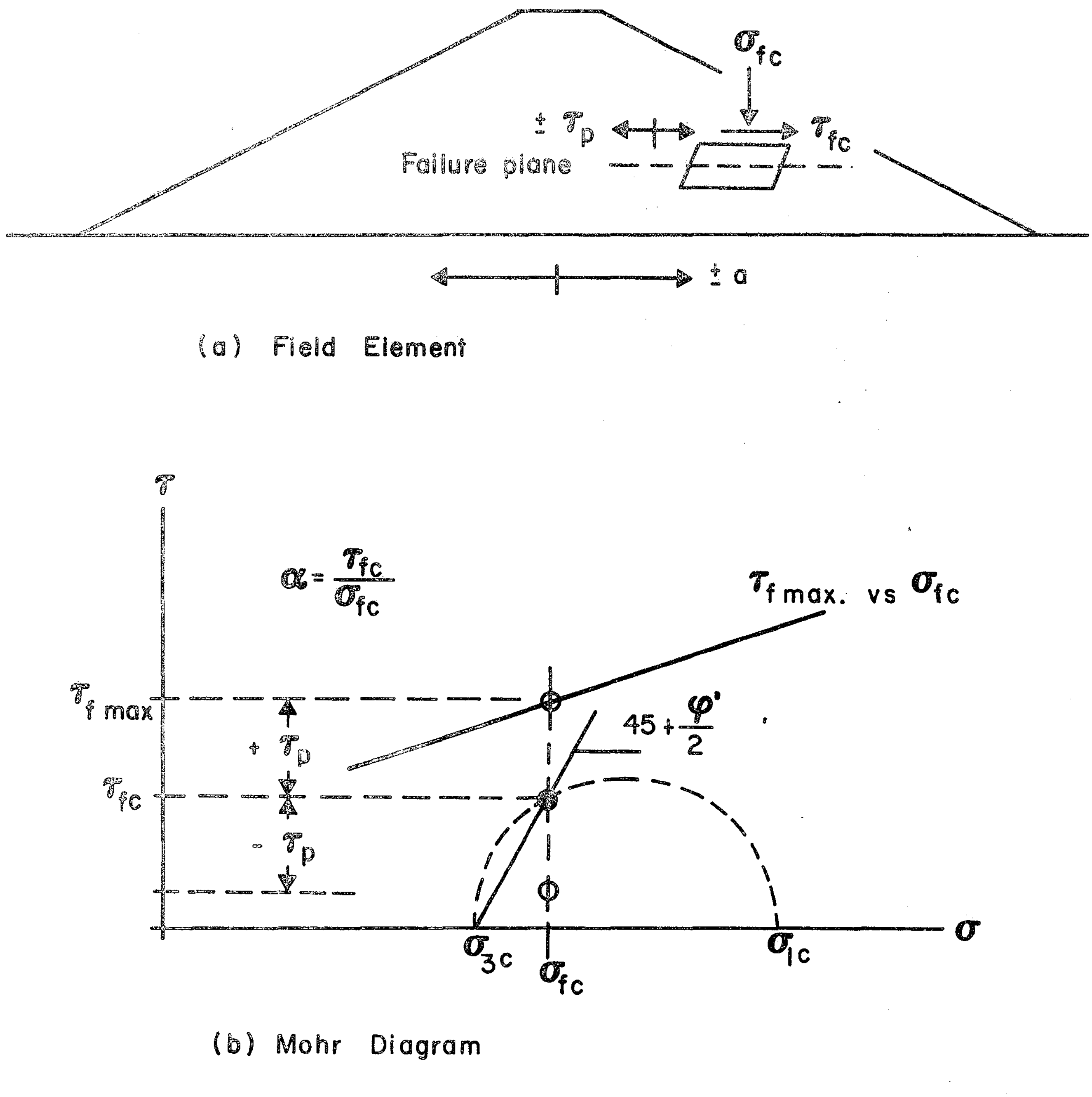

FIG. I CYCLIC LOADING SIMULATION BY SIMPLE SHEAR TEST.

by cyclic ground accelerations $\pm$ a, which cause cyclic or pulsating shear stress changes $\pm\ \tau_p$ on horizontal planes. If these pulsating stresses are large enough, then large permanent shear deformations or shear failure may occur on the horizontal planes, hence the subscript f is used as a reminder that the stresses are acting on the plane of potential shear failure.

The strength of the soil element under these conditions may be determined directly in a cyclic loading simple shear test which closely reproduces the complete stress history of the field element on a small sample of soil in the laboratory. The stress conditions on the field element and in the ideal laboratory simple shear test are described by the Mohr diagram on Fig. 1b. For ease in interpreting the results of laboratory tests, it is convenient to perform a number of tests on identical samples, each consolidated to the same normal stress σ_{fc}, and shear stress ratio $\alpha = \frac{\tau_{fc}}{\sigma_{fc}}$. The results of a series of such tests will define a strength envelope $\tau_{f\,max}$ vs σ_{fc} as indicated in Fig. 1b. Repeating these tests for different α consolidation conditions provides data from which the pulsating loading strength at any element within the embankment may be readily determined.

Unfortunately, the laboratory equipment and procedures required for performing cyclic loading simple shear tests are somewhat complicated, and at the present time (1973) the equipment is only available in a few laboratories. However, because of the relatively simple and long tradition of using triaxial tests, many laboratories are presently equipped to perform cyclic load triaxial tests. The relationship between the laboratory triaxial test and the field element is illustrated in Fig. 2. Since the potential failure plane is horizontal in the field, the element representing a

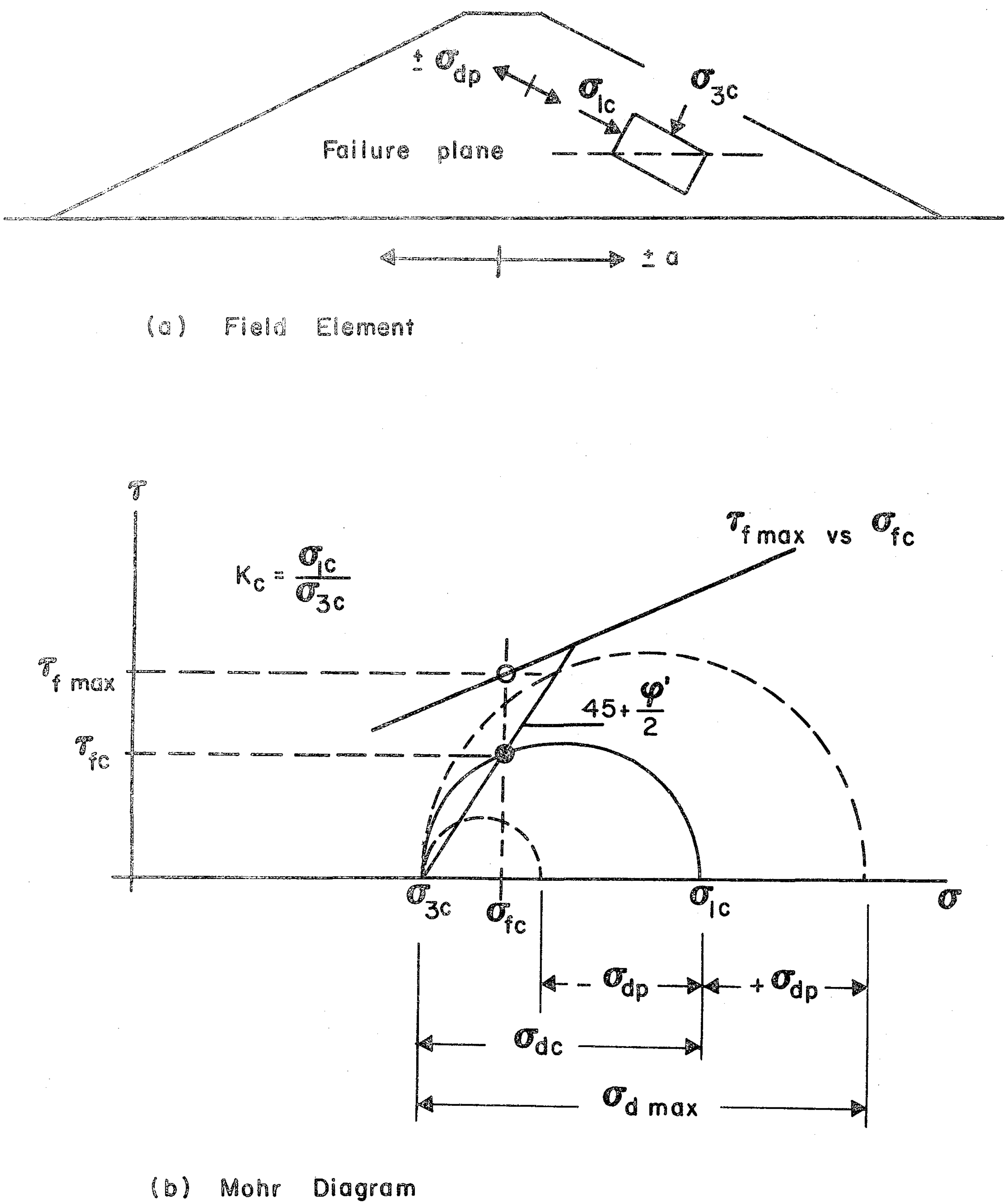

FIG. 2 CYCLIC LOADING SIMULATION BY TRIAXIAL TEST.

triaxial test specimen must be considered oriented at $45 \pm \phi/2$ to principal stress axes.

A triaxial test is limited in that the only stresses which can be controlled directly are the axial stress and the confining pressure. Changes in shear stress along the potential failure plane must therefore, be produced by changing these principle stresses. Thus, to produce the desired pre-earthquake static shear stress on the potential failure plane, the triaxial specimen must be anisotropically consolidated to the appropriate principal stresses σ_{1c} and σ_{3c}.

In earlier studies (12) it was shown that for undrained cyclic loading tests on saturated samples the cyclic shear stresses on the failure plane could be appropriately changed by cycling only the axial or deviator stress by an amount $\pm \sigma_{dp}$, while holding the chamber pressure in the triaxial cell constant.

A Mohr diagram of both static and cyclic loading stresses is shown on Fig. 2b. The Mohr circle shown by the solid line represents the stress conditions caused by anisotropic consolidation under the principal stress σ_{1c} and σ_{3c}. If the potential failure plane is inclined at $45 + \phi/2$ from the major principal plane then the static normal and shearing stresses on this potential failure plane are readily determined. Furthermore, from geometric considerations, there will be a direct definable relation between the major principle consolidation stress ratio $K_c = \sigma_{1c}/\sigma_{3c}$, which is conveniently used for handling triaxial test data, and the normal to shear consolidation stress ratio $\alpha = \tau_{fc}/\sigma_{fc}$ which is convenient for use with simple shear data and for field applications.

The dashed line Mohr diagrams represent the stress conditions at each extreme of the pulsating axial stress, on a total stress basis. It is convenient to consider failure as defined by the maximum axial stress $\sigma_{dc} + \sigma_{dp}$, which corresponds to the larger of the two dashed Mohr circles. Thus, as shown on Fig. 2b, potential failure is readily defined and can be plotted versus the pre-earthquake static normal consolidation stress σ_{fc}.

From the results of a series of such tests, each consolidated to the same K_c ratio, but different values of σ_{3c}, it is possible to define a strength envelope $\tau_{f\,max}$ vs σ_{fc}. Other series of tests are performed at different K_c ratios to cover the range encountered in the embankment. The strength envelopes for constant K_c are converted to envelopes for constant α, and used in a stability analysis.

Because the triaxial test does not correctly reproduce some of the aspects of cyclic loading on field elements, it is necessary to correct the triaxial test data for these discrepancies. Seed and Peacock (20) have reported a comprehensive study to determine correction factors for cyclic loading triaxial tests on samples consolidated isotropically ($K_c = 1.0$) which correspond to a field or simple shear condition of $\alpha = 0$. This condition is encountered in the central part of an embankment or at any location in the ground under a near level surface. A suggested factor C_r is applied to reduce cyclic loading triaxial test data to field conditions according to the following equation.

$$\left(\frac{\tau_p}{\sigma_{fc}}\right)_{\substack{\text{field} \\ \alpha = 0}} = C_r \left(\frac{\sigma_{dp}}{2\,\sigma_{3c}}\right)_{\substack{\text{lab triax} \\ K_c = 1.0}} \qquad (1)$$

Values of C_r vary with relative density of granular soil as shown in Table 1.

Table 1

C_r Values Suggested for $K_c = 1$, $\alpha = 0$ Conditions For Granular Soil

D_r - %	C_r
40	0.55
60	0.60
70	0.65
80	0.68
90	0.73

Values of C_r given in Table 1 are only valid for $K_c = 1$, $\alpha = 0$ conditions, and for saturated granular soils. In another study, Seed, Lee and Idriss (6) found that as K_c increased, the difference between cyclic triaxial and cyclic simple shear decreased. These studies were made on a slightly plastic silty sand, and led to the suggested that for K_c 1.5, no correction need be applied to convert cyclic triaxial test data for use directly in field stability analysis. Within the range 1.0 K_c 1.5, it seems appropriate to use a linear interpolation between $C_r = 1.0$ and the appropriate C_r value given in Table 1.

The results obtained directly from a pulsating load test performed on an anisotropically consolidated sample ($K_c = 2.0$) are shown on Fig. 3. At the end of the anisotropic consolidation stage the axial or deviator stress was 19 psi. The cyclic axial stress was $\sigma_{dp} = \pm 12$ psi. As is typical with these tests, the excess pore pressure increased somewhat as the cyclic loading continued but did not increase sufficiently to cause liquefaction

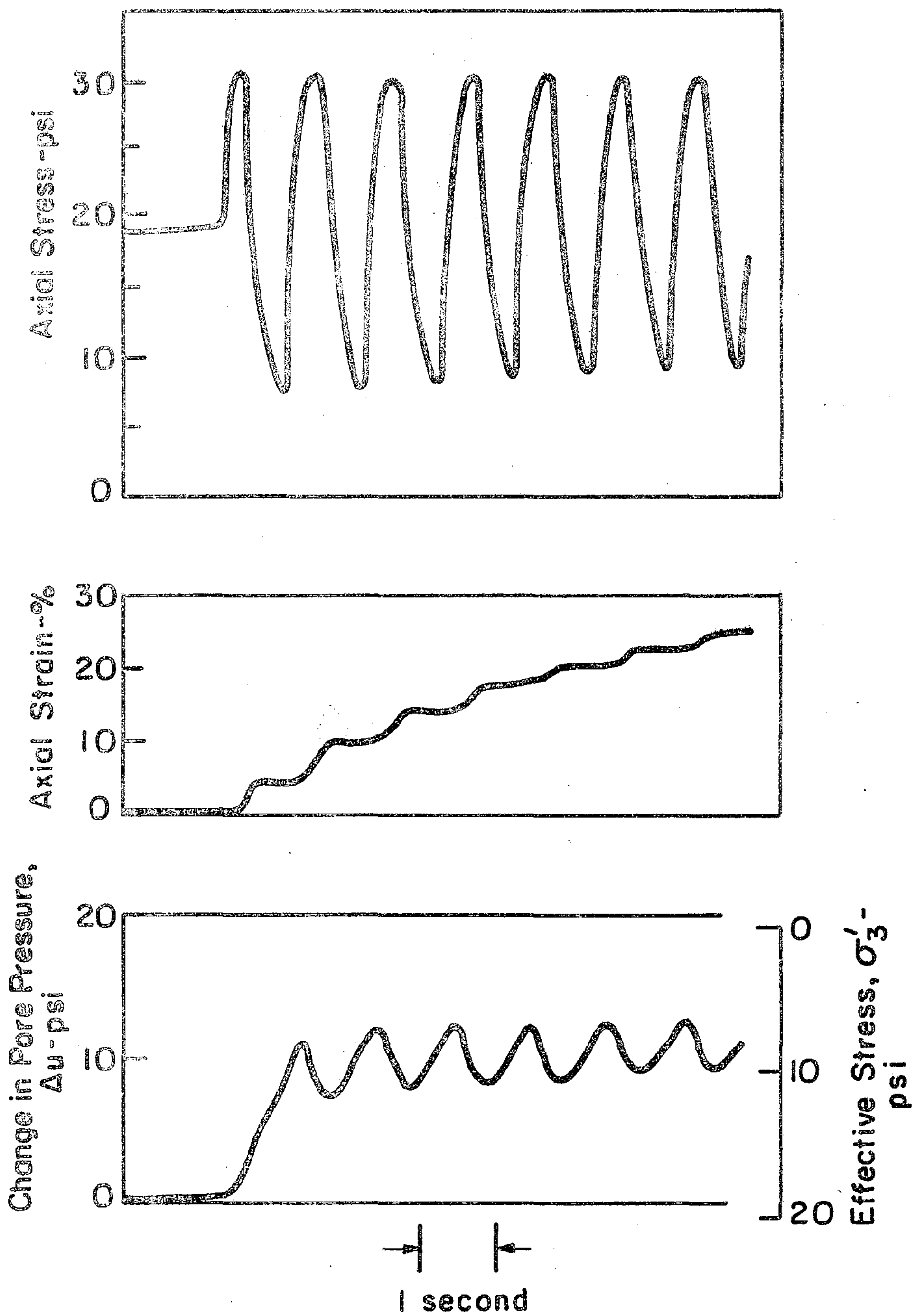

$D_r \approx 50\%$ $\sigma'_{3c} = 19$ psi $K_c = 2.0$ Loading rate = 1 Hz

Fig. 3 TYPICAL PULSATING LOAD TESTING RECORD.

or sudden loss in strength. The axial strains increased with each cycle in the direction of the major principle stress, and there was an insignificant recovery when the cyclic stress was reduced. Thus, there was no well defined failure point, yet after seven cycles, the triaxial specimen had suffered a compressive strain of about 25 percent, which most engineers would take to be less than satisfactory performance under this applied loading. Other samples tested in a similar manner behave similarly, the amount of accumulative strain increasing with each pulsating load cycle depending on the stress conditions. With the special exception of loose saturated sands at $K_c \approx 1.0$, there is no well defined point of failure (12). Thus, the point of failure has been arbitrarily selected as the stress conditions and number of cycles which produce a specified axial strain, with 5 percent strain being commonly accepted for many design purposes (7,14,16,17).

Having thus selected the failure criteria, it is a straight forward matter to obtain by interpolating from the results of a number of tests, the pulsating loading strength of any element of soil within the embankment. Comparison of the earthquake induced stress to the pulsating loading strength leads to an assessment of the relative seismic stability of each element, and finally of the entire embankment.

To summarize, a seismic stability analyses of an earth embankment using current (1973) methods with finite elements involves the following steps, in addition to the considerations given for non-earthquake analyses procedures.

1. Select a design earthquake base motion.
2. Perform a seismic response analyses on the embankment to find the maximum horizontal seismic shear stress τ_{max} at each element.
3. Determine the equivalent number of uniform cycles of shear stress N_{eq}, and the corresponding ratio of average to peak shear stress $R_{TO} = \tau_{av}/\tau_{max}$.

4. From 2 and 3 above, calculate the average horizontal cyclic shear stress τ_{av} induced by the design earthquake.

5. Perform a static stress analysis to determine the equilibrium, pre-earthquake normal and shear stress (effective stress basis) on horizontal planes at every element.

6. Perform cyclic load triaxial tests on representative samples of soil from the embankment at anisotropic consolidation stress representation of the pre-earthquake stress conditions.

7. Convert the lab triaxial test strength data to equivalent field strength conditions τ_f for N_{eq} cycles and a predetermined failure criterion of say 5 percent strain in the cyclic triaxial test.

8. Compare the measured cyclic loading strength τ_f to the calculated seismic stress τ_{av} at each element and note the relative stability or factor of safety of each separate element.

9. Consider the entire embankment, note the relative stability or factor of safety in each element, and make an assessment of the probable performance of the entire embankment.

From a designers point of view, one of the most questionnable aspects of the above method has to do with the arbitrary selection of the failure criterion and its use in assessing the stability of the embankment. In general, the samples do not suddenly collapse unless the soil is loose and $K_c = 1.0$. Thus, the selection of any failure criterion, say 5 percent in the laboratory test, is rather arbitrary and does not follow from a well defined change in soil behavior. Furthermore, there is no analytical correlation between soil strain in the laboratory cyclic load test and deformation of the element, or of the entire embankment in the field. Qualitatively, it seems reasonable that larger strains in the laboratory would correlate with larger field deformations, but there is as yet no method by which these can be correlated on a quantative basis. Justification for using 5 or 10 percent axial strain as a failure criterion is based on the results of analyses made of dams which performed less than satisfactory in the field during earthquakes (7,9,16,17).

Like the static equilibrium slip surface analyses, the above described seismic stability analyses method allows an evaluation of only failure or non-failure of each element based on the arbitrary selected laboratory failure criterion. For static analyses, this equilibrium method is satisfactory for many cases because the loads are permanent and the only changes which occur are due to changes in geometry and perhaps soil strength as the slope deforms. For seismic conditions, the earthquake loads are transient, each acting for only a fraction of a second. If as suggested by Newmark (18) and as used by Seed and Goodman (19) for some model tests on clean sand embankments, it would be possible to consider each pulse separately and integrate twice under the acceleration and velocity curves to calculate the transient displacements, these could then be summed to calculate the total accumulative deformation at the end of the seismic disturbance. However, difficulties in defining the strength changes at each element with each cyclic of loading, and the large amount of computation time involved to include these strength changes, does not encourage the practical use of this method at the present time. However, in an attempt to offer the designer an alternative to the present equilibrium method and provide a way of estimating the nature of permanent post-earthquake deformations which may be induced in an earth embankment, the following described method is presented.

Permanent Deformation Method

Reference is again made to the recorded results of a typical pulsating load triaxial test shown on Fig. 3, and it is again noted that the axial strains accumulate with each successive cycle. It is further noted that the strains occur when the maximum compressive portion of the load cycle is applied, and that when the pulsating load is reduced the strain remains approximately constant. This is typical of all tests for which the axial stress (or principal stress) is always in the same direction (compression) during the maximum and minimum stages of the pulsating loading. For other stress conditions which lead to a reversal of the direction of the principal stress changes during each cycle, a reversal in stress will also lead to a reduction or reversal of the axial strain on the unloaded cycle, followed by an increased strain on each succeeding cycle (14). Reversal occurs for $K_c = 1.0$ and reduction occurs for K_c slightly greater than 1.0 However, in all cases, the accumulative axial strain increases with each succeeding cycle. On the unloading portion of the cycle, the strain reduction does not begin to occur until the direction of the applied stress has changed to force the strain to reduce. Thus, the accumulative maximum axial strain which develops at the loading portion of each cycle can be taken as the permanent axial strain which would remain at the end of the pulsating loading (*).

In analyzing the test results, it is convenient to plot this accumulative maximum axial strain versus the accumulative number of cycles as shown on Fig. 4a. These data are for a series of typical tests on the same soil, at the same density and consolidated to the same anisotropic stress conditions. The only difference is in the amount of pulsating deviator stress $\pm \sigma_{dp}$ applied to each sample. The data points for strain at each cycle are shown for Test No. 45, but for clarity are omitted from the other curves on Fig. 4a.

If for example, failure was to be defined as the cyclic stresses causing 10 percent axial strain, then the number of cycles to failure could be readily determined for each test as shown. It is then convenient to plot the magnitude of the pulsating deviator stress $\pm \sigma_{dp}$ versus the number of cycles to failure (by the prescribed criterion) as shown on Fig. 4b.

(*) In this study cyclic strains are defined as follows: For $K_c = 1.0$ $\varepsilon_1 \approx \frac{1}{2}$ peak to peak strain amplitude; For K_c 1.0 ε_1 = compressive stain amplitude.

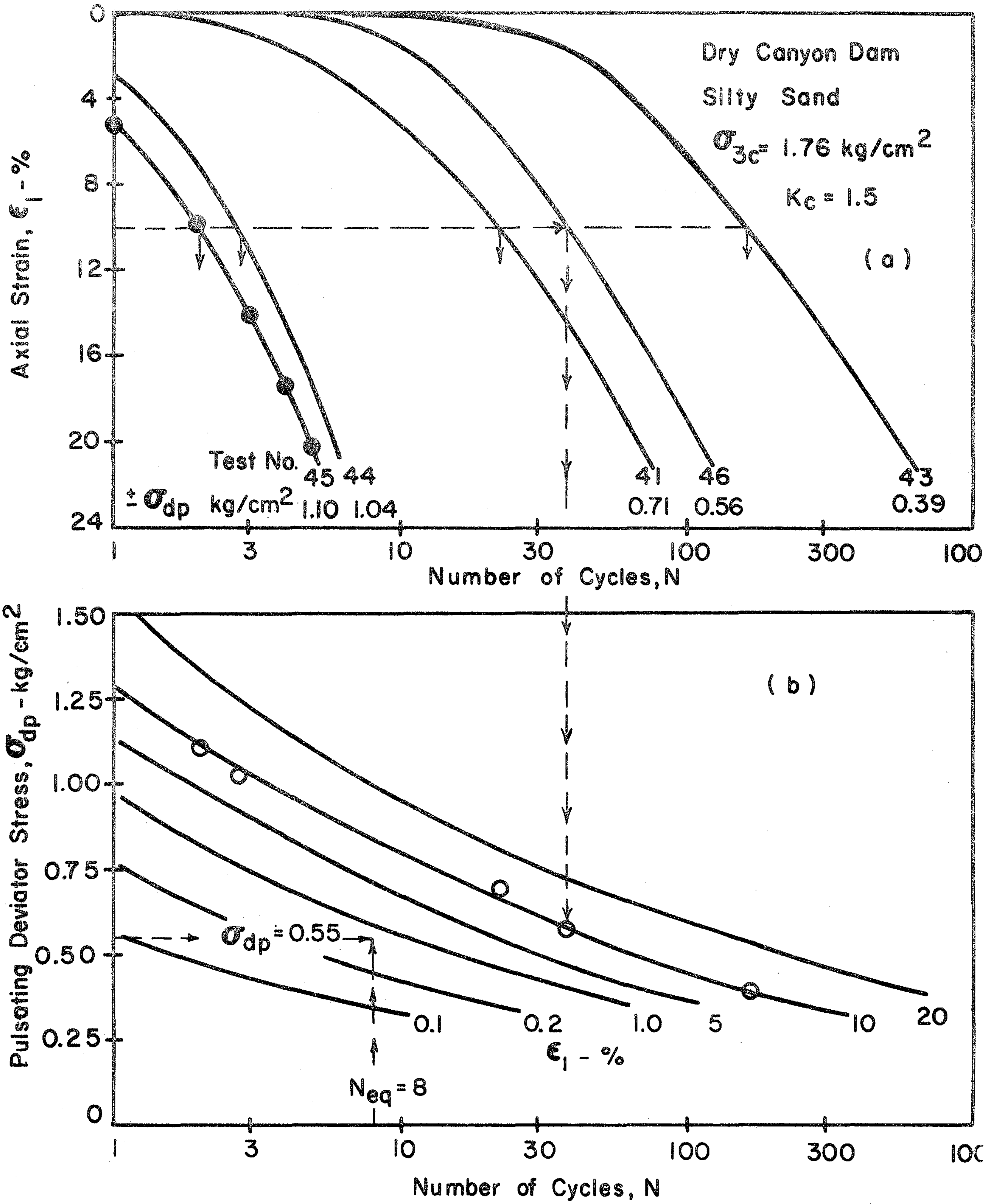

FIG. 4 DATA FROM TYPICAL PULSATING LOAD TESTS.

Data points for the failure criterion of $\varepsilon_1 = 10\%$ are shown. Other failure criterion may also be used and similar σ_{dp} - N curves drawn. These are also shown on Fig. 4b but for clarity the data points used to obtain these curves have been omitted.

It will be noted that the pulsating loading strength curves shown on Fig. 4b are plotted on semi-log paper, and the curves are not straight lines. The shapes are similar to curves from many tests on many other soils, and the semi-log presentation is convenient and clear for many purposes. As will be discussed later, these data define straight lines when plotted on log-log axes, and for this reason it is useful to plot the data on log-log paper in order to quantify it for later use in computer analyses. However, this brings the strength lines of Fig. 4b closer together and for convenience in explaining the procedure the semi-log plot will be used. Data plotted on log-log scales are presented in the appendices.

Suppose the data on Fig. 4 represent the conditions applicable to the element shown in the dam cross section of Fig. 1a. The equilibrium static consolidation stress conditions of the samples $K_c = \sigma_{1c}/\sigma_{3c}$ are equivalent to those on the horizontal plane in the dam $\alpha = \tau_{fc}/\tau_{fc}$. The cyclic deviator stresses $\pm\ \sigma_{dp}$ applied to the sample correspond to pulsating shear stresses $\pm\ \tau_p$ which may act on the element during an earthquake. The intensity of these equivalent uniform pulsating load cycles and the number of such cycles depends on the input earthquake motion, and on the characteristics of the embankment, but they can be readily determined by an appropriate seismic response analysis.

Let it be assumed that the field and the laboratory pulsating loads are related by a correlation factor C_r similar to that described by Eq. 1:

$$\left(\frac{\Delta\tau_{av}}{\sigma_f}\right)_{field} = C_r \left(\frac{\sigma_{dp}}{2\sigma_{3c}}\right)_{lab} \qquad (2)$$

For $K_c = 1.0$, $\alpha = 0.0$ conditions, C_r values given in Table 1. For $K_c \gtrsim 1.0$ and $\alpha \gtrsim 0.0$, C_r increases linearly with K_c to a maximum of 1.0 at $K_c \gtrsim 1.5$.

It is important to emphasize that the lines shown on Fig. 1b are not failure conditions in the sense of a sudden loss of strength, but merely indicate the σ_{dp} - N conditions which cause a certain amount of axial strain. The closer the lines are to each other, the more rapid will be the strains for each succeeding stress pulse, but unless the lines are over top of each other, the sample does not collapse once the failure condition is met.

Suppose that for the conditions depicted for the element shown on Fig. 1a, the earthquake induced stresses corresponded to $N_{eq} = 8$ cycles (21) and the corresponding pulsating deviator stress in a cyclic load triaxial test was $\sigma_{dp} = \pm 0.55$ kg/cm^2. Plottting these conditions on Fig. 4 indicates that these cyclic load conditions will produce an accumulative compressive axial strain in a triaxial test of about $\varepsilon_1 = 0.7$ percent. This same information could also be conveyed by considering that a laboratory had been subjected to a static load equal to σ_{dp}, provided the sample had a secant modulus.

$$E_p = \frac{\sigma_{dp}}{\varepsilon_1} \qquad (3)$$

For this case, $E_p = 0.55/0.007 = 78.6$ kg/cm^2 and this refers only to the end point deformations between the beginning and the end of the pulsating load following consolidation to equilibrium under the static stresses.

If the element in the field was truly represented by the triaxial test specimen, and if like the triaxial test specimen there were no other soil elements attached to it, then it would be reasonable to assume that the deformation of the single field element under the earthquake load could be calculated by a simple pseudo-elastic analyses using a Young's modulus E_p defined by Eq. 3, and an appropraite value for Poisson's ratio ν. Since the soil element is saturated and undrained during the short duration of the cyclic loading, it would seem appropriate to assume $\nu \approx 0.5$ for this load step. For partially saturated elements, or cases involving some compaction as a result of cyclic loading (36), a value for Poisson's ratio less than 0.5 would be appropriate.

However, the soil element in the field is not isolated from the surrounding soil, and its deformation will depend to a large extent on the deformation behavior of the surrounding soil. As an illustrative example, a metal bucket may contain saturated sand. When placed on a shaking table the sand may completely liquefy and lose virtually all of its shear strength. Simulated laboratory tests on samples of this sand would show very large strains after a certain number of cycles, and by Eq. 3 this would indicate a value of $E_p \approx 0$. But, as long as the walls of the bucket did not fail, the liquefied sand within the bucket would not suffer any permanent deformation, even though it possessed no shear strength, or in other words, a high potential for undergoing large shear deformations such as a fluid.

Therefore, the strains indicated by single tests as shown on Fig. 4 must be considered only as strain potentials, and the permanent deformation must include all connected elements taken together. This reasoning leads to the suggestion that the finite element method (FEM) may be a useful tool in a permanent deformation analysis.

The basic finite element analysis is a solution for the following matrix equation:

$$P = K\ U \tag{4}$$

In this equation, U represents the matrix of all nodal point displacements, which are the quantities sought in the solution. P is the matrix of all loads acting to cause the displacement, and K is the stiffness matrix which is made up of the elastic parameters of the system.

For the permanent deformation problem, the loads come from two sources: the gravity or dead weight loads of the soil, and the transient loads induced by the seismic accelerations. The elastic parameters may be defined by either Young's modulus E and Poisson's ratio ν, or by bulk and shear modulus B and G, or some other combination of elastic parameters.

The results from cyclic load laboratory tests on soil are interpreted by reducing them to a single strength value. However, because the seismic forces which act on the elements are not only transient in nature, but vary differently with time from nodal point to nodal point, it is difficult to represent each seismic nodal point force by a single constant value. Therefore in the permanent deformation analysis, it was decided not to represent the seismic forces themselves, but rather the effect of the seismic forces, by the change which they would produce in the stiffness of the structure as calculated from the changes caused in the soil modulus. This reasoning followed from consideration that only the end point deformation was desired and not the transient time dependent cyclic deformations.

Based on this reasoning, it follows that there is really no change in the load matrix P between the two end points; immediately before and immediately after the earthquake. Therefore, the earthquake induced changes in deformations Δ U as defined by Eq. 4 result from a change in stiffness K rather than for the usual FEM analysis where Δ U results from a change in P. Schematically, this concept is expressed by:

$$\Delta U = P(\Delta K)^{-1} \tag{5}$$

where P is constant. Solution of Eq. 5 for Δ U gives the earthquake induced permanent displacements at each nodal point. Direct solution of the equation as stated is not convenient, and therefore, an indirect two step method is suggested.

Step 1 In Solution of Permanent Deformation Equation: In the first step a simple gravity-turn-on analysis is performed and Eq. 4 solved in the usual direct manner to give values for nodal point displacements u_1, under the loading and soil conditions which exist just prior to the earthquake. These loads include the dead weight gravity forces plus any forces on the boundaries due to the reservoir water. Boundary water forces are used rather than seepage forces because the cyclic loading soil strengths are based on total stress and internal excess pore pressures are neglected. Also, it is reasoned that during the few seconds duration of the earthquake, the internal seepage force system may be disturbed to an unknown extent and the resulting permanent deformations will be due to the total stress system including the reservoir pressure acting on the relatively impervious boundaries of the dam. The elastic parameters E_1 and ν used for this first step gravity-turn-on analyses are selected somewhat arbitrarily, with attention to obtaining realistic numbers, especially with respect to relative values in different major zones of the dam.

Step 2 In Solution of Permanent Deformation Equation: Between Step 1 and Step 2, the dam will be effected by an earthquake, and this effect is included in the new stiffness matrix K of the finite element formation.

Evaluation of the new value of K is done as follows. The stiffness matrix k of each element is a function of the geometry, and of the elastic parameters E and ν or B and G. For reasons described later, the stress-strain matrix C is formulated in the computer in terms of B and G which are calculated from specified values of E and ν .

$$C = \begin{bmatrix} \frac{3B + 4G}{3} & \frac{3B - 2G}{3} & 0 \\ \text{(symmetrical)} & \frac{3B + 4G}{3} & 0 \\ & & G \end{bmatrix} \tag{6}$$

$$B = \frac{E}{3\,(1 - 2\nu)} \tag{7}$$

$$G = \frac{E}{2\,(1 + \nu)} \tag{8}$$

The formulation used for analyses thus far is strictly applicable only for the the case of saturated, zero volume change soils, thus the values of Poisson's ratio and the Bulk modulus B are assumed to be the same for both Step 2 and Step 1. The only change is in the shear modulus G as compared from the secant modulus E by Eq. 8. This change in the value of E from Step 1 to Step 2 for each element is illustrated as follows.

The seismic induced deformation can be formulated by considering a simple analogy of an axially loaded specimen with modulus E_i acted on by an initial axial stress σ_g and then subjected to some disturbance which softens the specimen to allow more deformation without changing the applied load. This concept is illustrated on Fig. 5*. The initial axial strain before

---

* An alternative line of deductive reasoning leading to Eq. 13 is presented in Appendix V.

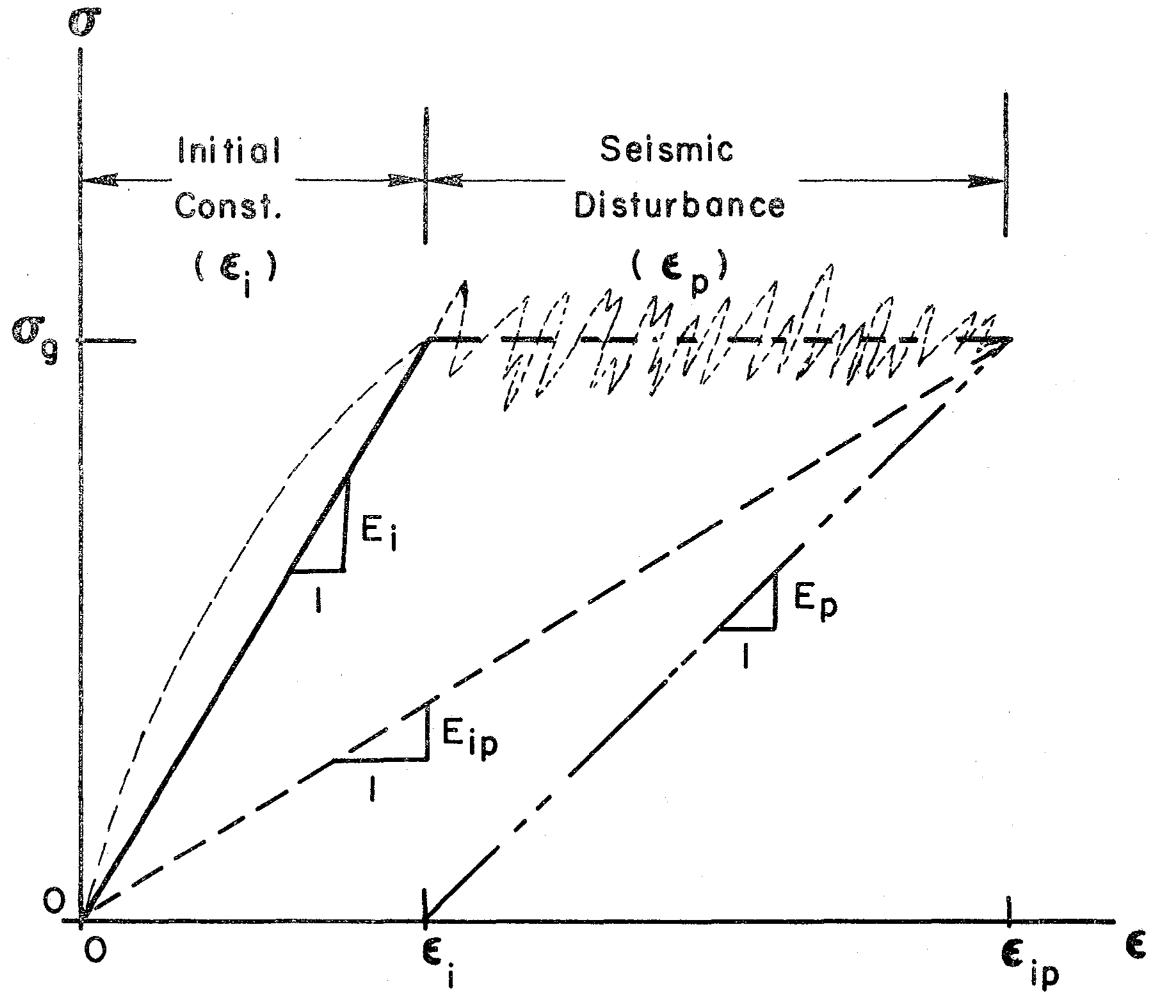

$$E_{ip} = \frac{1}{\frac{1}{E_i} + \frac{1}{E_p}}$$

FIG. 5 ANALOGY FOR SEISMIC INDUCED PERMANENT DEFORMATIONS.

disturbance is:

$$\varepsilon_i = \frac{\sigma_g}{E_i} \tag{9}$$

The value of E_i represents the initial assumed modulus for the soil element, and σ_g represents the gravity stress. Now consider that due to some disturbance the sample softens and deforms with no net change in applied stress. The incremental deformation due to this softening can be expressed in terms of a pseudo modulus E_p as defined by Eq. 3. Considering for the moment only the softened sample, if it were to be subjected to a load increment σ_g the corresponding strain ε_p would be:

$$\varepsilon_p = \frac{\sigma_g}{E_p} \tag{10}$$

Since σ_g is the same before and after softening, it follows that the total accumulative strain would be:

$$\varepsilon_{ip} = \varepsilon_i + \varepsilon_p = \sigma_g \left(\frac{1}{E_i} + \frac{1}{E_p} \right) \tag{11}$$

Stated another way, the accumulative strain ε_{ip} could be calculated from:

$$\varepsilon_{ip} = \frac{\sigma_g}{E_{ip}} \tag{12}$$

where

$$E_{ip} = \frac{1}{\frac{1}{E_i} + \frac{1}{E_p}} \tag{13}$$

This same procedure is used in the finite element calculations where the modulus is replaced by an element stiffness which is a function of the appropriate modulus. In Step 1 the initial reference deformations U_1 are calculated using initial values of Young's modulus E_i and Poisson's ratio.

Then in Step 2 of the finite element calculations, the value for Young's modulus is changed to E_{ip} computed from Eq. 13 where E_p is determined from an interpolation of the pulsating load triaxial test data for the appropriate element and Eq. 3. Using the same gravity loads, the accumulative deformations U_2 are calculated, thus the earthquake induced permanent deformations are obtained by subtraction.

$$\Delta U = U_2 - U_1 \tag{14}$$

Steps 1 and 2 are readily incorporated into the same computer program which automatically calculates the permanent deformations U at each nodal point.

It is seen from Eq. 13 that E_{ip} will always be less than E_i. For the case where cyclic loading causes very large strains, E_p will be very small, but as long as it is greater than zero, a value for E_{ip} can be determined.

For the analyses made thus far the stress-strain matrix shown by Eq. 6 uses the same bulk modulus for Step 2 as for Step 1 computed for $\nu \approx 0.5$ to insure that near zero volume changes will be calculated in the saturated undrained soil. The shear modulus is computed from Eq. 8 using $E = E_{ip}$. A more refined analysis would include volume changes caused by cyclic loading by allowing ν to change. However the available data (36) suggests that this component of strain is likely to be small.

Soil Parameters For Analysis

The soil parameters for the permanent deformation analysis are E and ν for both the pre-earthquake and the post-earthquake conditions. A simple linear elastic gravity-turn-on analysis is performed for both cases. For the pre-earthquake condition E_i and ν_i are rather arbitrarily selected. Since the pre-earthquake deformations resulting from E_i and ν_i are subtracted from the final results, an elaborate method for selecting these parameters is not justified. Suggested values of E_i are within the range of about 300 to 1000 kg/cm^2 with values of $\nu_i = 0.3$ to 0.4 for partially saturated soils and $\nu_i = 0.45$ to 0.49 for saturated soils which will not drain during the few seconds duration of the earthquake.

Post-earthquake values of ν are kept the same as the pre-earthquake values, and the bulk modulus is computed within the computer for Eq. 7 using the pre-earthquake value of E_i. The post-earthquake value of E is taken as E_{ip} calculated from E_p from Eq. 12 where E_p is calculated as described, from the results of pulsating loading triaxial tests. This latter calculation is done automatically in the computer for each element, from the test data for the appropriate consolidation stress conditions such as shown on Fig. 4b.

By replotting the curves of Fig. 4b and from other tests on log-log paper, it is possible to define the pulsating load strength results in terms of 9 parameters. These are described in Appendix I which also presents actual test data for the several soils used in this study.

Comparison of Calculated to Observed Permanent Deformations

In order to demonstrate the suggested analysis method, and to illustrate how well, in its present form, it predicts actual observed cases, five different dams were selected for study. Four of these dams have been studied previously and their observed behavior compared with predictions from an equilibrium stability analysis method. Thus a considerable amount of data was already available, which has been used where appropriate in these permanent deformation studies. The dams analyzed in this study were as follows:

1. Dry Canyon Dam - cracked during the 1952 Kern County, California earthquake (16,17).

2. Sheffield Dam - failed during the 1925 Santa Barbara, California earthquake (6).

3. Upper San Fernando Dam - badly cracked during the 1971 San Fernando, California earthquake (7).

4. Lower San Fernando Dam - failed during the 1971 San Fernando, California earthquake (7).

5. Hebgen Dam - crest settled during the 1959 Montana Earthquake (37, 38, 39).

The analyses performed on each of these dams are presented in the following sections. The studies were performed together, and therefore, not all of the parametric studies were performed on each dam.

Dry Canyon Dam

The Dry Canyon Dam is an old partial hydraulic fill structure located on the Los Angeles Aqueduct System some eight miles north of the Los Angeles City limits. The embankment is 63 feet high, and is founded on about 60 feet of recent silty-sandy-gravelly alluvium. During the 1952 Kern County earthquake, M 7.7, it was cracked longitudinally and appeared to have approached an unstable condition. The dam was taken out of service in 1966, and at the time of the 1971 San Fernando earthquake, the reservoir was completely dry.

The Dry Canyon Dam was studied by Lee and Walters (16,17) using an equilibrium slip circle analyses with a seismic coefficient calculated by shear slice seismic response analyses, and soil strengths obtained from cyclic load triaxial tests. Using strengths defined by 5 percent axial strain in cyclic load tests, the analyses showed the seismic factor of safety to be close to 1.0. Much of the data concerning this dam were taken from the Lee and Walters earlier study.

The dam was constructed in 1911-1912 using both wagon rolled and hydraulic fill procedures. The maximum cross section of the dam is shown on Fig. 6. The boundaries between the various zones are only approximate as no good records are available. The epicenter was about 46 miles from the epicenter of the earthquake. Several strong motion records were obtained of this earthquake. Peak accelerations from these records are shown in Fig. 7 along with other comparative data. Taken together the data suggest that the peak acceleration in rock at the damsite was probably between about 0.07 and 0.16 g. For many of the parametric analyses the peak acceleration was assumed to be 0.1 g. Other parametric analyses were also made using different accelerations for other illustration purposes.

Several longitudinal cracks were formed in the embankment as a result of the earthquake. The most serious was a 2 inch wide crack which ran along most of the crest of the dam as shown on Fig. 8a. A test pit was excavated into the fill to explore the extent of this crack, and it was followed to a depth of about 16 feet where it became too small to observe. A photograph of this crack as it appeared in one wall of the test pit near the surface is also shown on Fig. 8b. For scale, the brace is a 2 inch pipe. Surveys taken before and after the earthquake showed that points along the crest of the dam settled about 0.2 to 0.3 feet, and moved upstream by equal amounts.

A finite element representation of the maximum cross section of the Dry Canyon Dam is shown on Fig. 9 along with a sketch showing the zones of different materials used for the analyses. The same FEM grid and material zones were used for the seismic response analyses and for the subsequent permanent deformation calculations.

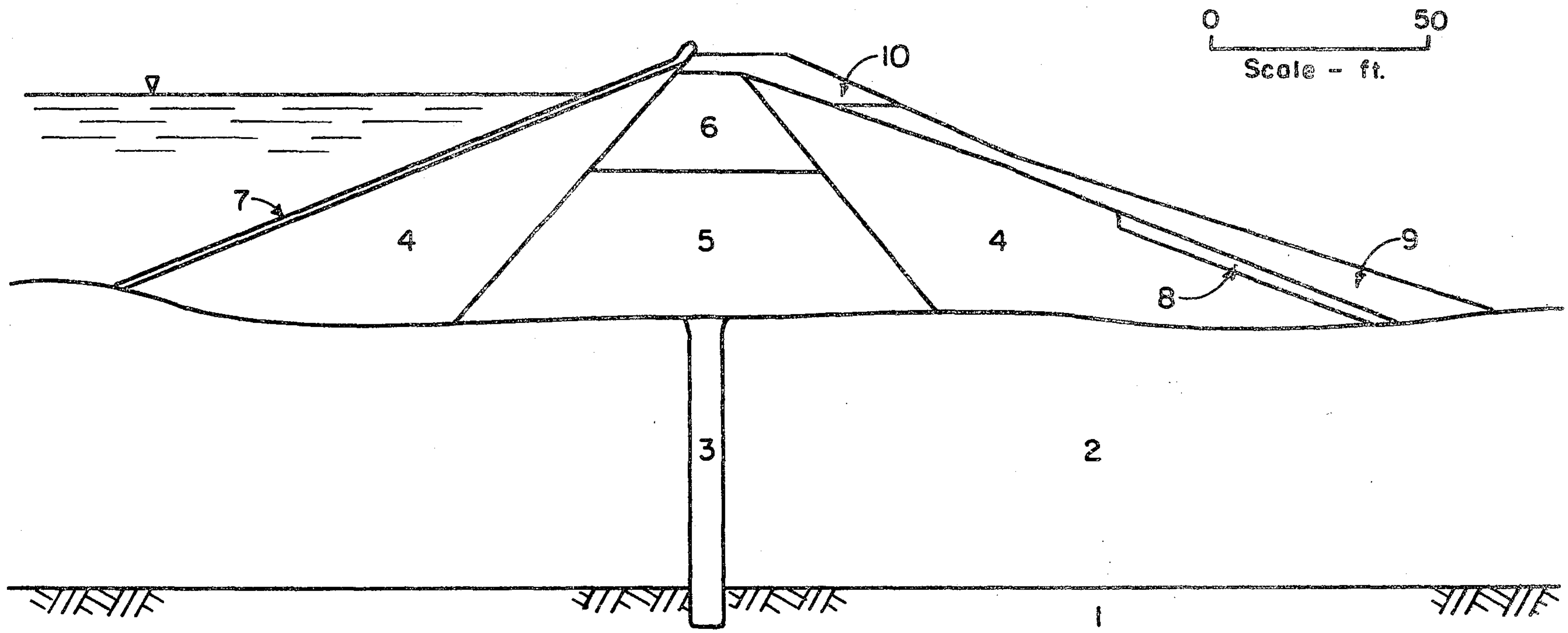

Boundaries between zones are very approximate

1	Bedrock (Shale and sandstone)	6	Wagon Rolled Core (1912)
2	Recent Alluvium (silty sand and gravel)	7	6" Thick Concrete Face (1912 and 1933)
3	Puddled Clay cut-off wall	8	Sand Filter (1933)
4	Shell (silty sand) (1911-1912)	9	Uncompacted SS and Shale (1933)
5	Hydraulic Fill (silt-sand) (1911-1912)	10	Compacted SS and Shale (1933)

Fig. 6 MAXIMUM CROSS SECTION OF DRY CANYON DAM. 1952

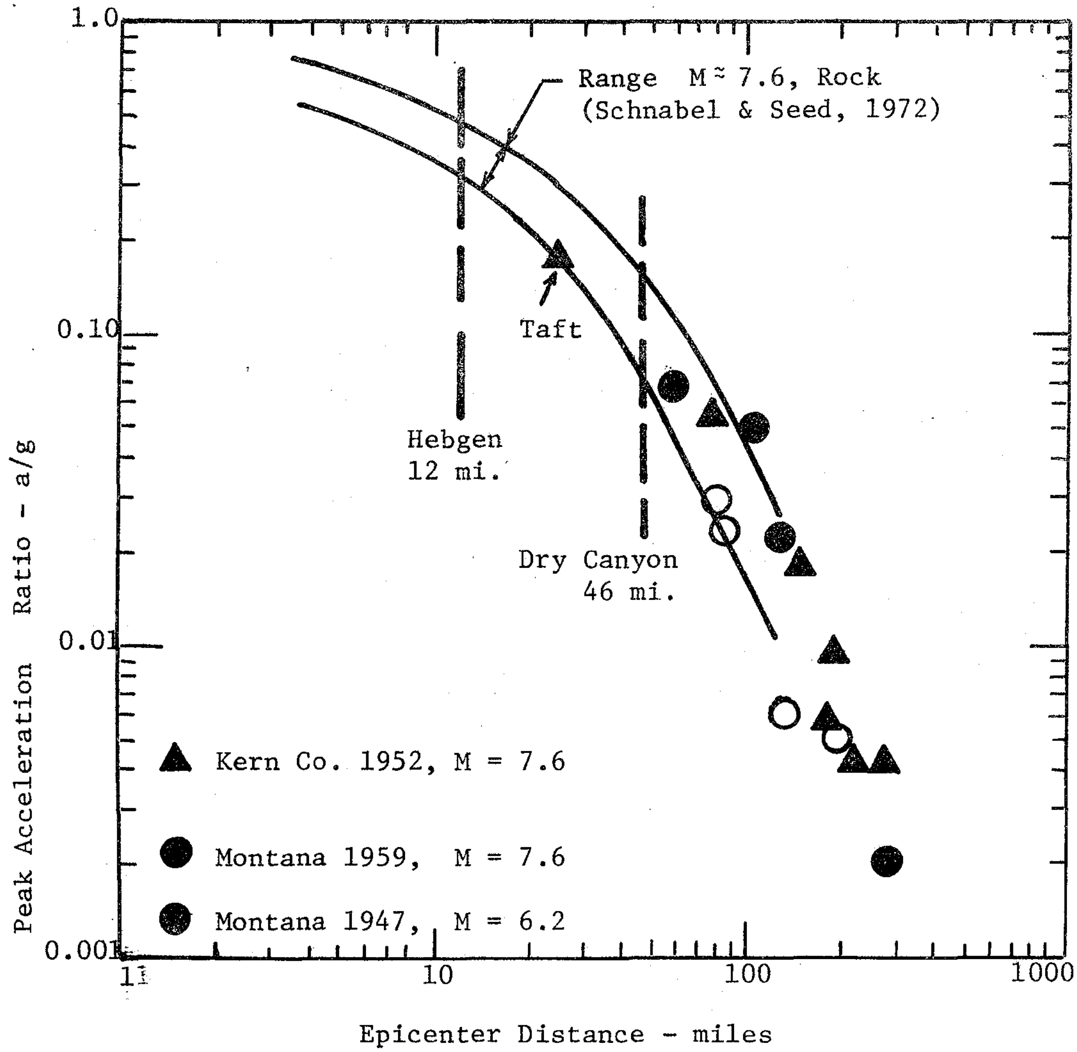

Fig. 7 Basic Data Used to Select Design Earthquake, Dry Canyon and Hebgen Dams

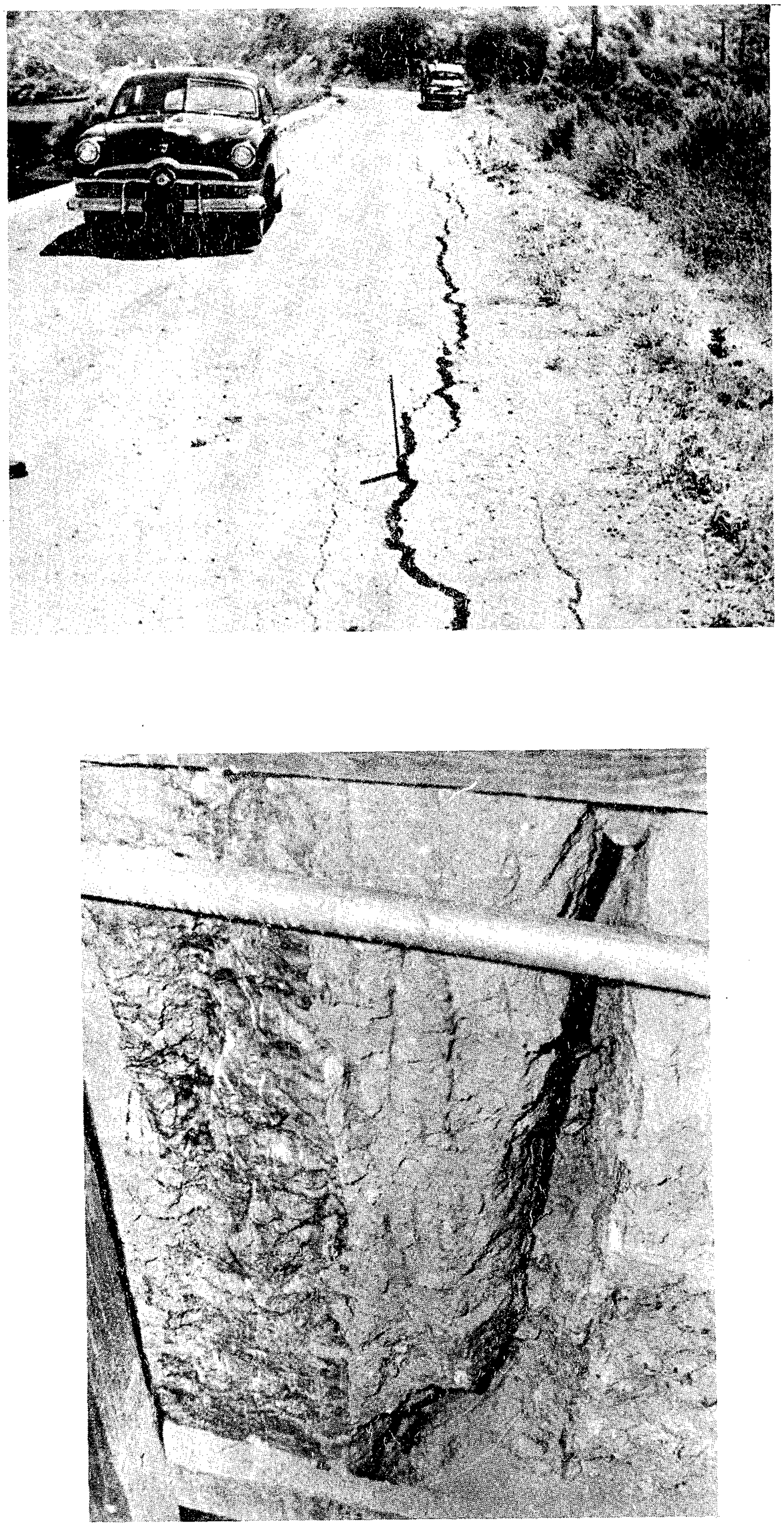

Fig. 8 Longitudinal crack along the crest of Dry Canyon Dam produced by the 1952 Kern County earthquake

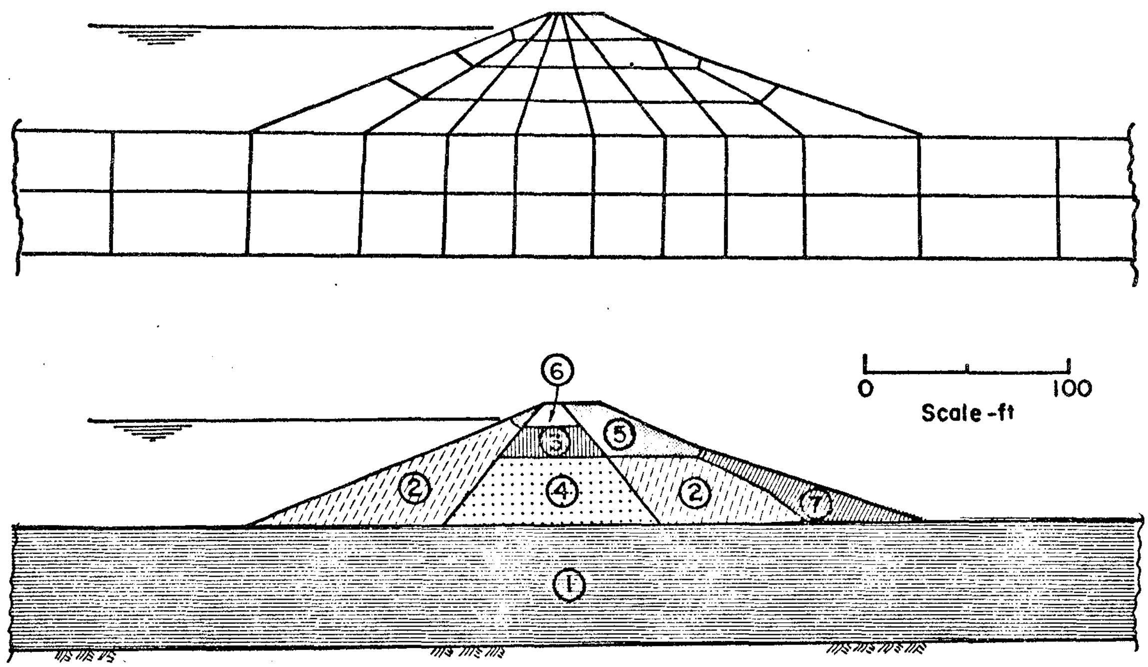

Zone	Below WT	Above WT	Dr - %
Foundation	1	—	77
Shell	2	5	62
Wagon Rolled Core	3	6	68
Hydraulic Fill Core	4	—	47
Stabilizing Berm	—	7	80

FIG. 9 FINITE ELEMENT SIMULATION OF DRY CANYON DAM.

The earthquake accelerations used in the seismic response analyses were the S69°E horizontal component and the vertical component recorded at Taft some 25 miles NW of the epicenter. The maximum horizontal acceleration recorded at Taft was 0.18g. Therefore, all accelerations on these records were multiplied by 0.10/0.18 to give a maximum horizontal acceleration of 0.1g at the bedrock level below the dam. Soil properties used for the static analyses are shown in Appendix I.

The deformed shape of the Dry Canyon Dam as indicated by the permanent deformation of each nodal point computed by the suggested method is shown on Fig. 10. The calculated deformations indicate 1.4 to 2.2 feet vertical settlement and 0.6 to 0.8 feet upstream movement at the crest. These movements are the result of relative distortions within the embankment as shown.

For reference it is recalled that the embankment fill was 63 feet high. This movement represents 1 to 4 percent of the height of the fill. By comparison, the measured crest movements at the actual dam were about 0.3 feet settlement and 0.3 feet upstream deformation. Thus, for this first illustrative calculation the suggested method over estimated the actual movements.

Parametric Studies-Dry Canyon Dam

Other analyses were also made to study the effects of different possible input parameters. These are described below. Some of the analyses using realistic input data gave calculated movements which were in closer agreement to the observed movements than indicated in Fig. 10.

2-D Versus 1-D Seismic Stress Analysis. One of the basic parameters investigated was the effect of 1-D (horizontal accelerations only) versus 2-D seismic response analyses in calculating the seismic shear stresses in the elements. Actually, the 2-D program only became available near the end

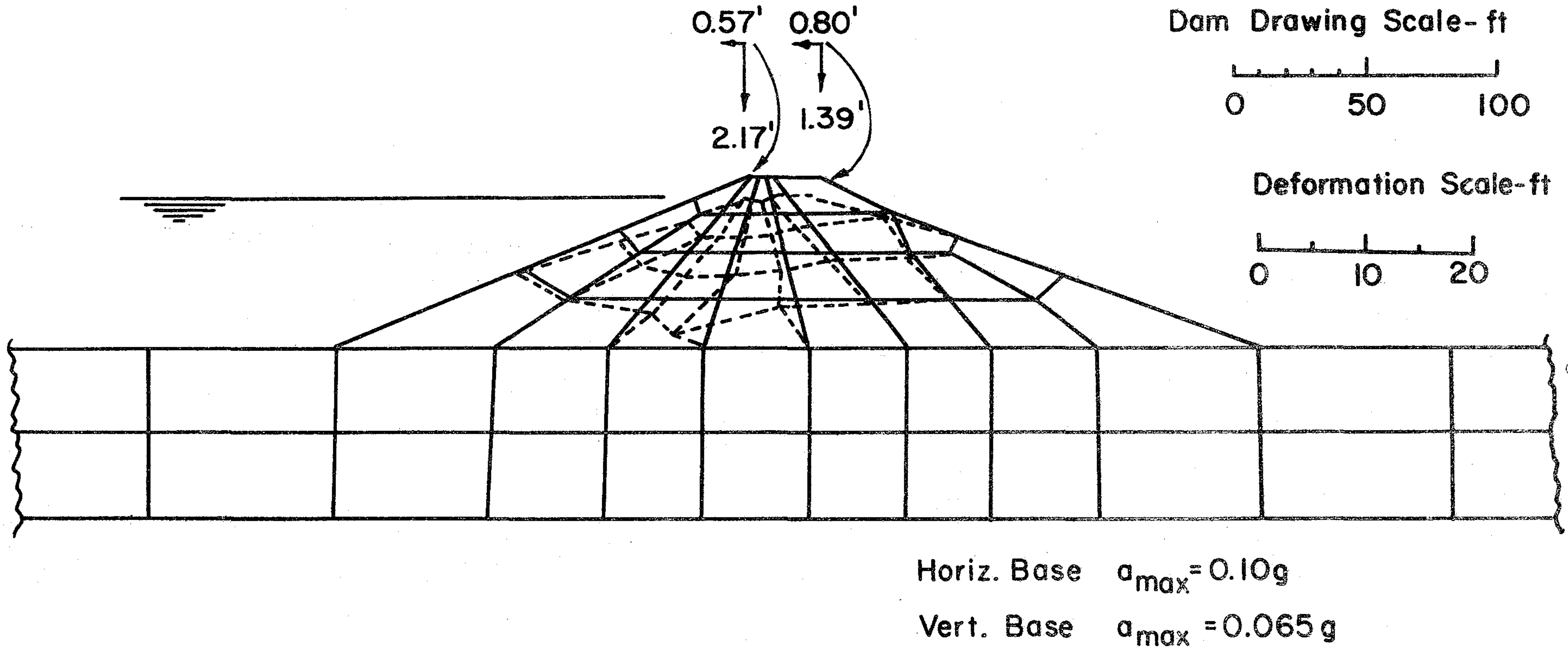

FIG.10 PERMANENT DEFORMATION PATTERN OF DRY CANYON DAM.

of the study, so all of the analyses were first made with a 1-D seismic finite element program. However, because the 2-D analyses may be more realistic, it was desirable to investigate the effect of 2-D versus 1-D seismic response calculations.

The first step was to perform a 1-D and a 2-D seismic response analysis on the same dam, with the same properties to see the effect of the vertical component of acceleration on the calculated seismic shear stresses. This effect is shown on Fig. 11 which presents a summary of the ratio of 2-D to 1-D shear stresses at every element. The ratio varies from 1.0 to a maximum of 1.3, with an average of 1.13 for all elements. This suggested that approximate or "simulated" 2-D seismic shear stresses could be obtained by multiplying the already calculated 1-D stresses by 1.13.

The next step was to see how well the permanent deformations using these "simulated" 2-D seismic shear stresses would compare with permanent deformations calculated from the actual 2-D shear stresses. This is illustrated on Table 2 for 5 typical nodal points. For all but very small calculated movements, there is good agreement between the results from the actual and the simulated 2-D method. On this basis, to save time and computer costs, the rest of the 2-D analyses were "simulated" by the above method from the 1-D analyses already completed.

Effect of Peak Acceleration. Another parameter investigated was the effect of peak acceleration. As already mentioned, based on tremds from available data, the maximum acceleration in rock at the damsite could have been as low as about 0.07 g or as high as about 0.16 g. It was of interest to investigate the effect of different maximum base accelerations on the calculated permanent deformations.

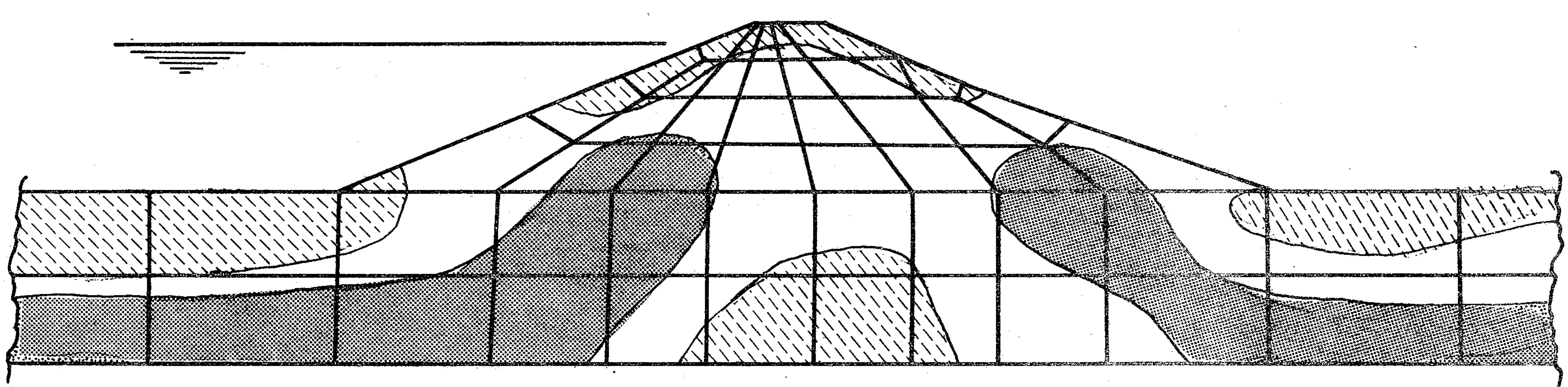

Legend

1.0 to 1.1

1.1 to 1.2

1.2 to 1.3

FIG.11 RATIO OF MAXIMUM SHEAR STRESS FROM SEISMIC ANALYSIS, 2D/1D, DRY CANYON DAM.

Table 2

Comparison of Displacements at Typical Nodal Points

for Actual and Simulated 2D Base Motion

Dry Canyon Dam - 2D Analysis

A_{max} = 0.10g horiz., 0.065g vert.

Nodal Point		12	21	42	19	47
Vert. movement - ft (+ up)	2D Actual	0.08	-2.40	-0.97	-2.17	-1.39
	2D Simulated	0.03	-2.22	-0.83	-1.97	-1.22
Horiz. movement - ft (+ downstream)	2D Actual	-0.70	-0.10	0.02	-0.57	-0.82
	2D Simulated	-0.56	-0.03	0.04	-0.52	-0.72

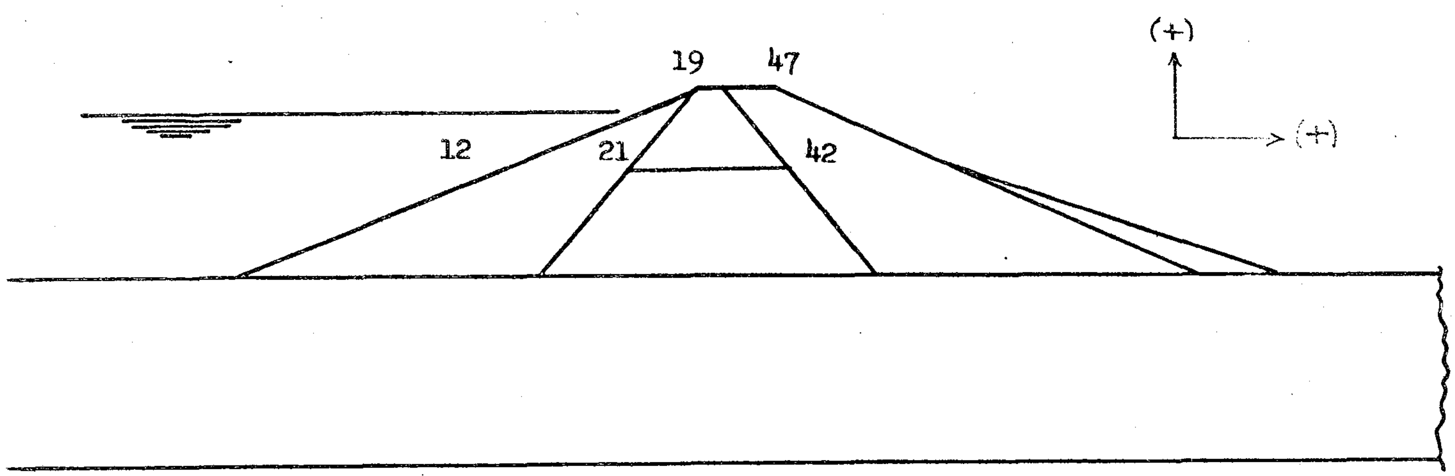

It was fairly clear that smaller accelerations would lead to smaller calculated permanent deformations. It was not so clear, however, that larger accelerations would lead to large enough deformations to give a postiive indication of failure. For this reason, calculations were made for peak horizontal base accelerations of 0.13g and 0.20g respectively as well as for a low peak acceleration of 0.075g. The peak seismic shear stress to static normal stress ratios calculated for several elements along the center line of the dam are shown on Fig. 12. For comparison, the calculated 2-D stresses are also shown for a_{max} = 0.1g and 0.075g.

The finite element program used to compute the seismic shear stresses used non-linear soil modulus and damping which varied with strain. Thus, it is not surprising that at high accelerations the calculated shear stresses also show a non-linear increase with acceleration.

The permanent deformations of the crest of the dam is shown on Fig. 13. for the 4 different base accelerations, and for 1-D and 2-D analyses. From the trend in the data it is clear that a peak base acceleration of 0.2g would have been sufficient to cause excessively large crest deformations of the order of 5 feet vertically and 12 feet horizontally. Such large deformations in a 63 foot high dam, with a loose silty sand hydraulic fill clay core would probably have led to the outer shell breaking up and result in even larger flow slide type of movements such as have been observed at other dams. The finite element analysis used for these studies cannot handle such problems of cracking and disintegration of the various parts. It is based on small strain theory, and on the assumption that all elements maintain their integrity and their connections to each other.

On the low acceleration side, the trend suggests that a maximum horizontal base acceleration of about 0.07 to 0.08, would have led to crest

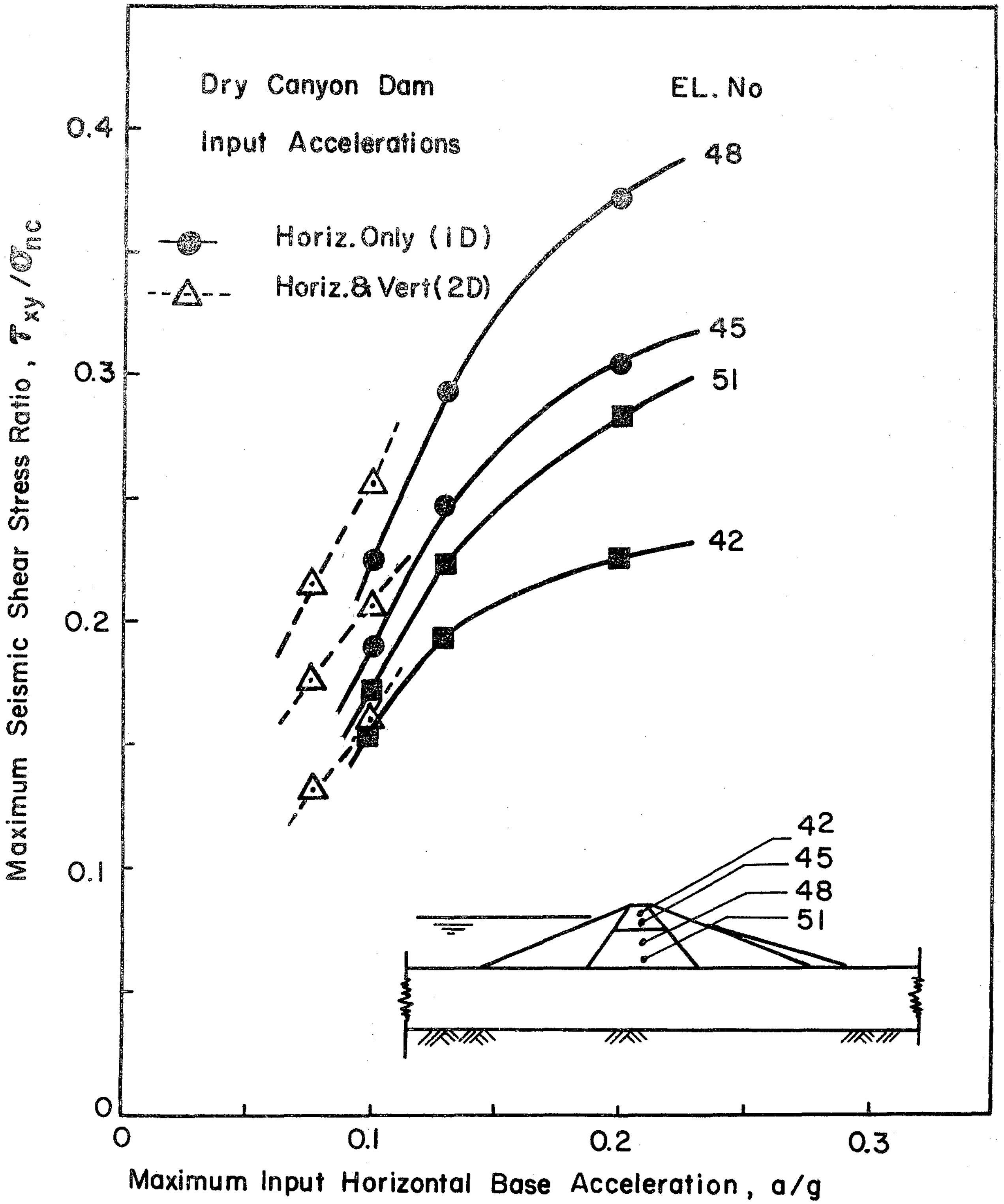

FIG. 12 SHEAR STRESS RESPONSE TO DIFFERENT BASE ACCELERATION.

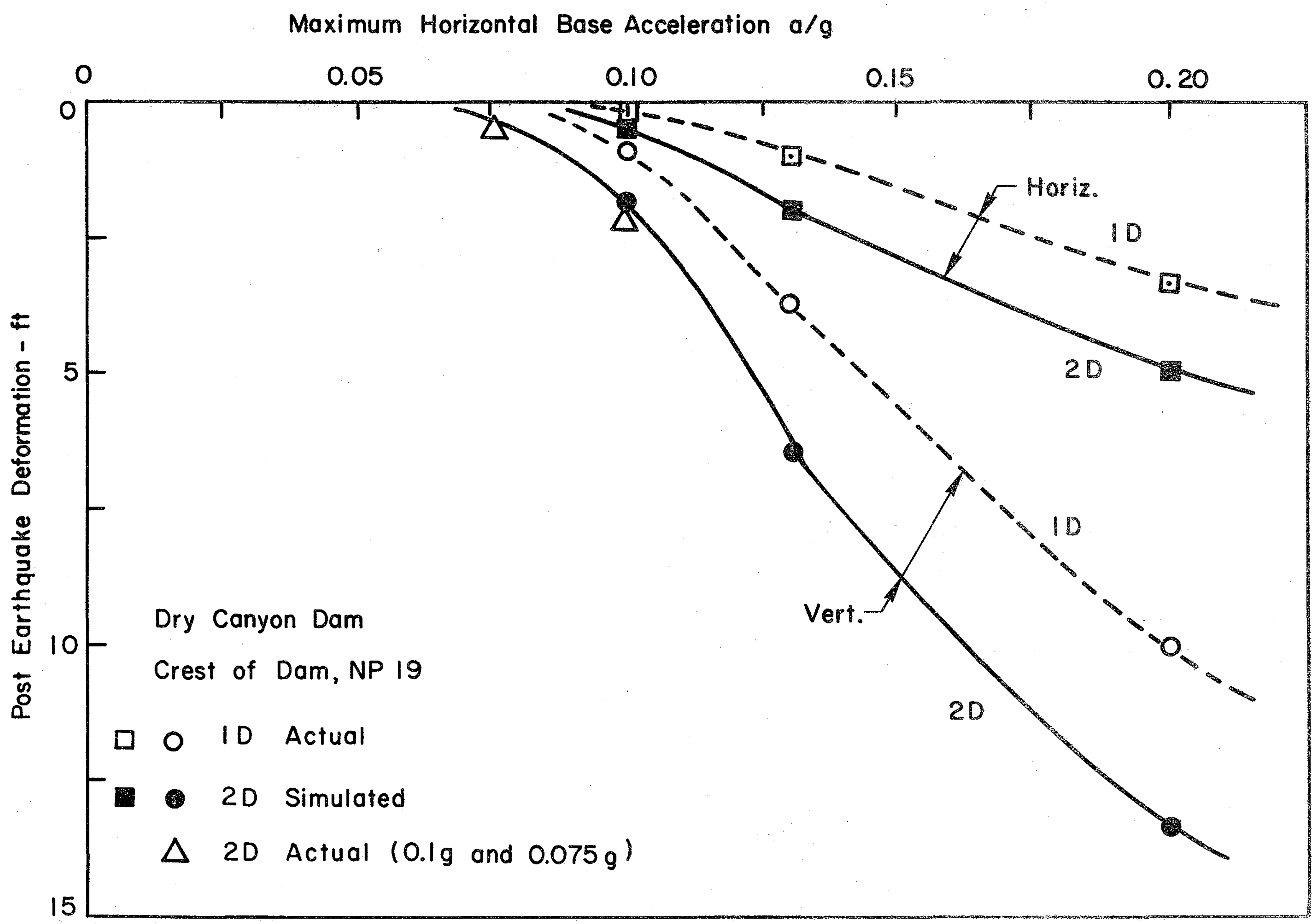

FIG. 13 COMPARISON OF CREST DISPLACEMENT FROM 1D AND 2D, INPUT BASE MOTIONS.

deformations of the order of 0.3 feet, which were actually measured. Considering the wide variation in maximum ground accelerations recorded at similar epicenter distances for the San Fernando 1971 earthquake (22,23) it is not unreasonable to suppose that the peak accelerations in rock at the Dry Canyon Dam in 1952 may have been as low as 0.07 to 0.08 g instead of the 0.10g assumed for the first analysis.

Equivalent Number of Cycles. Lee and Chan (21) have described the method employed in seismic stability analyses of earth structures for computing the equivalent number of uniform cycles of stress from the irregular time history which results from a seismic response analysis. A summary of the method is presented in Appendix III. The basis of the method equates the effect of an actual irregular stress time history to the effect of an equivalent number N_{eq} of cycles of uniform stress intensity τ_{av} which is some specified ratio R, of the maximum peak of the irregular stress.

$$R = \frac{\tau_{av}}{\tau_{max}} \qquad (15)$$

The evaluation is made on a single element basis. For each element there is no unique number N_{eq} and R, but rather a whole family of possible values, each combination of which will affect the soil in the same way as the actual irregular stress history. Thus a small number of large stress cycles will be equivalent to a large number of small stress cycles. Each appropriate combination will cause the element or sample of soil to strain the same amount.

The computer program developed by Lee and Chan computes N_{eq} for values of R = 0.65, 0.75, and 0.85 for each desired time history. From these data it is straight forward matter to select any appropriate combination of N_{eq} and R to represent the actual time history of stresses.

Calculations made for several elements in a dam show similar, but not exactly the same N_{eq} - R relation. Also, calculations based only on the input base acceleration show a similar N_{eq} - R relation to that of the time history response at any other location. The N_{eq} - R relations calculated for base, crest, and two center elements in the dam are shown on Fig. 14. From this data the values N_{eq} = 10 and R = 0.72 were selected for all of the analyses described thus far and unless specifically mentioned, for all other analyses. These values correspond to the central zone of the experimental data.

Because the N_{eq} - R data do show some scatter, it is of interest to investigate what effects may be involved by choosing other possible values of N_{eq} - R combinations. The results of several analyses using different combinations are summarized on Table 3. All data on this table refer to the calculated crest displacement, at Nodal Point 19. All other data were similar and, therefore, are not shown.

The first three sets of data correspond to N_{eq} - R combinations selected along the mean curve of Fig. 14. Cal. No. 17 corresponds to N_{eq} = 10 and R = 0.72 which has been discussed previously. The displacement pattern for this entire dam for this case is shown on Fig. 10, and the horizontal and vertical crest displacements are listed on Table 3. According to the reasoning behind the calculations of N_{eq} - R values, any combination along the same curve shown on Fig. 14 should produce the same effect on the soil. This is confirmed quite well by the results shown for the other two combinations along the mean curve. The slight differences in computed displacements (2.14, 2.17 and 2.48 feet horizontally) are not considered to be significant.

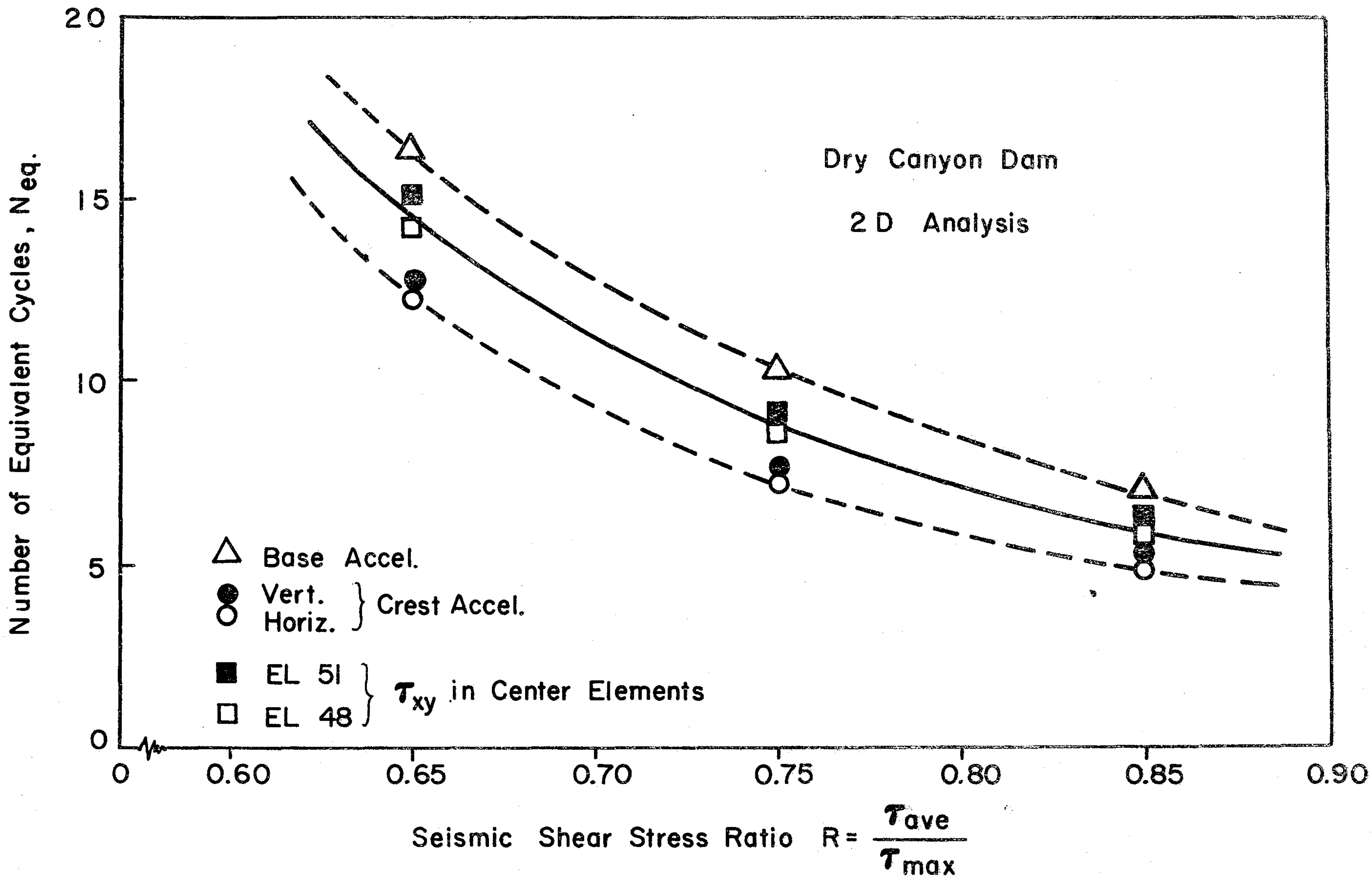

FIG. 14 EQUIVALENT NUMBER OF CYCLES FOR DRY CANYON DAM.

Table 3

Effect of Different Neq. & R

Dry Canyon Dam, 2D, horiz. $A_{max} = 0.10g$

Calc. No.	Neq.	R	Crest Deformations (NP No 19)		Remarks (Refer to data Fig 12)
			Horiz. (US) ft	Vert. (down) ft	
19	14.5	0.65	0.57	2.14	Mean Curve
17	10.0	0.72	0.57	2.17	Mean Curve
20	6.0	0.85	0.67	2.48	Mean Curve
29	10.0	0.68	0.38	1.56	Lower Limit Curve
17	10.0	0.72	0.57	2.17	Mean Curve
30	10.0	0.76	0.82	2.90	Upper Limit Curve

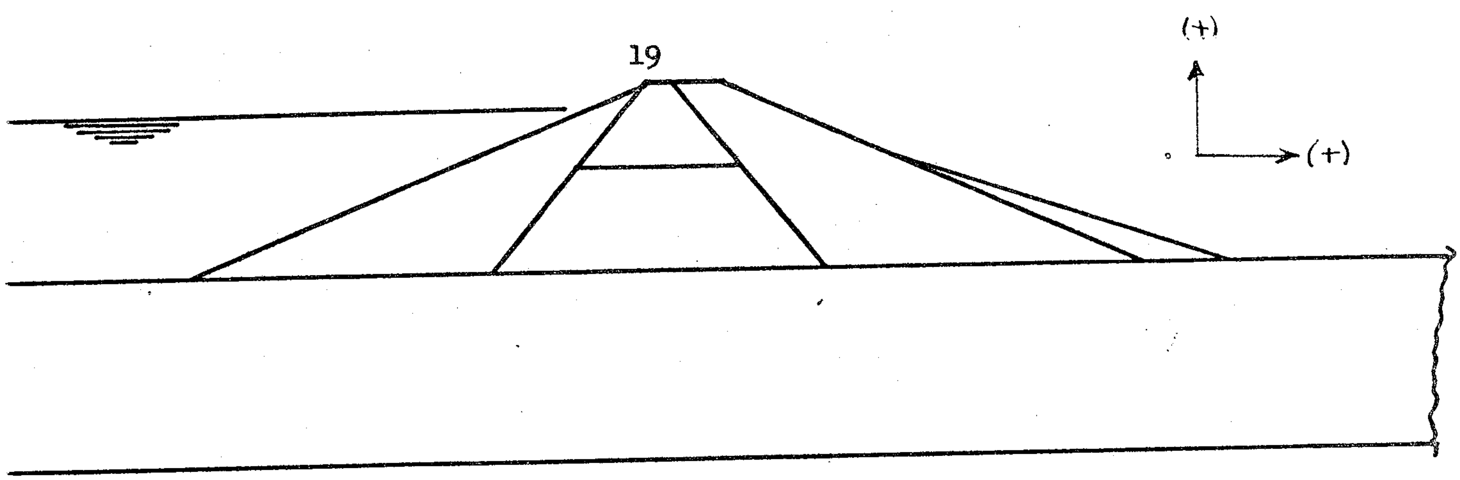

The second assumption inherent in the use of an N_{eq} - R combination for seismic stability analyses is that the same combination applies everywhere in the structure. The band width of curves shown on Fig. 14 illustrates the extent to which this actual data deviate from this basic assumption. The effect of this variation on the computed permanent deformations is shown by the lower three items on Table 3. These calculations were each made for N_{eq} = 10 but with R = 0.68, 0.72 and 0.76 corresponding to the lower mean and upper limit curves of Fig. 14. The corresponding vertical movements of 1.56, 2.17 and 2.90 illustrate the variation that can be expected from selecting different plausible combinations of N_{eq} and R.

Effect of Pre-Earthquake Static Modulus. The description of the suggested method of permanent deformation calculations stated that the values of pre-earthquake modulus E_i for each material could be chosen rather arbitrarily, with some caution in selecting relative values from one soil zone to another. To investigate this assumption, three calculations were made using identical data except for the values of E_i. The results of these calculations are summarized on Table 4, which show calculated permanent displacements for 5 typical nodal points from the three calculations.

The basic calculation used $E_i = E_o$, where E_o represents the values of Young's modulus used in the several zones of the dam, for all other calculations. These values are shown in Table I-7 of Appendix I, along with other data used in the calculations. The two other calculations used E_i = 0.5 E_o and 2.0 E_o respectively. As shown in Table 4, the calculated nodal point displacements for each case are quite similar, and the variations do not appear to be significant. Thus it would appear that values of E_i used for the various materials in the embankment may be selected rather arbitrarily.

Table 4

Comparison of Displacements at Typical Nodal Points
For Different Static Modulus Values

Dry Canyon Dam - 2D Analysis

A_{max} = 0.1g horiz., 0.065g vert.

Nodal Point		12	21	42	19	47
Vertical Movement - ft (+ up)	$E_i=0.5E_o$	0.09	-2.82	-1.08	-2.52	-1.59
	$E_i=E_o$	0.08	-2.40	-0.97	-2.17	-1.39
	$E_i=2E_o$	0.07	-2.15	-0.89	-1.94	-1.26
Horizontal Movement - ft (+ Downstream)	$E_i=0.5E_o$	-0.68	0.02	0.09	-0.61	-0.89
	$E_i=E_o$	-0.70	-0.10	0.02	-0.57	-0.82
	$E_i=2E_o$	0.71	-0.15	-0.02	-0.54	-0.76

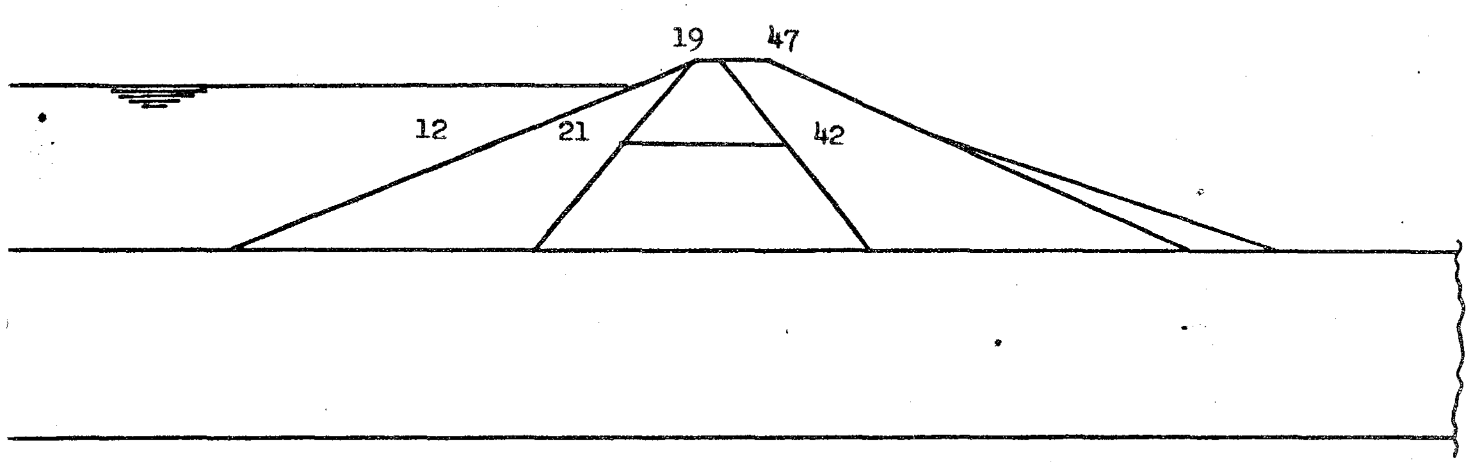

Effect of Pre-Earthquake Equilibrium Static Stresses. One of the important calculations in this method of analysis as well as in the equilibrium methods is to determine the static equilibrium stresses in the dam prior to the seismic disturbance. This is important because the response of soil to pulsating loading is quite dependent on the static consolidation stresses to which it has been subjected prior to the cyclic load applications. In many analyses, these static stresses are computed by means of a static loading finite element method which uses incremental loading to simulate construction of the embankment and non-linear stress-strain properties. A popular program is one developed at Berkeley (24) which uses stress dependent hyperbolic stress-strain Poisson's ratio parameters.

On the other hand, Clough and Woodward (25) found in early studies that if stresses alone were the only properties desired, a simple gravity-turn-on analysis using a linear elastic finite element computer program would give reasonably accurate values. Subsequent investigations by the writer and others have tended to confirm this early finding. In a major design problem it is probably best to use a non-linear program. The costs in time and computer charges are not prohibitive. The major cost involved is in obtaining the necessary non-linear static soil properties from laboratory tests.

However, for a research oriented parametric study such as described herein, it is relatively costly, time consuming and inconvenient to use a non-linear program because to do it correctly would require extensive laboratory testing to get the necessary non-linear soil parameters. If a simple gravity-turn-on analysis will give similar results, and if they will be consistent from case to case, then it would seem to be acceptable to use the simpler linear elastic gravity-turn-on method for calculating the static stress distributions within the embankments.

A comparison of the static stresses computed by a simple gravity-turn-on analysis and by two different non-linear incremental loading analyses is shown on Fig. 15.

The Non-linear Method A is the hyperbolic stress dependent method developed by Duncan and his colleagues at Berkeley and modified to include seepage forces. The Non-linear Method B is a new method currently under development by the writer using strain dependent formulations. Properties for the programs were estimated from published data, and selected to be as similar as possible from one program to another.

Each of the programs calculated the static stresses due to loads from the appropriate total or buoyant weight of elements plus seepage forces under full reservoir steady state conditions. The distribution of normal and shearing stresses on horizontal planes through the center of the lowest row of elements in the embankment is shown.

The two non-linear methods give similar results. The gravity-turn-on method gave slightly higher normal stresses than either of the non-linear methods, but the shearing stresses were similar. Considering the limitations of all of the methods to accurately simulate all aspects of the problem there is little to suggest that the stresses computed by any one method are more appropriate to use in the subsequent seismic stability analyses than another.

Permanent deformation calculations were made for one seismic stress condition, using the static stresses computed by the three different methods described above. The deformations at 4 representative nodal points are summarized in Table 5. There appears to be an almost random variation with one method computing slightly larger movements at one point, and slightly smaller movements at another. However, for all three methods, the calculated

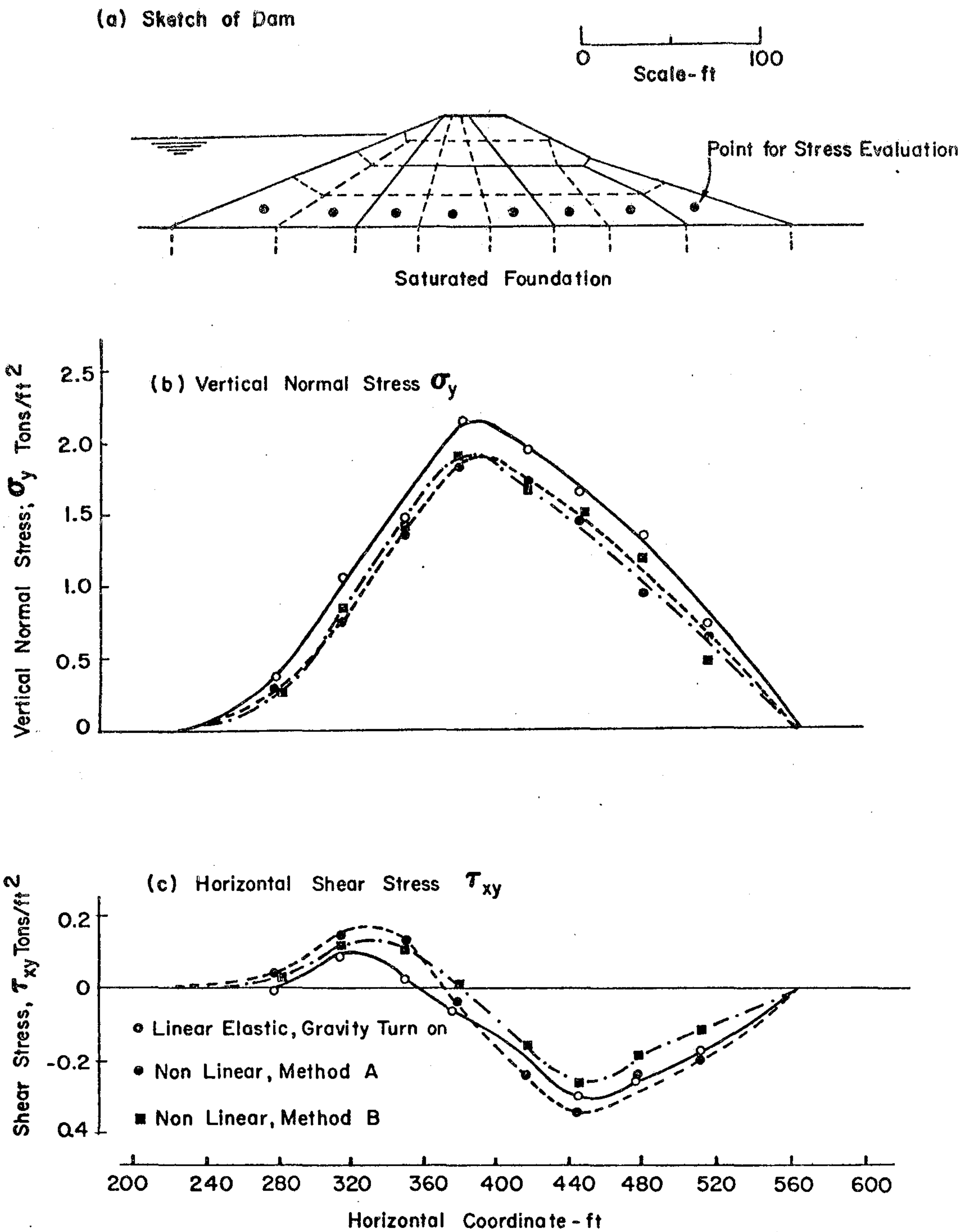

FIG. 15 STATIC STRESSES AT CENTER OF LOWEST ELEMENTS IN EMBANKMENT, DRY CANYON DAM.

Table 5

Comparison of Displacements at Typical Nodal Points

For Different Pre-Earthquake Static Stress Analyses Methods.

Dry Canyon Dam. 2D Motion
0.1g Horiz.
0.065g Vert.

Nodal Point	19		47		21		12	
Direction	H	V	H	V	H	V	H	V
Linear elastic gravity-turn-on	-0.57	-2.17	-0.82	-1.39	-0.10	-2.41	-0.70	-0.80
Non-linear incremental Method A	-0.49	-3.06	-0.98	-1.98	-0.23	-2.91	-0.34	-0.11
Non-linear incremental Method B	-1.09	-2.97	-1.31	-1.77	-0.13	-3.83	-0.20	-0.06

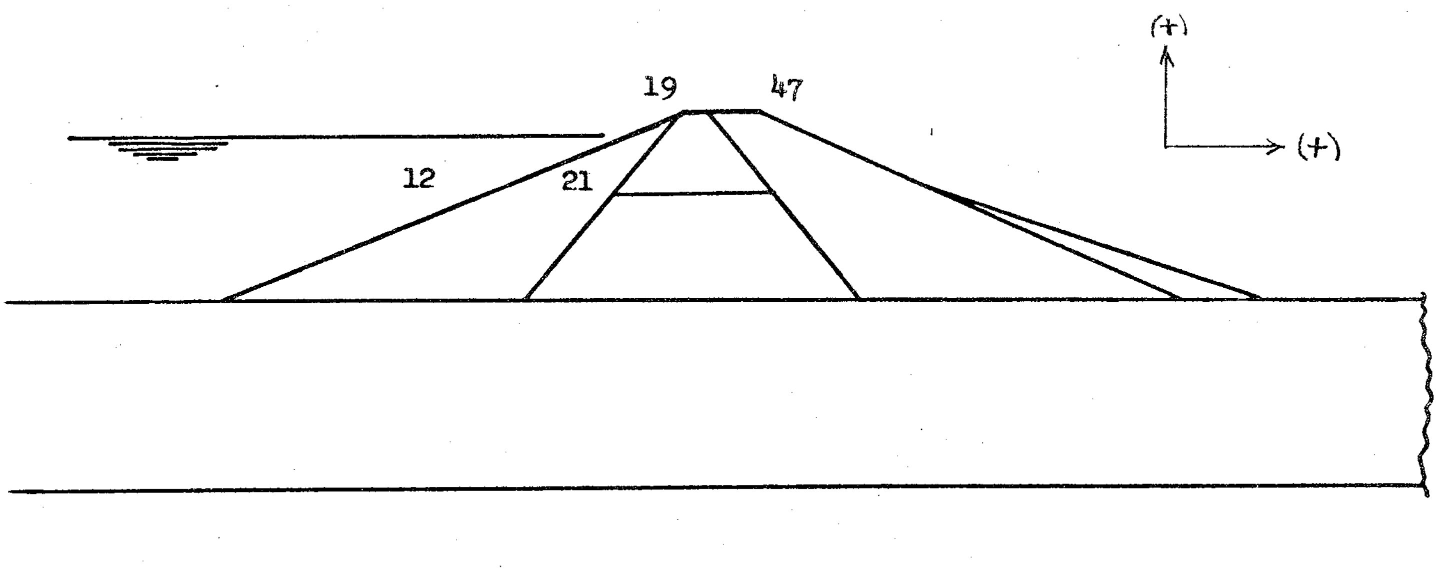

movements are of similar magnitude. Thus, for the purpose of this study at least, the simple gravity-turn-on linear elastic method of analysis seems to be sufficient for determining the pre-earthquake static stresses. Therefore, this method was used for all other cases studied.

Sheffield Dam

A detailed equilibrium method of seismic stability analysis of the Sheffield Dam along with a description of the dam and its observed behavior has been published by Seed, Lee and Idriss (6). Only a brief summary will be presented here for background and continuity.

The Sheffield Dam was constructed in 1917 in a ravine north of the city of Santa Barbara, California. The embankment was only 720 feet long and 25 feet high. It was constructed of sandy silty soil excavated from the reservoir area. Compaction was probably limited to that obtained by routing the construction equipment over the fill. The upstream face was designed to include a 4 foot thick clay blanket on the upstream face extending into the foundation and covered with a 5 inch thick perforated concrete slab. There are few available records of the actual construction to indicate how this upstream impervious clay face and cutoff were actually built, or to what extent it functioned as an impervious barrior. Photographs of the dam do show the concrete face, but the city engineer at the time wrote that there was no downstream drainage, and that although there was no leakage through the upstream core, seepage around and under the cutoff had saturated the main structure prior to the earthquake.

A cross section through the dam is shown on Fig. 16 which indicates the position of the freatic surface estimated by Seed, Lee and Idriss for their analysis.

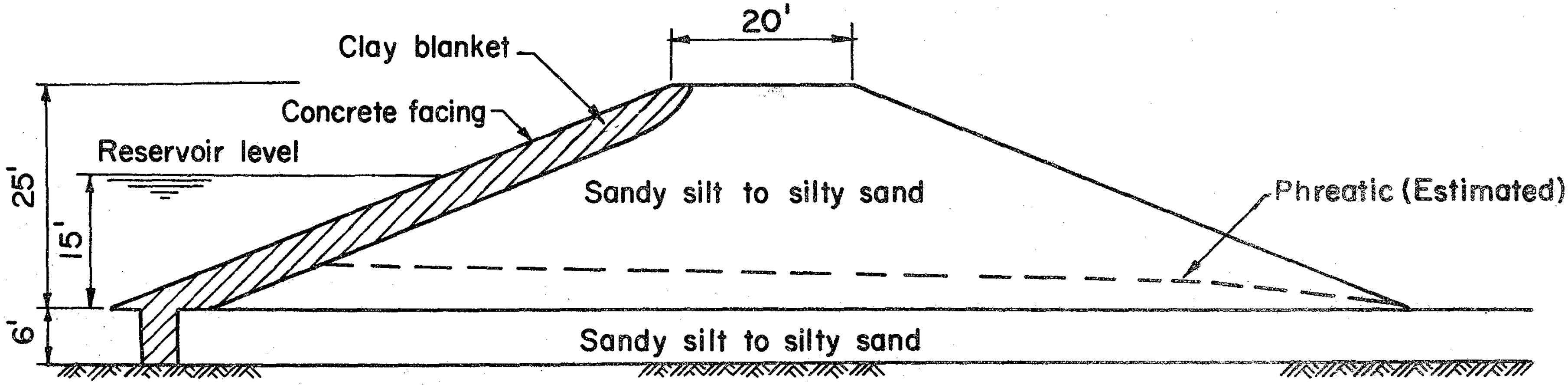

FIG. 16 CROSS SECTION THROUGH EMBANKMENT.

The Santa Barbara earthquake of 1925 had a magnitude of 6.3 and was located some 7 miles northwest of the dam site. It completely destroyed the dam. The city manager described the failure as follows. "After examination by several prominent engineers, the conclusion has been reached that the base of the dam had become saturated, and that the shock of the earthquake---had opened vertical fissures from the base to the top; the water rushing through these fissures simply floated the dam out in sections." (26).

Photographs looking along the upstream face of the dam with the reservoir empty, before and after the earthquake, are shown on Fig. 17.

The studies described by Seed, Lee and Idriss (6) found that the upper layers of natural soil near the old dam site was loose silty sand and sandy silt with an average dry density of about 90 pounds per cubic foot, corresponding to about 76 percent of the maximum standard AASHO density. It was estimated that this corresponded to about 40 percent relative density. The material in the embankment was the same as the foundation, and because of the minimal amount of compaction provided by the hauling equipment of that time, was probably about the same density as the upper part of the foundation. Only a few cyclic triaxial tests had been performed for the earlier seismic stability study. Most of the tests were cyclic simple shear. Unfortunately, most of the original test data had been misplaced, therefore, cyclic loading parameters required for this study were estimated from the compilation of data from the other soils for which large amounts of data are available. (See Appendix I).

No strong motion recording equipment was in use at the time of the earthquake so that the input motion at the base of the dam had to be estimated from other records obtained from other earthquakes at later dates. The Seed et al. (6) study suggested that the strong motion at the dam site

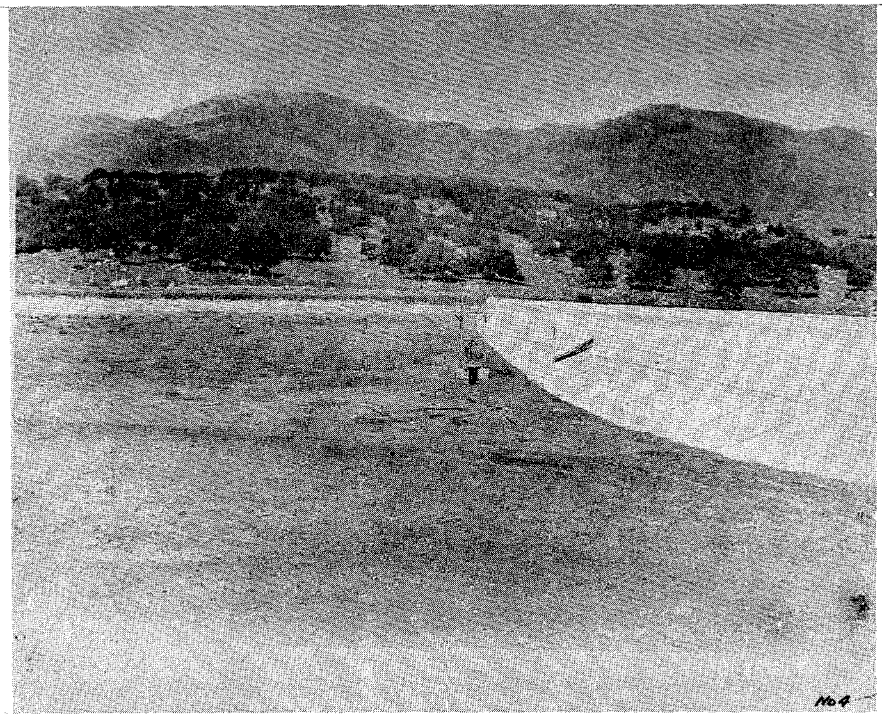

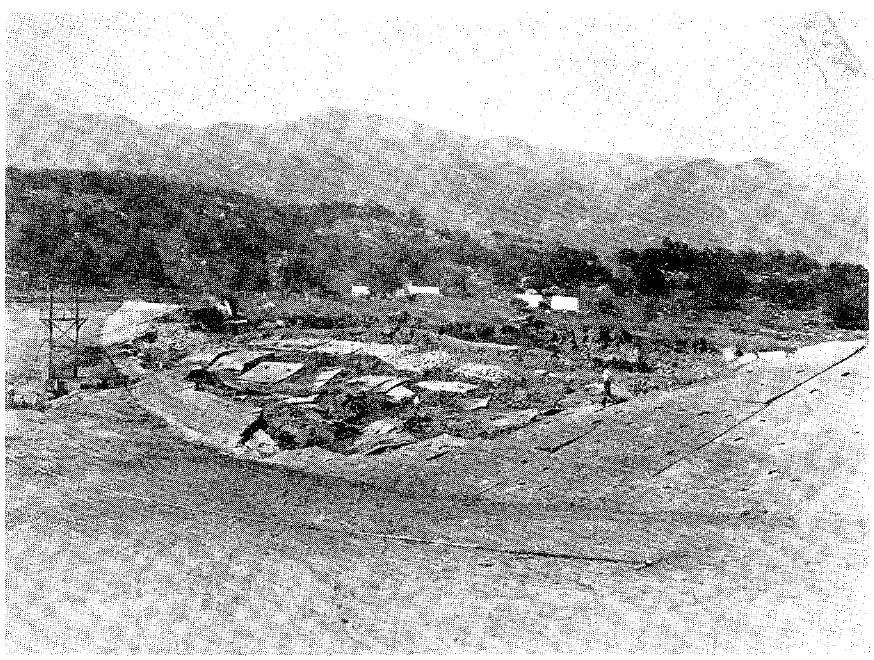

Fig. 17 Views of the Sheffield Dam before and after the Santa Barbara earthquake, 1925

might be defined approximately as follows: maximum acceleration = 0.15g, duration of shaking = 15 seconds, predominant frequency of accelerations = 3 cycles per second, and the time history might be approximated by appropriate scaling of the 1940 El Centro NS record. This same modified El Centro time history was used in these permanent deformation analyses. All accelerations were multiplied by the same constant required to reduce the maximum peak acceleration to 0.15g. The time scale of the recorded El Centro accelogram was multiplied by 1.50 to provide a predominant period in the acceleration response spectra of 3 Hz.

The finite element simulation used for the Sheffield Dam is shown on Fig. 18. The soil properties used in the analyses are summarized in Table I-8 of Appendix I. Although provision was made for different materials in the embankment as in the foundation, the available information was not sufficient to justify use of different properties in the analyses. The only difference in material properties which were used corresponded to differences between saturated material below the water table and moist material above the water table. Because of uncertainty of the position of the freatic surface and saturation zones prior to the earthquake, two different analyses were made with different assumed water table positions. These are designated by RUN 1 and RUN 2 on Fig. 18.

As discussed in connection with the Dry Canyon Dam analyses, the seismic response calculations had already been made for 1-D horizontal accelerations only at the time that the 2-D computer program became available. Therefore, a "simulated" 2-D analyses was made for this dam as well, by multiplying the 1-D seismic shear stresses by 1.13 as was done for the Dry Canyon Dam. An analysis of the time history records at several elements indicated that the equivalent uniform cyclic stress conditions could be

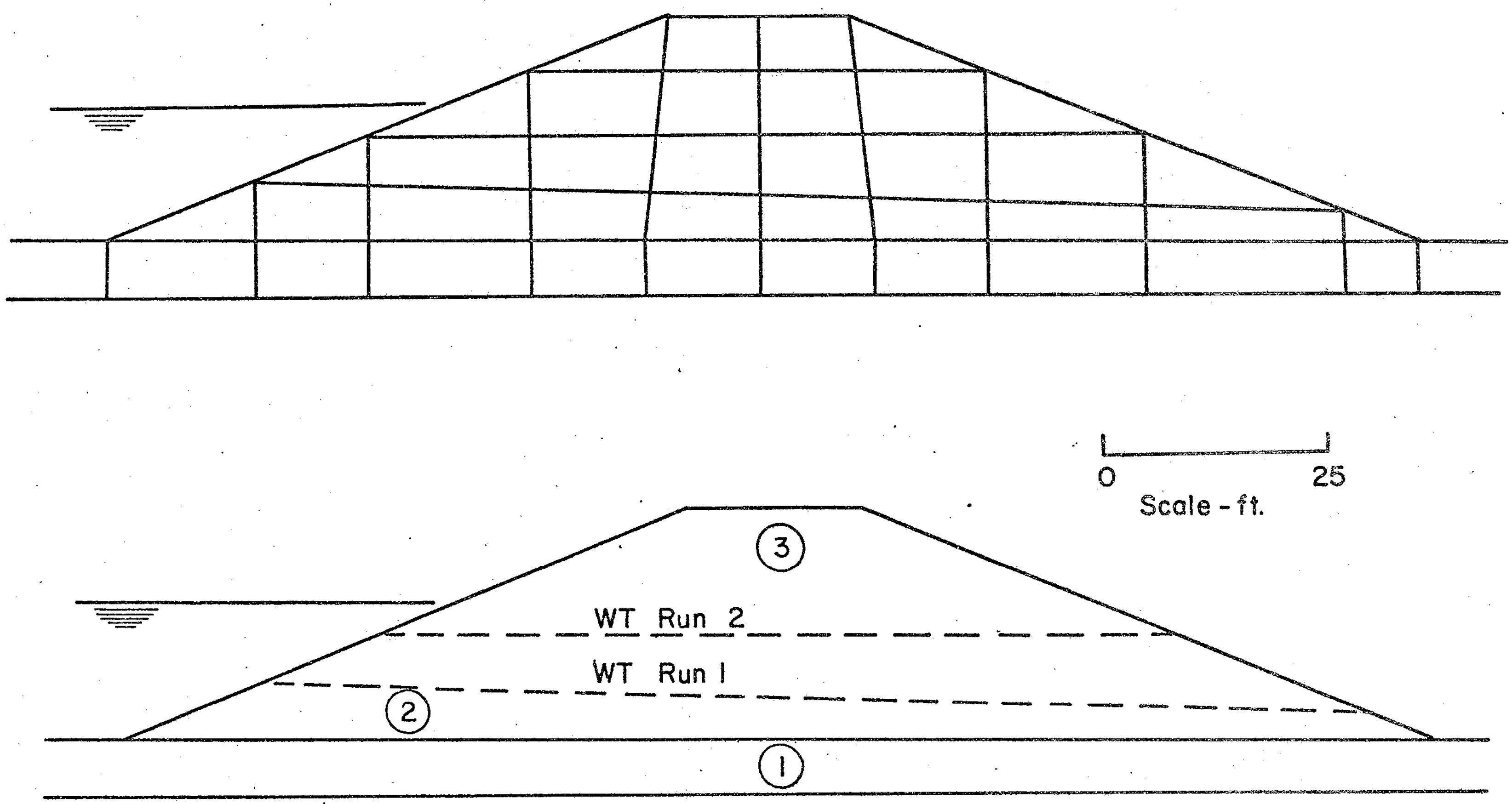

Zone	Below WT	Above WT
Foundation	1	—
Embankment	2	3

FIG.18 FINITE ELEMENT SIMULATION OF SHEFFIELD DAM.

represented by the combination $N_{eq} = 10$ and $R = 0.72$.

The permanent deformations calculated from RUN 1 with the low position of the water table in the embankment were too small as compared with the observed performance of the dam. A summary of the calculated crest deformations for RUN 1 is shown on Table 6 for 4 typical nodal points. The maximum calculated deformation was only 0.8 to 1.0 feet vertical settlement whereas the actual dam was known to have failed.

A second calculation RUN 2, was made for the assumed position of the water table coincident with the next highest element layer as shown on Fig. 18. This led to large calculated deformations. These are also summarized on Table 6 for typical nodal points. The calculated settlement of the crest ranged from 6.7 to 8.7 feet whereas the height of the dam was only 25 feet and the freeboard at the time of the earthquake was only 7 to 10 feet.

The calculated deformed shape of the dam from RUN 2 are shown on Fig. 19. Clearly such large vertical deformations would be almost enough to cause the reservoir water to flow over the dam. On the other hand, the large deformations would probably lead to the formation of cracks through which the water could begin to escape, and because of the erosive nature of the material, would rapidly destroy the entire embankment. This latter hypothesis agrees with the descriptions by engineers who visited the dam following the earthquake (26).

Other analyses could have been made to further bracket the range of uncertainties in the basic input data; position of water table, maximum acceleration, time history, and soil properties. However, considering the uncertainty in all of these data, further detailed studies did not appear to be justified at this time. The analyses which were performed showed

Table 6

Calculated Displacements At Sheffield Dam

Using Two Different Internal Assumed Distribution of Saturation

Nodal Point	9		21		33		44	
Component	H	V	H	V	H	V	H	V
Lower 5 ft. of embankment saturated-Run 1	-0.4	0.1	0.0	-1.0	-0.2	-0.8	0.2	0.1
Lower 12 ft. of embankment saturated-Run 2	-6.16	1.86	-1.9	-8.7	-3.0	-6.8	0.2	1.5

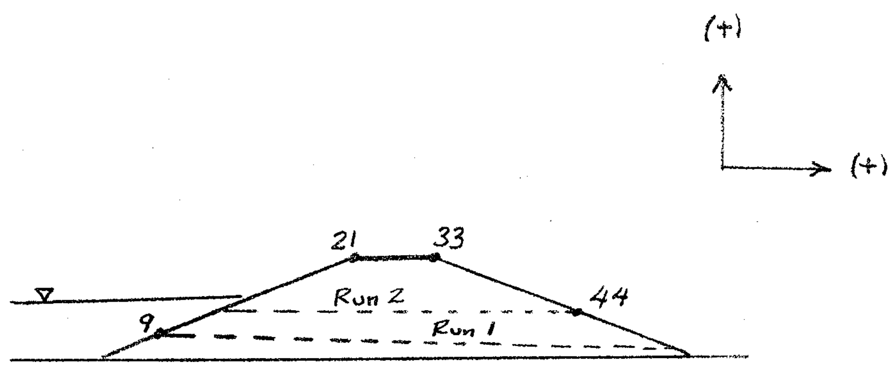

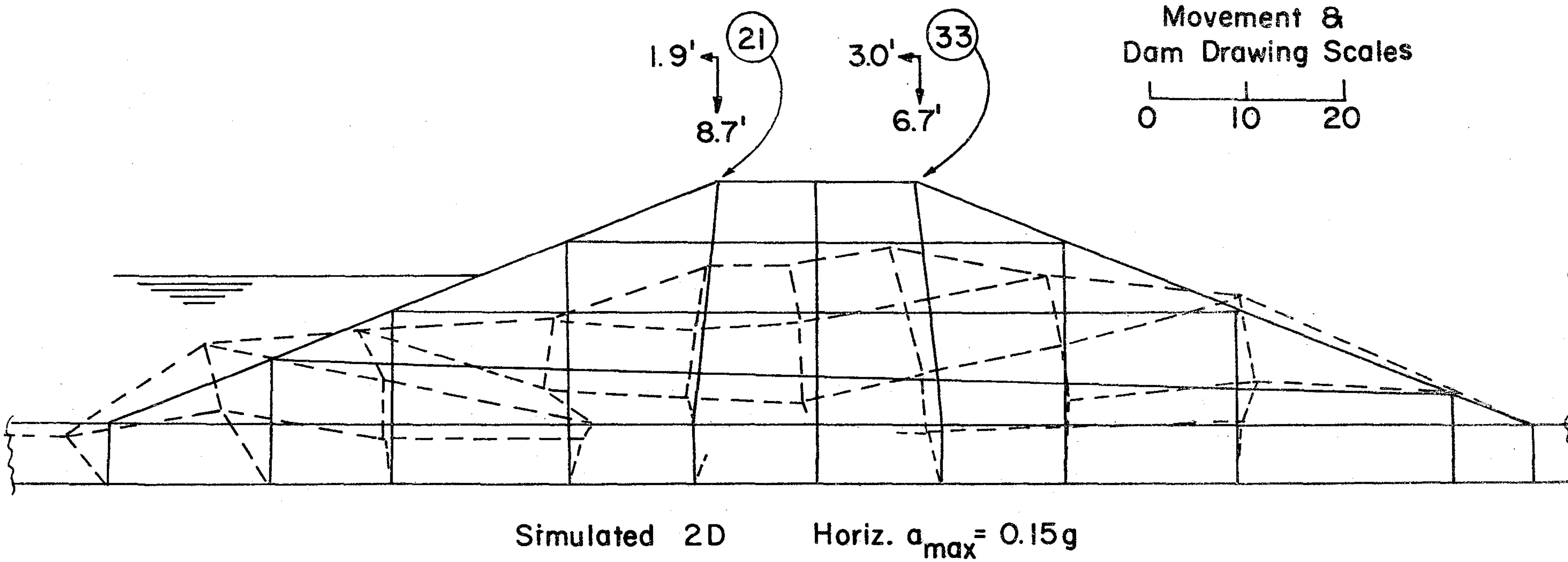

FIG. 19 PERMANENT DEFORMATION PATTERN OF SHEFFIELD DAM, RUN 2, WATER TABLE HIGH.

that the calculated permanent deformations were sensitive to the position of the water table within the dam, and a reasonable assumption of the water table led to calculated deformations in good agreement with observed field performance.

Upper and Lower San Fernando Dams

A comprehensive description and seismic equilibrium analyses of the behavior of these two dams during the February 9, 1971 earthquake has been presented by Seed, Lee, Idriss and Makdisi (7). Much of the data used in the following permanent deformation studies came from this earlier report, and only a brief summary will be repeated here for background information and continuity.

These dams provided the terminal storage for water from the Los Angeles aqueduct system. They are some 15 miles below the Dry Canyon Dam previously described in this report. The Lower dam was built in the year 1912 with additions up to about 1940. The Upper dam was constructed in 1921-22. Early construction work on these dams was by hydraulic fill methods with some wagon hauled material placed in the outer shells. Later construction used rolled compacted fill.

The Upper and Lower San Fernando dams were located some 1½ miles apart and about 8½ miles southwest of the epicenter of the February 9, 1971 earthquake. This was about 7 miles from the energy center as defined by Duke et al. (22). The magnitude of the earthquake registered about 6.6 on the Richter Scale. Both dams were seriously damaged by the earthquake, the Lower dam much more seriously than the Upper.

Numerous accelerogram records were obtained from the shock. The maximum recorded acceleration was 1.25g at the abutment of the concrete arch

Pacoima Dam. However, because of the peculiar topographic and geologic features of this site, this large acceleration has been discounted somewhat as far as its application to other more level sites. A seismoscope record from the abutment of the Lower San Fernando Dam was converted into a time history accelerogram by Scott (27). However, it too had some questionable peaks. Based on the available data, Seed, et al., (7) assumed that the maximum acceleration at the San Fernando dam sites was about 0.55 to 0.60g, with a time history similar to that recorded at Pacoima Dam, or as calculated from the seismoscope record at the Lower San Fernando Dam. The seismic stresses calculated in this earlier study from these two records for the two dams were used directly in the following described permanent deformation analyses.

Upper San Fernando Dam

An aerial photograph of the Upper San Fernando Dam taken 12 days after the earthquake is shown on Fig. 20. The slide scarps visible on the upstream face were below the water level at the time of the earthquake. Two close-up photographs along the crest of the dam are shown on Fig. 21 and illustrate the surface nature of the permanent deformations. Not shown by these photographs was downstream movement and a pressure ridge about $2\frac{1}{2}$ feet high at the downstream toe of the embankment.

A cross section through the dam is presented on Fig. 22 which also shows the extent of permanent deformations following the earthquake. Surveys made along the crest of the dam indicated that the abutments moved upstream about $1\frac{1}{2}$ feet while the center moved downstream about $3\frac{1}{2}$ feet with respect to a reference away from the site. The net movement at the center of the crest of the dam with respect to the abutment was, therefore, about 5 feet

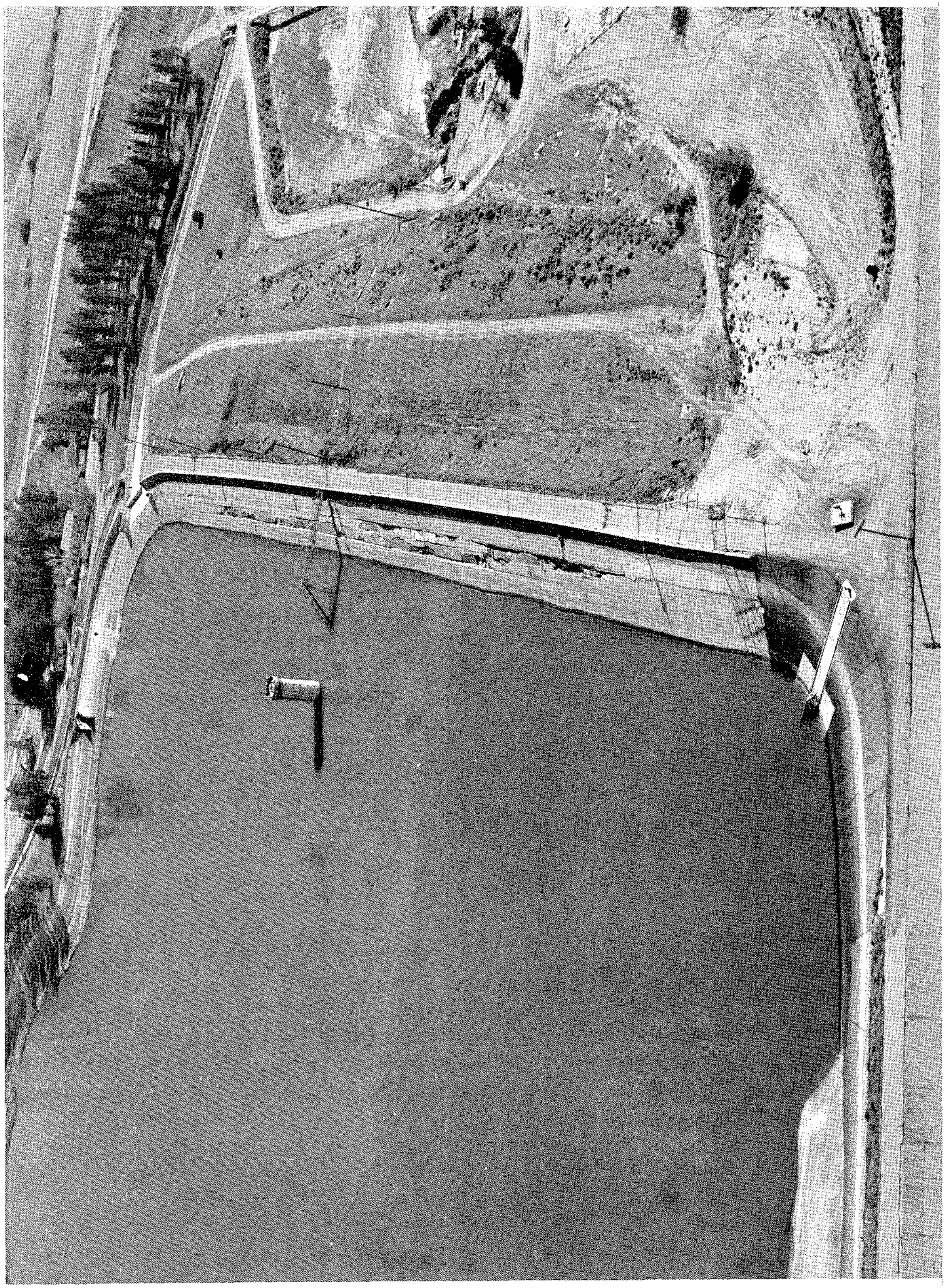

Fig. 20 Upper San Fernando Dam, February 21, 1971, following the February 9, 1971 earthquake

Fig. 21 Two close up views of the Upper San Fernando Dam following the Feb. 9, 1971 San Fernando earthquake

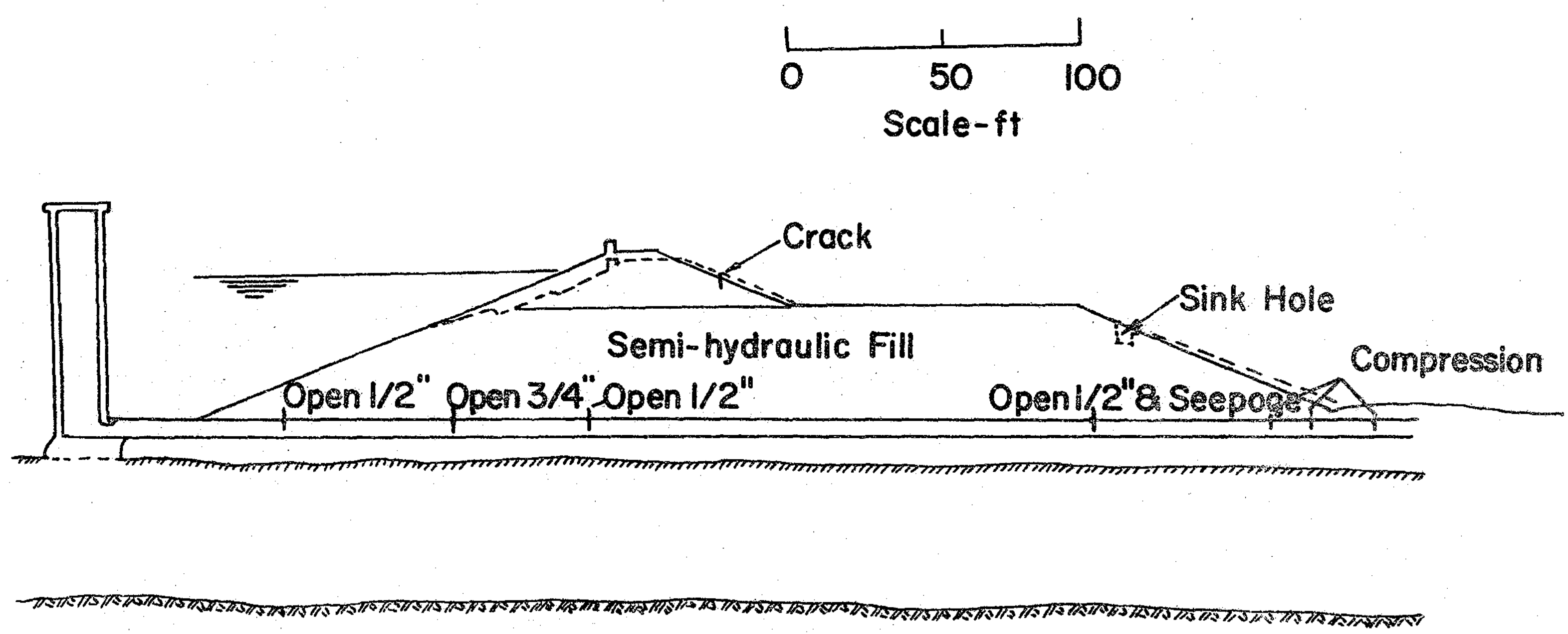

FIG. 22. CROSS-SECTION THROUGH UPPER SAN FERNANDO DAM SHOWING MOVEMENTS CAUSED BY THE EARTHQUAKE.

downstream and about 3 feet settlement. This was accompanied by the formation of two well defined shear scarps at the upstream face, compression and extension zones along the outlet conduits through the embankment, and a $2\frac{1}{2}$ foot pressure ridge at the toe. The embankment is about 65 feet high and constructed over about 120 feet of alluvial soil foundation.

The finite element model used in the analyses is shown on Fig. 23 along with the various soil zones. A description of the soil properties used in the permanent deformation analyses is presented in Appendix I.

The seismic stresses were computed from the response of the dam to a modified Pacoima record (a_{max} = 0.60g) as described in detail elsewhere (7), and then used directly in the permanent deformation analysis described herein. Calculated permanent deformations for three typical nodal points on the surface of the dam are shown on Fig. 24, along with other data to be described later. The calculated permanent deformation at the crest was approximately 1.0 feet vertical settlement and 0.4 feet horizontal movement downstream. The movements were smaller than the 3 and 5 foot movements which were actually measured at the crest.

It was reasoned that because of the scatter in observed maximum accelerations from various records of this earthquake (22,23) it is not reasonable that the maximum acceleration at the dam may have been 20 percent higher. Assuming that 20 percent increase in accelerations would lead to 20 percent increase in seismic shear stresses, a new permanent deformation analysis was made using seismic shear stresses which were 20 percent higher than for the previous analysis. The results of these calculations for the same 3 nodal points are also shown on Fig. 24. For this case, the calculated deformations at the crest were about 1.7 feet vertical settlement and 1.2 feet horizontal downstream movement.

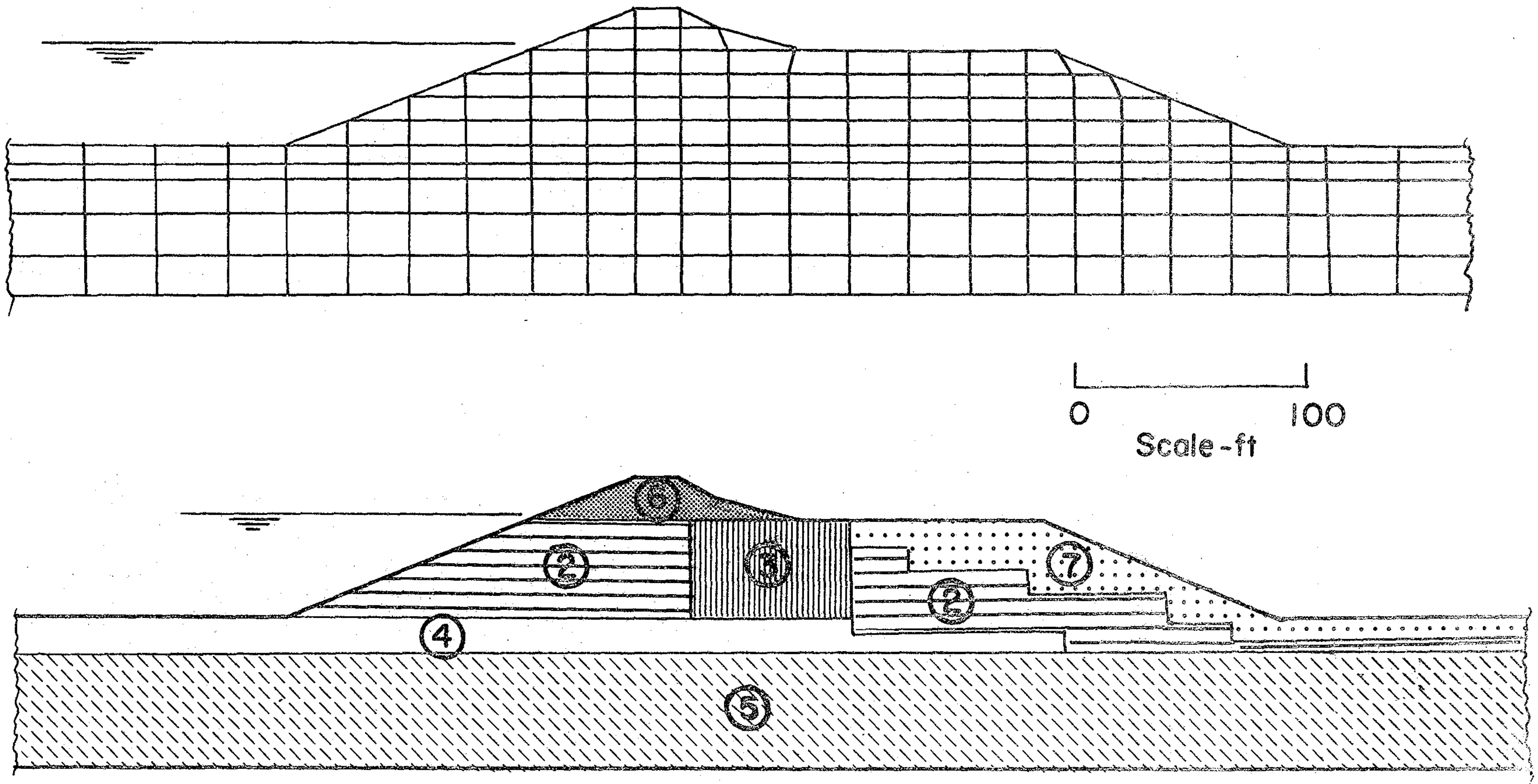

Zone	Belowe WT	Above WT
Rolled Fill Cap	1	6
Hyd. Fill Sandy Shell	2	7
Hyd. Fill Clay Core	3	–
Upper Alluvium Fnd.	4	–
Lower Alluvium Fnd.	5	–

FIG. 23 FINITE ELEMENT SIMULATION OF UPPER SAN FERNANDO DAM.

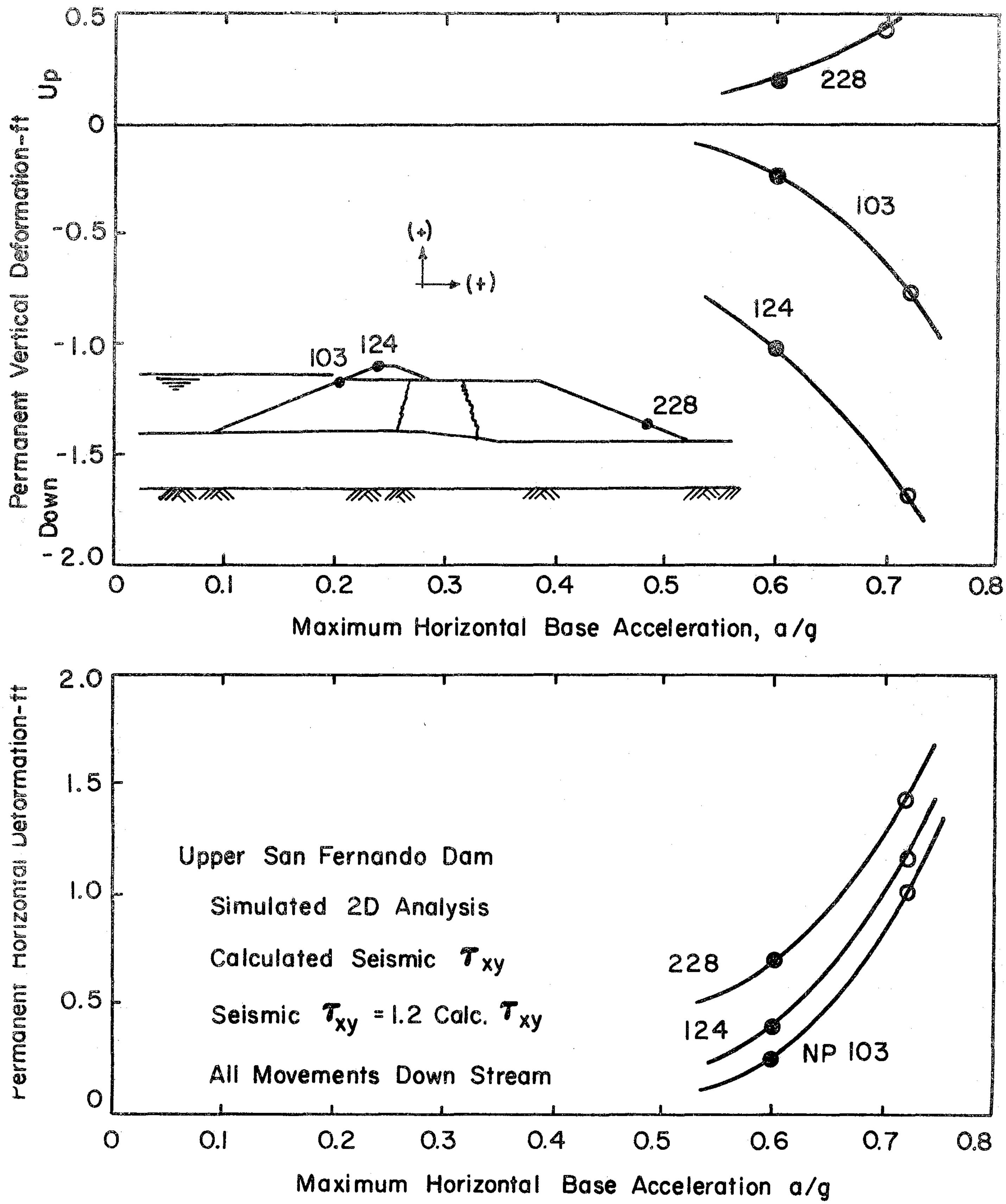

FIG.24 EFFECT OF BASE ACCELERATION ON PERMANENT DEFORMATIONS, UPPER SAN FERNANDO DAM.

These calculated movements agreed in direction with the observed movements, but were only about half as large as those measured. It is recalled that the actual dam developed a visible shear scarp at the upstream face, and a pressure ridge suggesting a shear scarp at the downstream toe, along which much of the total observed movement appeared to have taken place in these zones. In its present form the finite element program used to calculate the permanent deformations could not predict or handle a shear plane of failure, but rather was based on small strain theory and elements which remained intact. On this basis, calculated deformations of about 1 to $1\frac{1}{2}$ feet do not seem unreasonable in comparison with the observed movements which developed along a well defined shear surface.

The pattern of calculated permanent deformations at all nodal points within the Upper San Fernando Dam, for seismic stresses 20% greater than given by 0.6g peak acceleration, is shown in Fig. 25. For clarity, the deformation pattern is drawn to approximately double the basic drawing scale. The general nature of the movements, crest settlement, and sliding in a downstream direction is readily apparent. It is noted that like the Sheffield Dam, there is considerable calculated distortions in the internal elements, but this is not reflected to the same extent at the boundaries.

Because of the pre-earthquake stress conditions, and the partially saturated soil above the freatic surface, the soil elements near the outer faces of the dam are stronger than the internal elements. The previously mentioned water bucket analogy is recalled in which even though the internal material is no stronger than a fluid, there can be no overall movement unless the walls fail.

In the actual dam, the outer "walls" did fail and developed shear scarps along which some movement developed. Unfortunately, in its present

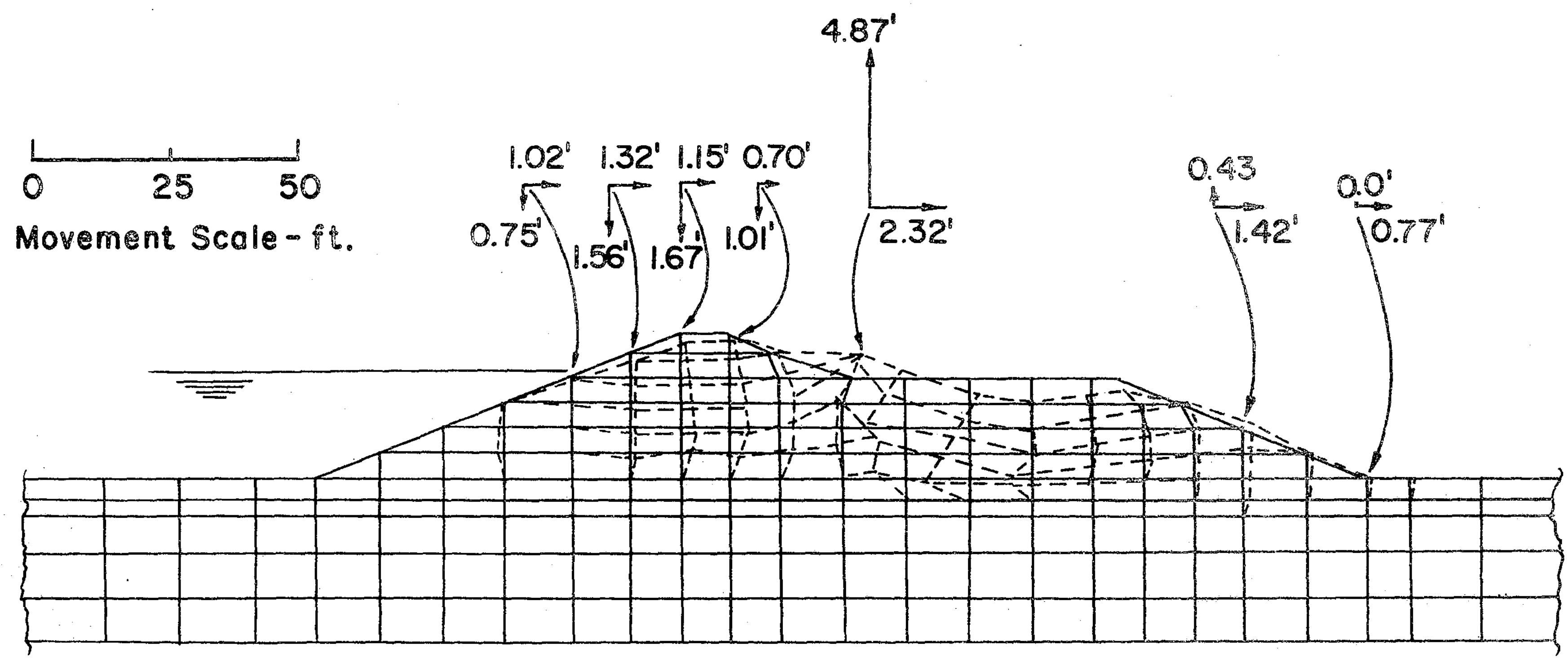

Simulated 2D , Horiz. a_{max}=0.7g

FIG. 25 PERMANENT DEFORMATION PATTERN, UPPER SAN FERNANDO DAM.

form, the finite element method used for these calculations cannot predict or handle the formation of cracks and shear zones. If the dam had not developed these shear zones in the outer shell the actual deformations would have probably been smaller, and in better agreement with the calculated values. Further analytical development of permanent deformation analyses needs to provide a method of analyzing for shear scarps which may develop through the stronger shell materials of dams.

As with the Dry Canyon Dam, a limited number of analyses were made on the Upper San Fernando Dam to investigate the effect of the N_{eq} - R combination selected for the analysis. The calculated N_{eq} - R values for several locations within the dam, and for both the Scott seismiscope and modified Pacoima acceleration records, are shown on Fig. 26. The basic analyses which have been discussed thus far used $N_{eq} = 5.5$ and $R = 0.75$ as obtained from the mean curve. Calculations were also made for two other locations along this mean curve. The calculated crest deformations for these three cases are shown in the upper part of Table 7. According to the theory involved in calculating the N_{eq} and R, any combination of values along the same curve should lead to the same final results. Comparison of the data on Table 7 indicate this to be approximately the case.

Calculations were also made for one point on the upper limit curve, $N_{eq} = 7.0$, $R = 0.75$ to compare with the same calculations for the mean curve. The resulting permanent deformations from these calculations are shown on the lower part of Table 7. In this case there is not a large difference in calculated permanent deformations from using one curve as opposed to another. This suggests that one should not look toward improving the accuracy of the calculated permanent deformations.

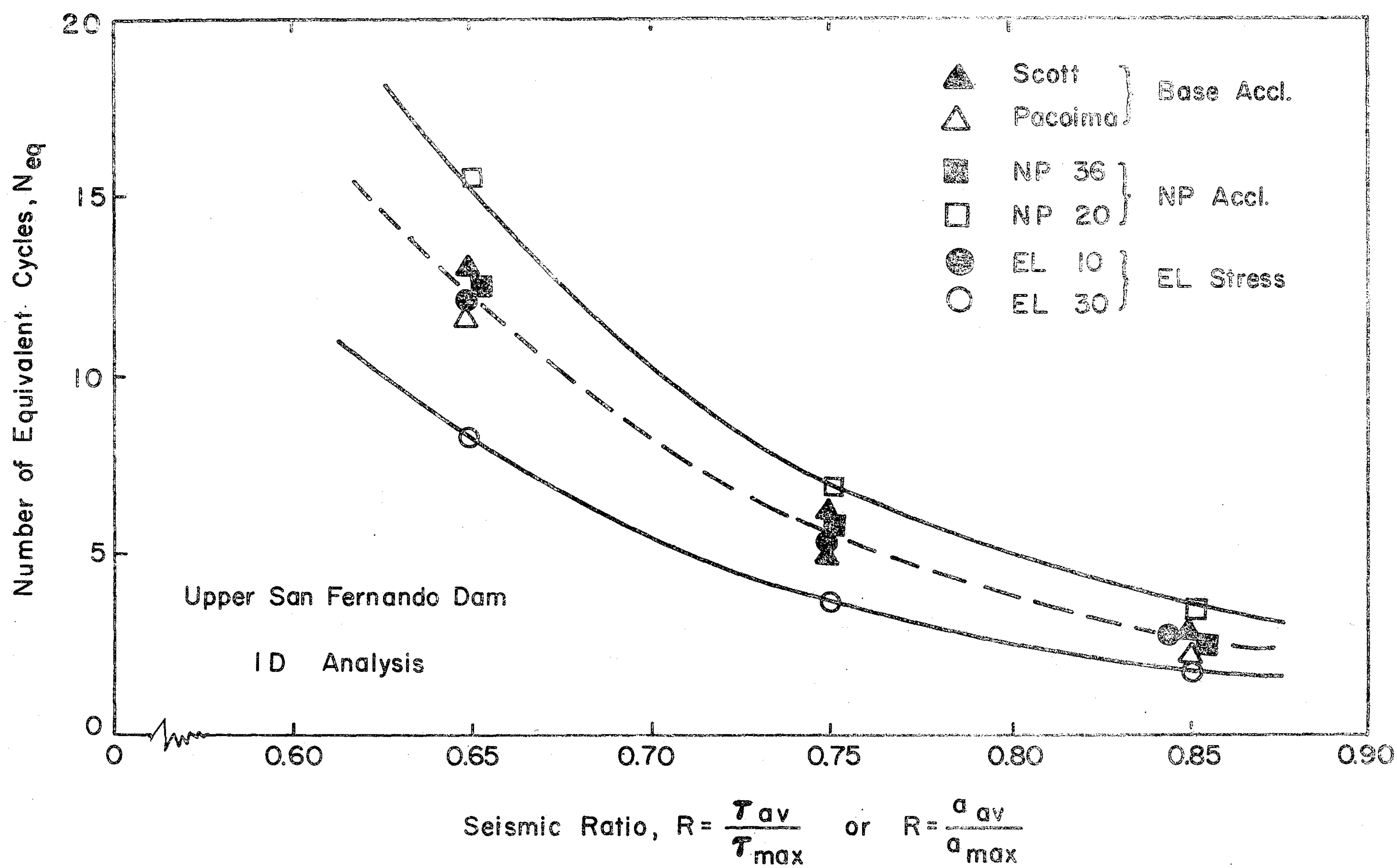

FIG.26 EQUIVALENT NUMBER OF CYCLES FOR SAN FERNANDO DAMS.

Table 7

Effect of Different N_{eq}. and R

Upper San Fernando Dam, Simulated 2D, Horiz. A_{max}=0.6g

Calc. No.	N_{eq}	R	Crest Deformation (NP No 124)		Remarks (Refer to Data Fig.)
			H ft.	V ft.	
13	12.5	0.65	0.48	1.26	Mean Curve
12	5.5	0.75	0.42	1.09	Mean Curve
11	3.0	0.85	0.42	1.03	Mean Curve
12	5.5	0.75	0.42	1.09	Mean Curve
14	7.0	0.75	0.56	1.29	Upper Limit Curve

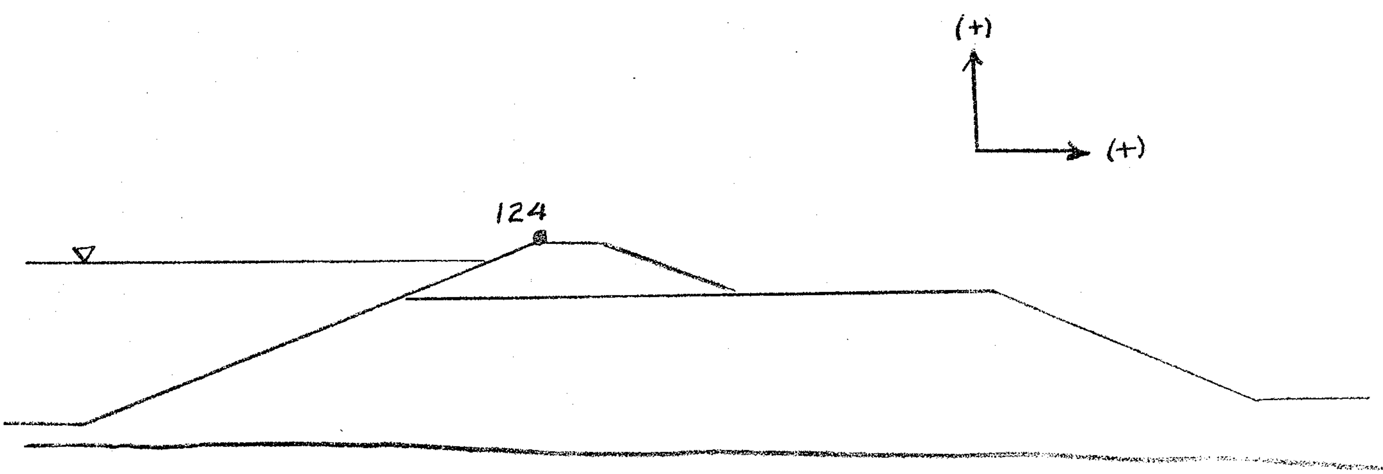

Lower San Fernando Dam

An aerial photograph of the Lower San Fernando Dam taken 12 days after the earthquake is shown on Fig. 27. As described elsewhere (7) the entire upstream zone of the dam extending back beyond the crest, slid upstream into the reservoir. Fortunately, sufficient embankment material remained in place to contain the reservoir water until it could be lowered through controlled drainage.

Cross sectional views through the central main section of the dam are shown on Fig. 28. These are taken from a previous report by Seed, et al. (7) and show the relative position of the various zones before the earthquake, after the earthquake and as reconstructed to illustrate how the movements developed. The outlet tower shown on Fig. 28 was knocked down during the slide, and is lying out of sight below the water in Fig. 27.

According to the previous study, a large portion of the hydraulic fill shell on the upstream side liquefied during the earthquake. The resulting loss of strength in this zone allowed relative movements of the overlying material, which soon broke into blocks and slid down over and into the liquefied material to a final resting place as shown. Some of the liquefied shell erupted through the overlying material near the toe to form sand volcanoes.

The maximum height of the embankment above the alluvial foundation before the earthquake was about 130 feet. The surveys after the earthquake indicated that the crest had moved upstream about 20 feet and settled vertically about 40 feet. Other parts along the upstream face suffered different amounts of movement. A small structure supporting a walkway to the central tower, and located midway along the upstream face moved upstream about 70 feet.

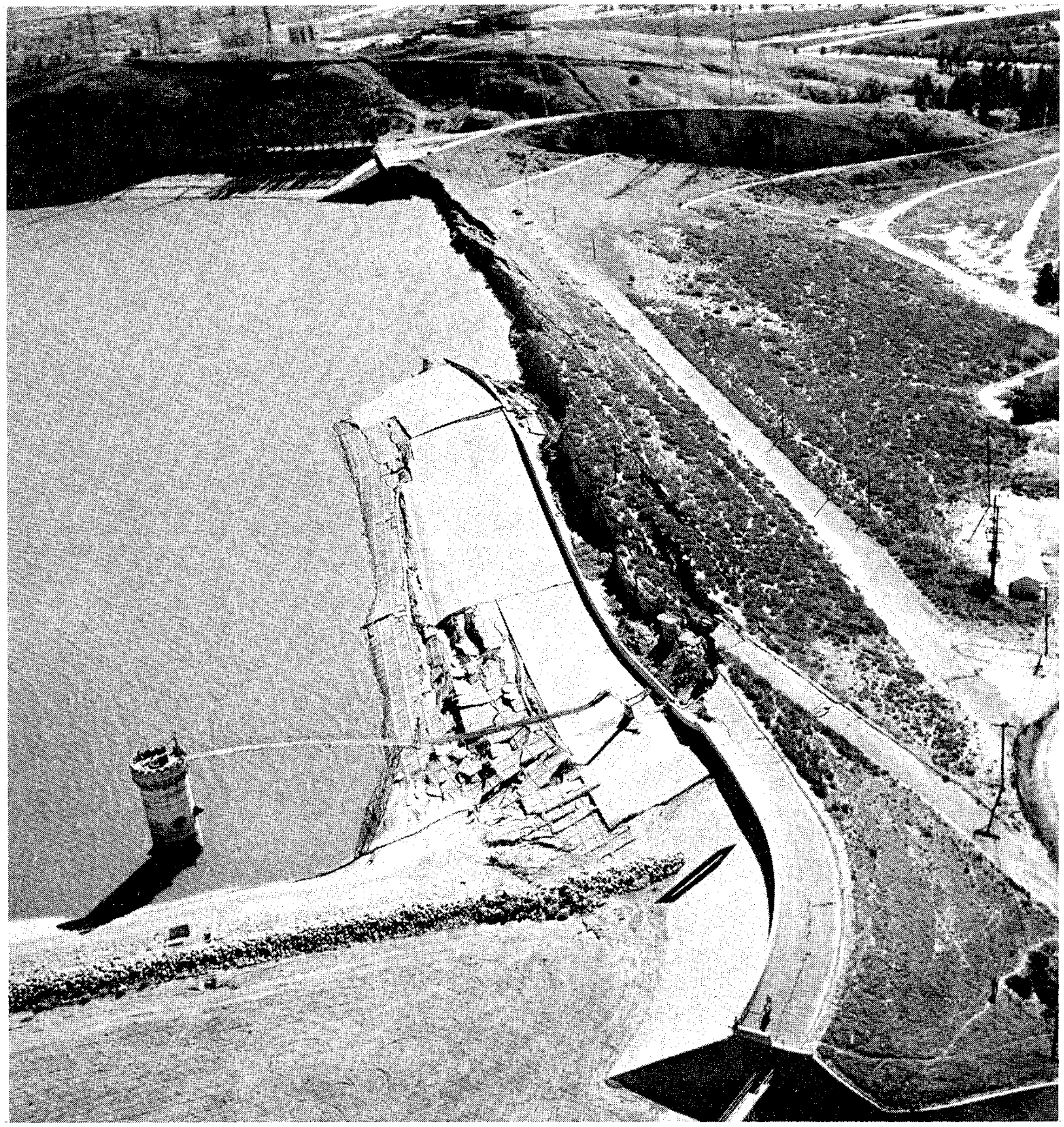

Fig. 27 Lower San Fernando Dam, February 21, 1973 following the February 9, 1971 earthquake

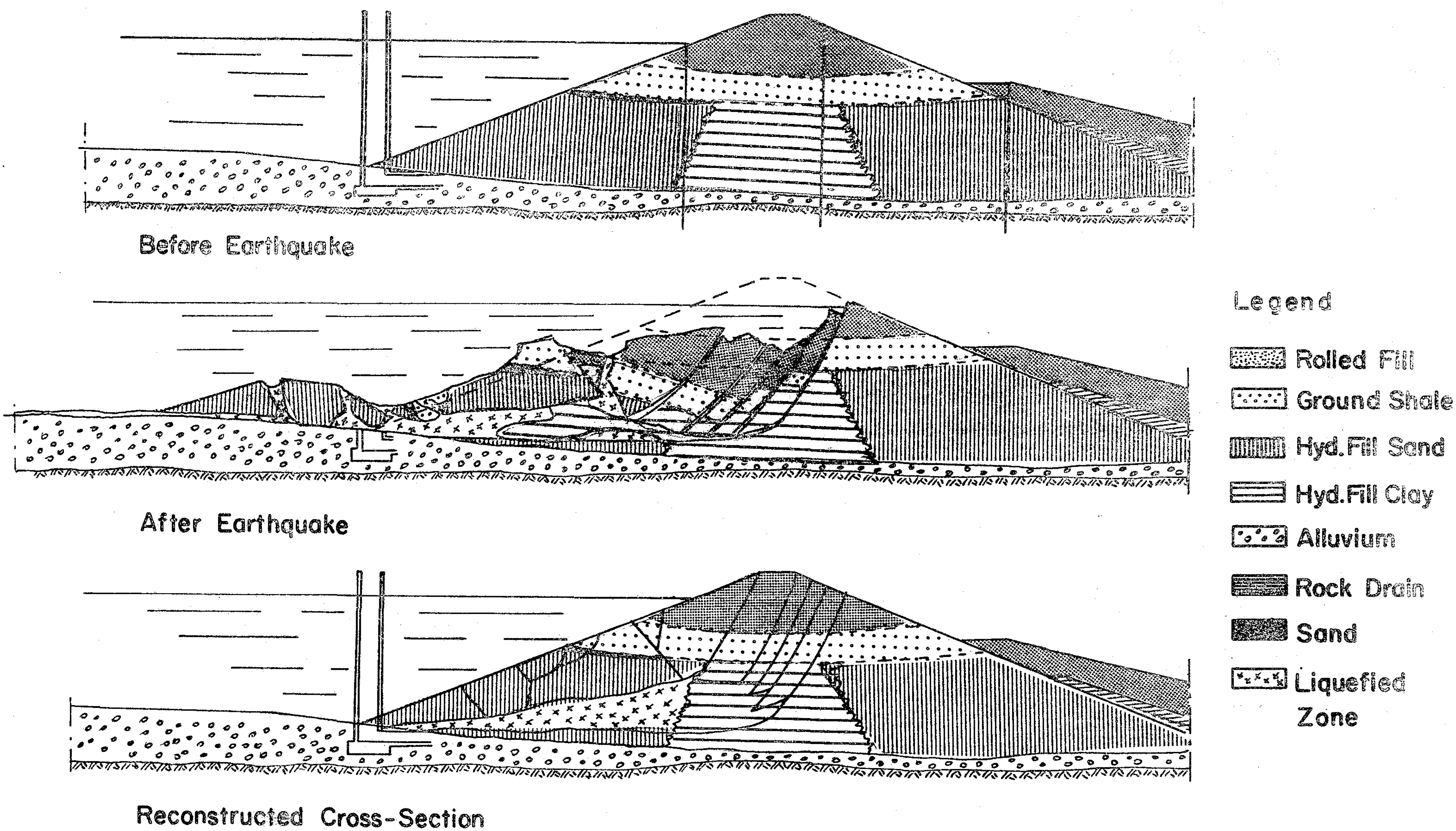

FIG. 28 CROSS SECTIONS OF LOWER SAN FERNANDO DAM BEFORE AND AFTER EARTHQUAKE, SHOWING FAILURE MECHANISM.

According to the previous analysis, some of the hydraulic fill shell material on the downstream side of the dam also liquefied, but no serious movements developed, presumably because of the large downstream berm of stronger compacted material.

Two seismoscopes were located at the Lower San Fernando Dam. One instrument was located on the east abutment near the top of Fig. 27. The other was located near the center of the dam, the crest which participated in the major slide movements. It slipped below the water level, and came to rest badly tilted, but was recovered after the water level had subsided. Both instruments wrote very good records which are reproduced on Fig. 29. As mentioned previously, Scott (27) has converted the abutment record into a time history accelerogram which was used in the seismic analyses of these dams. The crest record has not yet been analyzed in this fashion. However, even without detailed analyses, the two records illustrate at least one important point related to this study. Both records show a considerable amount of strong motion, extending over a fairly long period of time. It appears that the instrument on the crest functioned about as long as that on the abutment, during which time several major excursions were recorded by each. These observations indicate that the dam remained intact throughout the strong earthquake motions and it was only after the major shaking had subsided that the large permanent sliding deformations occurred to put the crest instrument out of service.

This conclusion is also corroborated by testimony of the caretaker who came to the crest of the dam within about 5 minutes following the shaking. He observed no significant wave action, which would indicate that the failed portion of the dam must have slipped slowly and steadily into the water over a period of time much longer than the 10 to 15 seconds of strong shaking.

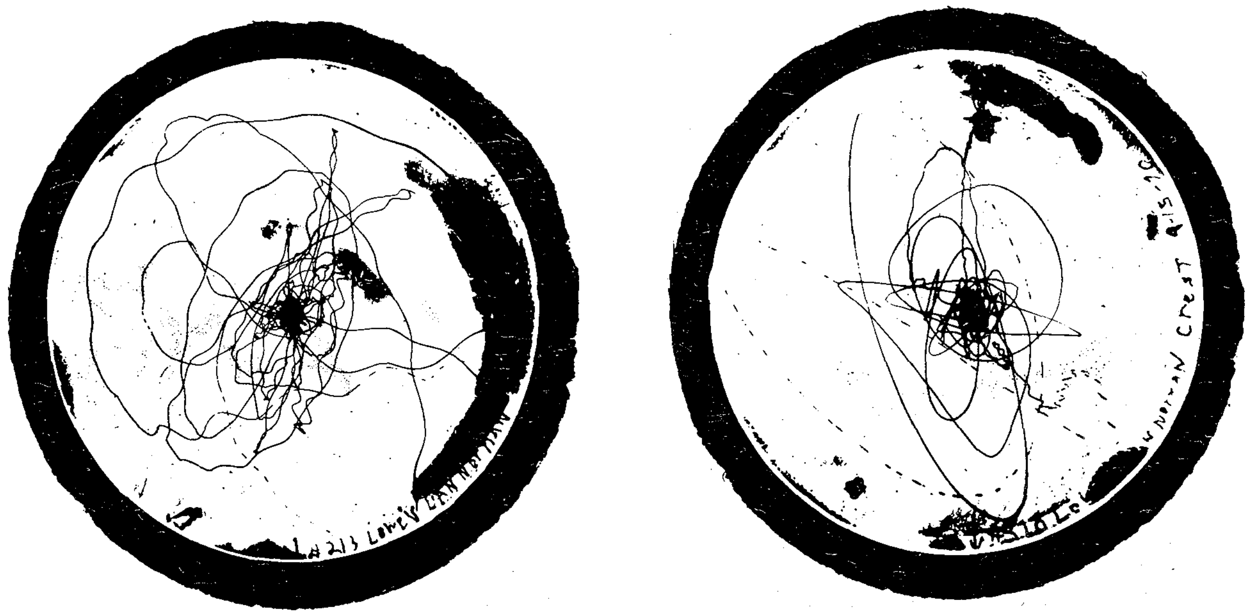

Abutment

Crest

Fig. 29 Seismoscope records obtained at the Lower San Fernando Dam

It will be recalled that the formulation of the permanent deformation analyses method used herein is in good agreement with this observed behavior. The effect of the seismic disturbance is to weaken the soil, and the resulting permanent deformations are due to the steady gravity and water load forces acting on the weakened structure.

Unfortunately, as mentioned previously, the finite element method used cannot accurately accommodate a structure after it has broken up or undergone excessively large strains. Therefore, it cannot be expected that the calculated deformations for this dam would agree well with the final surveyed locations of the many broken pieces of the actual dam following the slide. However, if it is to be useful the method should predict large enough intact deformations for this dam that a designer would be concerned that it might break up.

The finite element grid used for these analyses is shown on Fig. 30, along with a sketch showing the various material zones. The properties of the different materials used on the analyses of this dam are described in Appendix I.

The first calculations were made using the Scott record converted from the seismoscope with a maximum acceleration of 0.56g. The calculated permanent deformations at the crest were 5 feet vertical settlement and 2 feet horizontal movement upstream. This amount of movement in a 130 foot high embankment occurring immediately following the earthquake would probably have been sufficient to signal a warning of possible cracking in the shell which would lead to escape of some internal liquefied soil and subsequent further deformations.

As discussed for the Upper dam, it was felt that the earthquake accelerations and corresponding seismic stresses could have been 20 percent

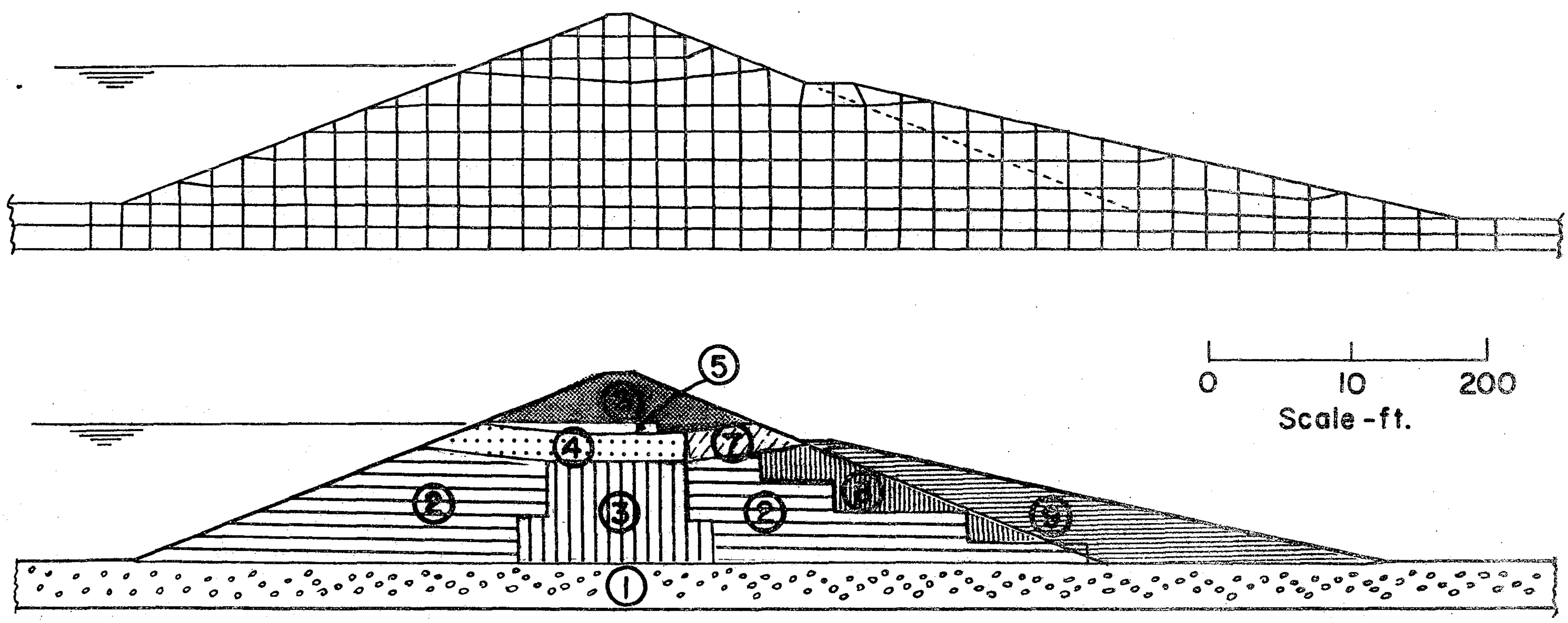

Zone	Below WT	Above WT
Alluvium Foundation	1	—
Silty Sand Hyd. Fill Shell	2	8
Clay Hyd. Fill Core	3	—
Ground Shale	4	7
Compacted Cap	5	6
Compacted Berm	—	9

FIG. 30 FINITE ELEMENT SIMULATION OF LOWER SAN FERNANDO DAM.

larger than those corresponding to $a_{max} = 0.56g$. For this reason, a second permanent deformation analysis was made using seismic shear stresses 20 percent larger. In this case, the calculated permanent deformation of the crest amounted to 12 feet vertical settlement and 5 feet horizontal movement upstream. This amount of calculated crest movement would have almost certainly signaled potential trouble had the results been available prior to the earthquake.

A summary of the calculated permanent movements for the crest as described above and for two other typical nodal points is shown on Fig. 31. The permanent calculated deformations at all nodal points are shown on Fig. 32 in relation to their pre-earthquake positions. The same scale is used for the movements as for the basic drawing. It is noted that the sense of the movements is the same as the actual displacements which were observed; horizontal upstream, settlement at the crest and bulging on the upstream face with virtually no movement in the downstream portion of the dam. The magnitude of the calculated movements are somewhat less than actually observed, but this is to be expected since the finite element program cannot handle cases where the soil breaks up into pieces, flows, or slides along thin shear zones. Nevertheless, the magnitude of the calculated movements (12 feet on the surface and 20 feet in the interior) are large enough to signal the probability that some break up and further sliding may take place.

Hebgen Dam

The Hebgen dam was damaged during the August 17, 1959 Montana earthquake. The general effects of this earthquake and the behavior of this dam in particular have been described by several investigators, but a

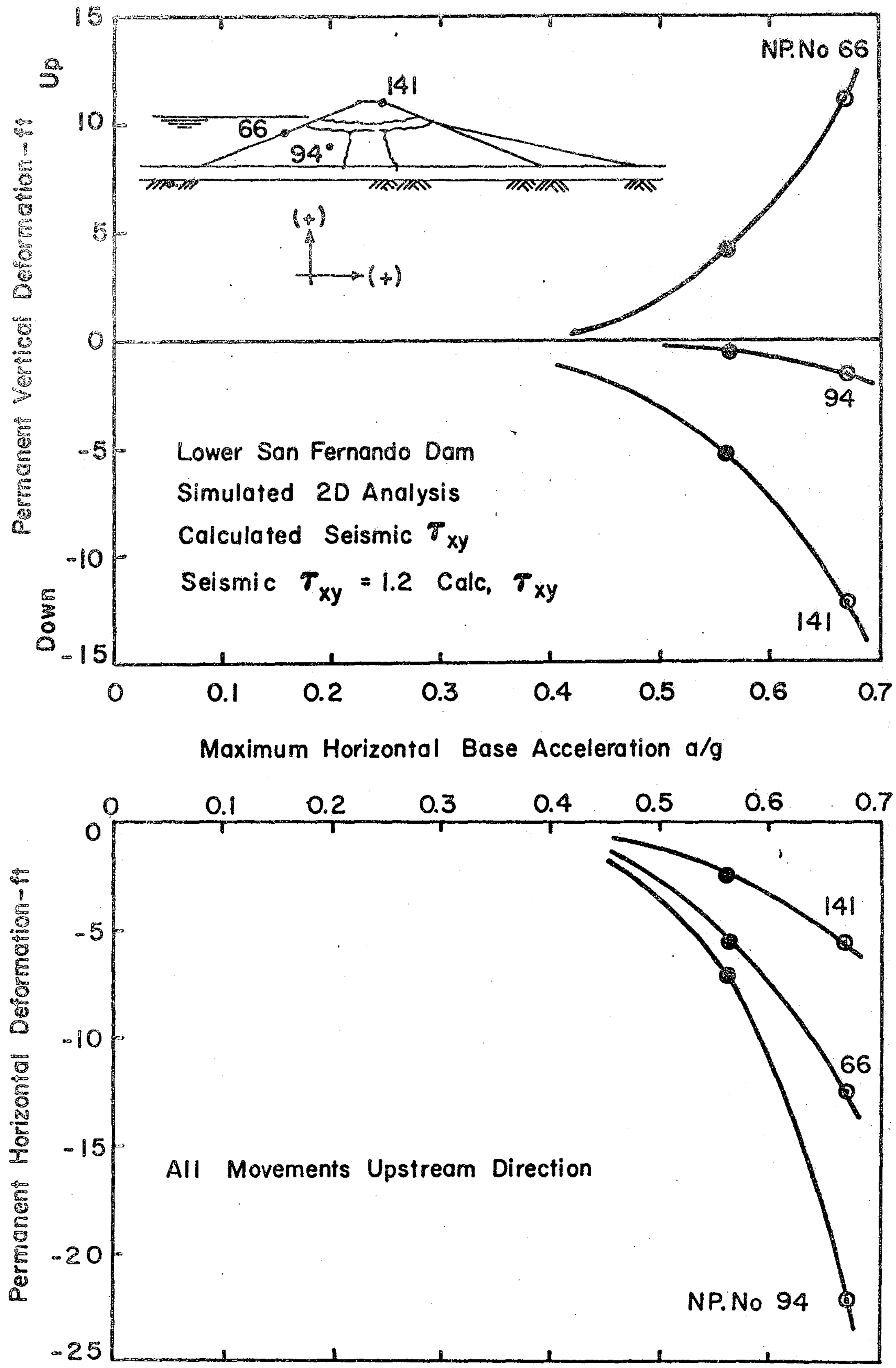

FIG.31 EFFECT OF BASE ACCELERATION ON PERMANENT HORIZONTAL DEFORMATIONS.

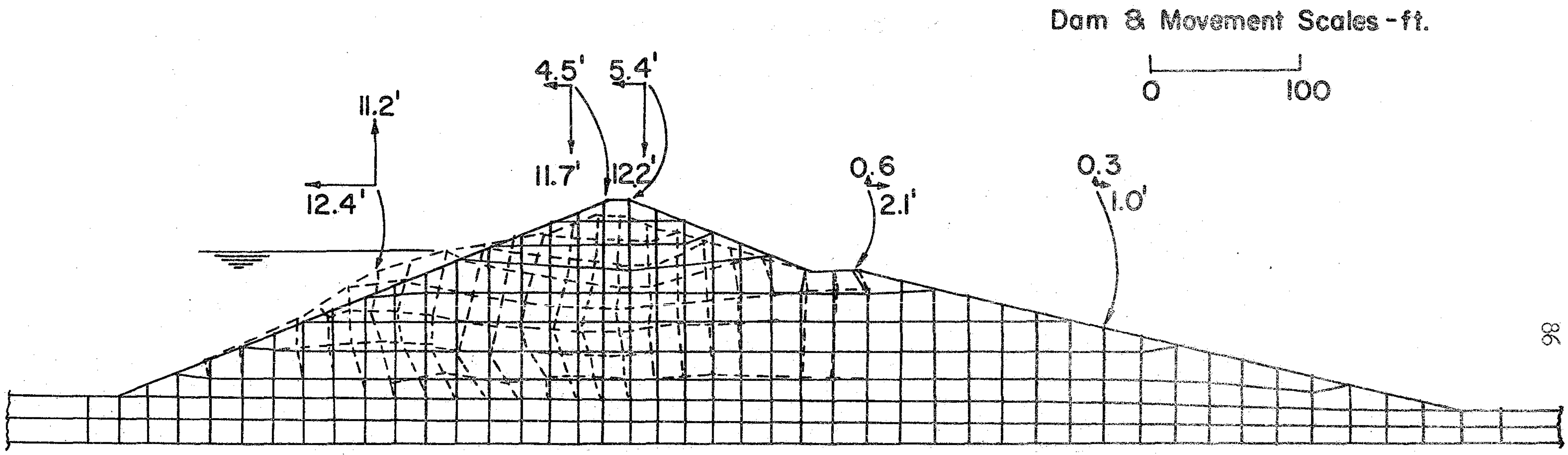

Simulated 2D. Horiz. a_{max}=0.67 g

FIG. 32 PERMANENT DEFORMATION PATTERN LOWER SAN FERNANDO DAM.

detailed seismic analysis of the dam has never been made.

The earthquake was located in a mountainous area of South Western Montana near Yellowstone National Park. Early reports give the magnitude of the earthquake as 7.1, but later reports (37, 39) give values of 7.5 to 7.8. Severe shaking occurred in the epicentral area for which maximum MM intensities of VII to X were assigned. The earthquake was accompanied by extensive and major vertical faulting. One 6 foot vertical fault scarp passed within less than 1000 feet of the east abutment of the dam. There was considerable regional and local tectonic movement in the area. Surveys indicated that the entire dam dropped about 10 feet. The bedrock in the area was quite severly warped. The north shore of the reservoir went down about 19 feet while the south shore rose about 9 feet.

The earthquake caused numerous landslides in the reservoir and mountainous areas. The most spectacular was a 3 million cu. yd. rock slide which completely blocked the Madison River about 7 miles below the dam. The slide debris formed a 200 ft. natural dam, which after some subsequent reshaping by construction equipment, still remains as a dam across the river.

In addition to the landslides and faulting, a Seich was set up in the Hebgen Lake reservoir. This Seich sent a flow of water over the Hebgen dam 4 times at about 10 to 15 minute intervals. The first and maximum wave was about 4 feet above the crest of the dam. Several strong motion instruments recorded the main shock of the earthquake, but none of them were located in the epicentral area where the dam and other areas of major damage were located. The closest instrument was located at Bozeman, Montana, some 59 miles from the epicenter, and it recorded a maximum horizontal acceleration of only 0.068g. Maximum recorded accelerations for this and other more distant stations are presented on Fig. 7, along with the limits for thismagnitude earthquake suggested by Schnabel and Seed (23). These limit lines appear to bracket the observed data rather well, and suggest that at the dam site, some 12 miles epicentral distance, the maximum horizontal acceleration was probably in the range of 0.3 to 0.5 g. The seismic response analyses which were made of this dam for the study reported herein used the Taft 1952 earthquake strong motion records scaled to give a maximum horizontal acceleration of 0.4g.

The Hebgen dam is an old earth and rockfill structure with a central concrete core wall, built in the period 1909 to 1914. The dam rises to a maximum height of about 80 feet above the natural soil foundation. A photograph and several cross section sketches of the dam are shown in Figs. 33 and 34. The dam embankment was constructed on a gravelly soil foundation of variable thickness, but the concrete core wall extends through this foundation soil and is keyed into the bedrock all across the length of the dam.

The concrete core wall was apparently quite effective in stopping. Water level measurements made over the years in open stand pipe type piezometers within the fill indicated that the water level in the fill downstream was about at the elevation of the top of the loose rock fill shown in Fig. 34.

In addition to the general subsidence and regional warping due to tectonic movements, the dam was also damaged on a local basis. Although it was overtopped 4 times by waves from the Seich set up in the reservoir, the erosion caused by this overtopping was surprisingly small. Photographs show grass and vegetation still growing on this soil over the exposed core wall following the wave action. However the embankment fill settled

Sections Shown Below

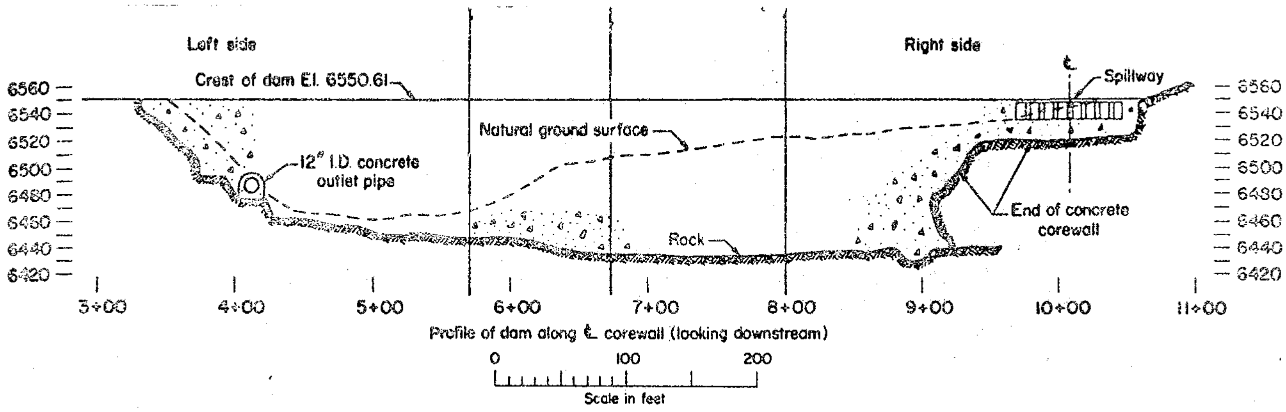

Fig. 3. Profile of Hebgen Dam.

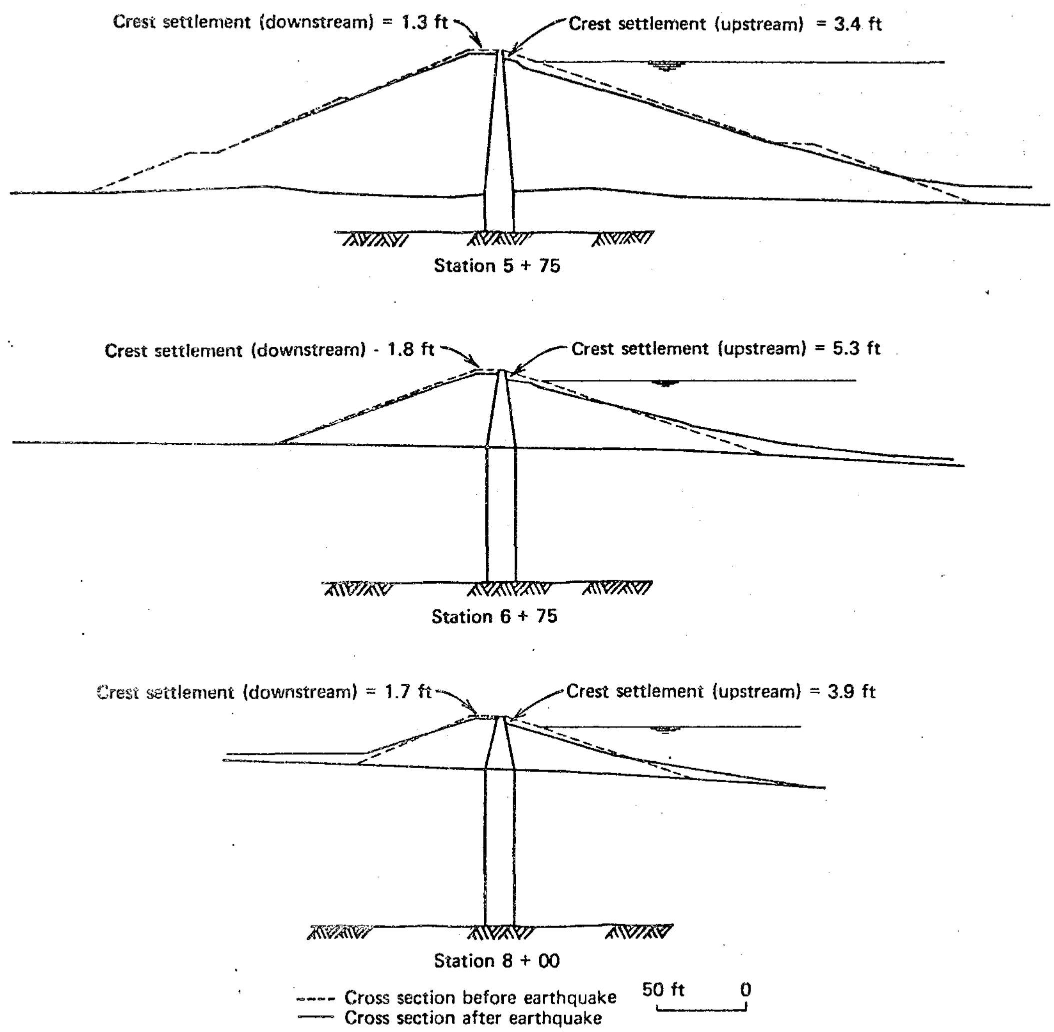

Fig. 33 - Cross Sections Through Hebgen Dam Before And After Earthquake (After Seed 1973)

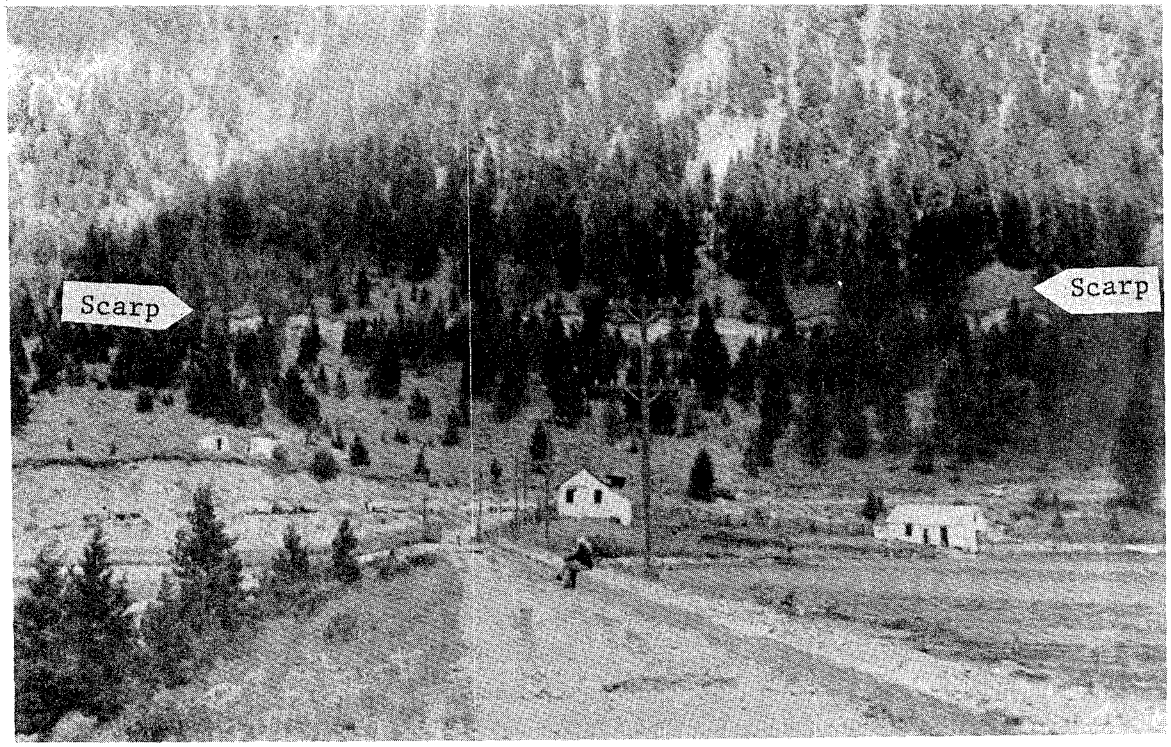

(K. V. Steinbrugge photo)

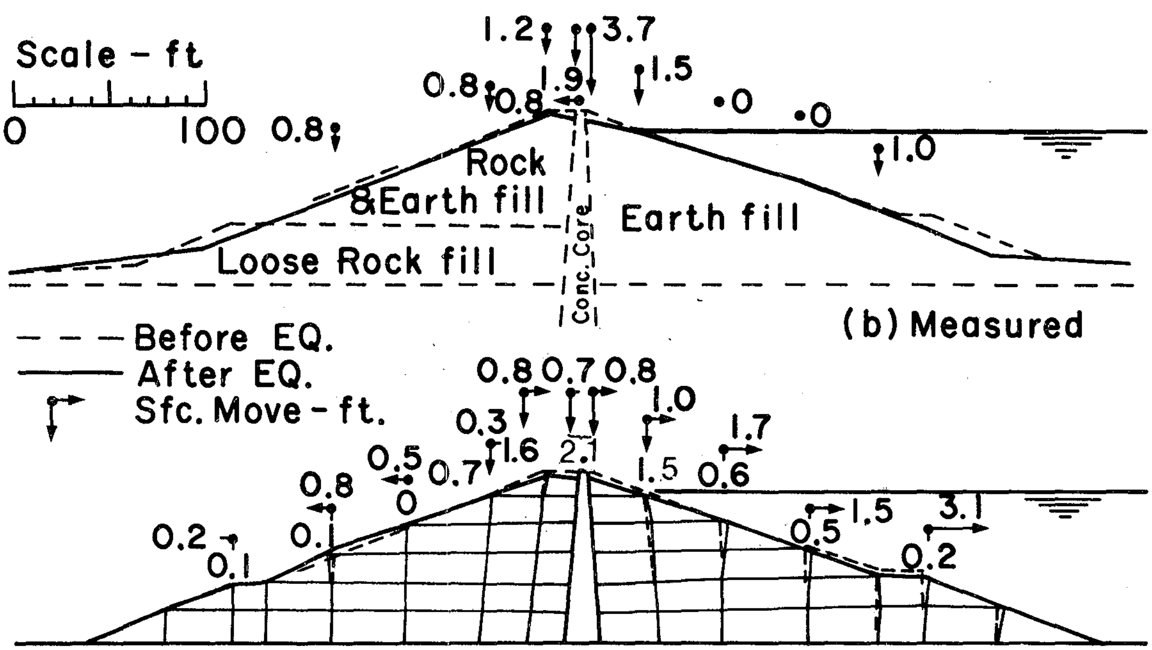

FIG. 34 PERMANENT DEFORMATIONS, HEBGEN, DAM, STA 5 + 00, 1959

significantly and some lateral bulging also occurred. The core wall was cracked in several places and moved laterally at the crest by amounts ranging from about 0 to 1 foot downstream at Sta. 4 + 00 to 7 + 50, and upstream by about 0 to 2 feet at Sta. 7 + 50 to Sta. 9 + 00. As indicated in Fig. 33., the vertical settlement at the crest by the core wall was greater (by 2 to 3 times) upstream as compared to downstream of the core wall. Seed (37) attributes most of the downstream settlement to compaction of the embankment fill whereas he attributes the greater upstream settlement to a combination of compaction and lateral spreading. The amount of vertical settlement ranges up to about 6 percent on the downstream side and up to 8 percent on the upstream side. Compared with the magnitudes of compaction due to seismic loading reported by Lee and Albaisa (35), and by Silver and Seed (36) (generally much less than 0.5 percent) it seems to this writer that movements on both sides of the core wall are probably due more to shear deformations than to compaction.

An interesting observation is reported by Steinbrugge and Cloud (38) in connection with the observed subsidence of the fill next to the concrete core wall. On page 216 of their report they state "Mr. George Hungerford, who had observed the event, replied to the authors inquiry (about the subsidence) by stating, 'When I first arrived at the dam there was very little if any settlement of the earthfill on either side of the core wall, although there was a separation of the earthfill and the spillway'. The U.S. Forest Service report, 'Hebgen Lake, Madison River, Earthquake Diaster', which was prepared shortly after the event, concludes that the earth settling at the dam occurred more than ½ hour after the principal shock". However Steinbrugge and Cloud also report that, "strong contrary opinion holds that the earth settlement occurred simultaneously, or nearly so, with the principal earthquake." To this writer, a delayed settlement appears to be logical and consistent. If the settlement were associated with build up of excess pore pressures, especially in the upstream portion, it would take a finite amount of time for these to dissipate, and during this period of pore pressure stabilization, volume change and shear deformations could be expected.

Little is known about the soils in the foundation or the embankment fill other than the simple descriptions given in Fig. 34: ie. earthfill upstream; loose rock fill, and earth and rock fill downstream. It was presumed that because of the era in which the dam was built the soil in the embankment was probably not compacted to a particular dense state. Furthermore to avoid having to estimate soil properties for the foundation, the section with the least foundation soil was used for analysis, Sta. 5 + 00, and the small thickness of foundation soil at this section was neglected in that the properties were assumed to be the same as assumed for the overlying embankment soil.

Because the concrete core was fairly thin, and not particularly bonded to the soil, it was treated as if it were a soil in the finite element stress analyses. If it had been treated as concrete, the stiffnesses of the concrete elements would have been significantly greater than the adjacent soil elements. Unless appropriate boundary elements had been placed between the soil and the concrete, the soil would have hung upon the core.

Some calculations were attempted with boundary elements in the form of very short bars, but even with double precision on the IBM 360-91 computer (15 significant figures) the results of the gravity stresses did not appear to be correct. Ghabaussi, Wilson and Isenberg (34) have pointed out problems of this nature can be expected from using this type of a boundary element, and have suggested another formulation to overcome these numerical difficulties. However, for the studies performed herein, the concrete was treated as soil throughout the analysis. Then finally, when reporting the end results, nodal points in the concrete elements were assumed to have suffered zero vertical displacement.

A sketch of the Hebgen dam showing the three major soil zones assumed for the analysis is presented in Fig. 35, along with an outline of the finite element grid that was used. The properties of the soils in the different zones are summarized in Table I-11. These properties were estimated from the trends presented in Appendix I, after first estimating appropriate values for relative density for the different soils. The rockfill was assigned a higher relative density than the earthfill. No laboratory test data was available for rockfill material, but it was felt that for equivalent method of placement rockfill material would probably be somewhat stronger and stiffer and resistant to seismic deformations than earthfill.

The results of the permanent deformation calculations are shown in Fig. 34, where they may be readily compared with the observed deformations. Compared to the scale of the dam, the deformations drawn to scale appear small, which of course they were. At this section the observed crest settlements were 3.7 ft. on the upstream side of the concrete core wall and 1.9 ft. on the downstream side. The corresponding calculated vertical movements at these two locations were each 2.1 ft. Movements at other locations along the faces of the dam are shown in Fig. 34. In all cases the agreement is remarkably good. If the analysis had included a provision for some volume change due to cyclic loading, the calculated vertical settlements might have been slightly greater, but probably still close to the observed movements.

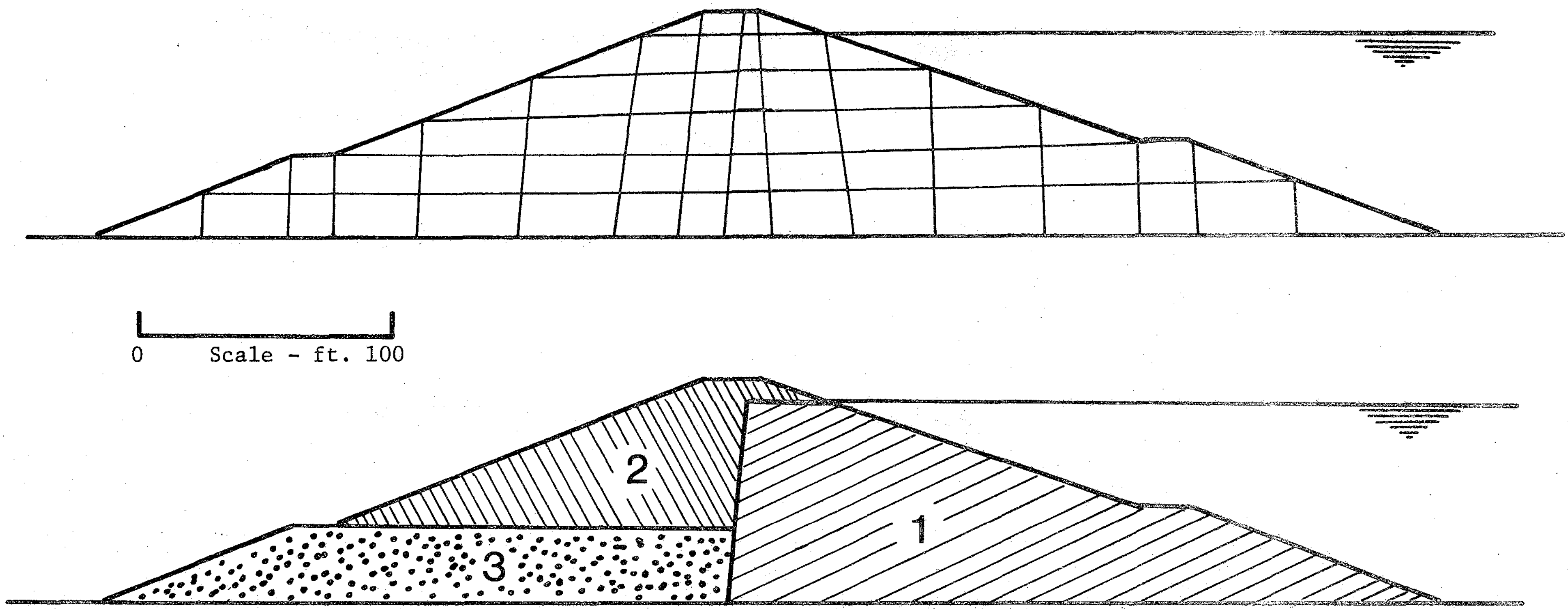

Zone
1 Earth Fill, Saturated
2 Rock and Earth Fill, above water table
3 Loose Rockfill, assumed saturated

Fig. 35 Finite Element Simulation of Hebgen Dam, Sta. 5+00

At this section, Sta. 5 + 00, the crest was observed to move downstream about 1.9 ft. whereas the calculated horizontal movement was about 0.7 ft. upstream. This is the only case studied where the direction of the calculated horizontal movement did not agree with the observation. Recalling that the concrete core was neglected in the analysis, and that the analysis was plane strain whereas the actual structure could have been affected by some lateral forces, this single slight discrepancy does not seem to be significant. Calculated horizontal movements at other points along the face of the dam appear consistent with the observed profile measured after the earthquake.

Summary Comment on Results, Assumptions and Limitations

Currently used methods of seismic stability analysis of earth embankments and slopes are based on equilibrium considerations. The shear stresses induced during the earthquake are compared to the soil strength under cyclic load conditions to obtain a factor of safety. The cyclic loading strength of the soil is obtained from the pulsating stress which produces a certain preselected amount of strain in a laboratory test specimen. Unfortunately, there is no simple relation between strain in an isolated laboratory sample and deformation of an element of soil surrounded by and connected to other elements of soil which have different seismic response characteristics. Thus, although the equilibrium methods of analyses can indicate which zones of the embankment become overstressed from the effect of the earthquake, they cannot lead to more than a qualitative guess at the nature or magnitude of the permanent deformations which may result therefrom.

The study presented herein was conceived as a step toward filling this gap by developing an approach for calculating the permanent deformations which may result in an earth embankment or slope subjected to a seismic disturbance.

The method described herein is intended only as a suggested first step towards the solution of this very difficult and complicated problem. The overall objective in this stage of the development was to obtain a realistic and workable method which was sophisticated enough to take into account the apparent most important factors related to the problem, usefully accurate and yet simple enough that it could be used in solving practical problems with todays' technology and limitations.

To meet these objectives simultaneously, it was necessary to make many simplifying assumptions, and to use theories and techniques which may very likely be superseded in the future. To illustrate the method and its ability to calculate permanent deformations resulting from earthquakes, five case histories were studied where in-service earth dams had been subjected to strong seismic shaking and had suffered various amounts of permanent deformation including settlement, significant cracking and complete failure. The overall results of these five case studies are summarized in Table 8 along with the observed movements and a few explanatory comments. Reference to the data in Table 8, and to the complete data presented in the foregoing pages, leads to the following general observations concerning the ability of the suggested method to predict permanent deformations.

1. The method correctly predicted the direction of movement. The only exception was the very small horizontal deformation at the crest of the core wall of the Hebgen dam which at the section studied was predicted to move slightly downstream but measured to move slightly upstream. Predicted movements at other points on this dam were in good agreement with observed movements. It is especially noted that the method correctly predicted that the crest of the Upper

TABLE 8

SUMMARY OF PERMANENT DEFORMATION OBSERVATIONS AND CALCULATIONS

Dam	Type	Height ft.	Earthquake	Mag.	Horiz. a_{max} (g)	Crest Deformation - ft. Observed (Calculated)		Remarks	Ref.
						Vertical	Horizontal		
Dry Canyon	Hydraulic fill and rolled silty sand	63	Taft 1952	7.7	0.075	0.3 D (0.8 D)	0.3 US (0.15 US)	2 inch crack. a_{max} is lower limit of range	7
Sheffield	Loose silty sand	25	Santa Barbara 1925	6.3	0.15	Failed (8.7 D)	Failed (1.9 US)	Dam failed and reservoir emptied. Assumed lower 12 ft saturated.	20
Upper San Fernando	Hydraulic fill silty sand	65	San Fernando 1971	6.6	0.6	3.0 D (1.0 D)	5.0 DS (0.4 DS)	Major crack on US slope. Pressure ridge DS toe. a_{max} from Ref. 22.	22
					0.7	(1.7 D)	(1.1 DS)	Seismic stresses 20% greater than for a_{max} = 0.6	
Lower San Fernando	Hydraulic fill silty sand	130	San Fernando 1971	6.6	0.56	40 D (5 D)	20 US (2.5 US)	Major slide upstream. a_{max} from Ref. 22.	22
					0.67	(12 D)	(5.5 US)	Seismic stresses 20% greater than for a_{max} = 0.56	
Hebgen Sta. 5+00	Loose soil and rock fill	87	Montana 1971	7.6	0.4	2.8 D (2.1 D)	0.8 DS (0.7 US)	Crest settled by core wall. a_{max} middle of range.	23, 24, 25

D = vertically down
DS = horizontally downstream
US = horizontally upstream

San Fernando Dam moved downstream and that the crest of the Lower San Fernando Dam moved upstream.

2. The method overpredicted the movements at the Dry Canyon Dam which were very small, and caused minor damage compared with the other dams studied. Although no field measurements were possible at the Sheffield Dam, which failed, it would appear that the method correctly predicted the magnitude of those movements. At the two San Fernando Dams the method underpredicted the observed movements, but it is noted that much larger movements were predicted for the Lower Dam than for the Upper Dam which is in agreement with the observation. Movements at these two dams involved extensive breaking up and sliding along thin shear zones, which is beyond the capacity of the method to handle. Movements at the Hebgen dam, which involved mostly crest settlement and lateral bulging along the slopes, were correctly predicted.

3. The method requires an integral structure, and cannot handle field problems involving break-up into pieces and subsequent large flow or shearing movements. Some of the discrepancies noted above involved this type of field movements. However, in these cases, the method did predict movements which were large enough to suggest that shearing or break-up might logically develop as a result.

4. The parametric studies conducted in connection with some of the cases demonstrated that reasonable variations in the assumed basic input data could lead to significant changes in the computed results to narrow the gap between observed and computed movements. This is especially significant for the assumed input notion, where reasonable variations in assumed maximum acceleration for a single earth-

quake can lead to comparatively very large variations in calculated movements.

Because of the dependency of the method on the basic assumptions, it is appropriate at this point to comment somewhat on the important assumptions and limitations in this suggested method. The basic assumptions may be classified in two major categories; analytical approach and input data. Some assumptions in the analytical approach include:

(i) Pre-earthquake stresses.

(ii) Solution of load stiffness equations by double gravity-turn-on method.

(iii) Shear stress distribution on horizontal planes.

(iv) 2-D vs. 1-D Seismic response calculations.

Some assumptions in the input data include:

(v) Input base accelerations.

(vi) Soil properties - computer storage of lab test data.

(vii) Soil properties - stiff and partially saturated soils.

The effects of these assumptions are discussed below.

(i) Pre-earthquake Stresses - The pre-earthquake stresses at various locations within the embankment were determined by a finite element procedure which included dead weight plus steady state seepage forces. For these studies a linear elastic gravity-turn-on program was used although it was recognized that non-linear incremental programs are available. Conceptually, a non-linear incremental method would seem to be better, but as first pointed out by Clough and Woodward (25) and as shown by one example presented on Fig. 15 herein, the calculated distribution of internal stresses does not appear to be greatly dependent on whether a linear or a non-linear method was used for the calculations. For hydraulic fill structures, which included three of the five dams studied, there is some question as to whether the incremental loading used in the non-linear method is a significantly more realistic approximation to the actual construction stress paths than the simple gravity-turn-on. It is unlikely that in the field, each layer of soil was completely consolidated before the next layer was placed. Judging by the example on Fig. 15 and by other similar studies, it was felt that while some refinement is warranted in calculations of pre-earthquake stresses, these improvements are not likely to have a major effect on the accuracy of the calculated post-earthquake permanent deformations.

(ii) Solution of Load-Stiffness Equations by Double Gravity-Turn-On Method

The suggested method for calculating earthquake induced deformations assumes that the deformations can be treated as though they followed immediately after the earthquake, as a result of a softening in the material due to the effect of seismic shaking. After the soil has thus been softened by the earthquake, the movements are assumed to be caused by readjustment to equilibrium under static gravity loading. For the case of loose saturated materials such as found in hydraulic fill dams, the actual behavior may be very close to this ideal simulation. For example, the seismoscope records at the Lower San Fernando dam indicate that the major movements there took place after the major shaking had subsided. Similarily, an eye witness account at the Hebgen dam stated that the movements took place more than one-half hour after the earthquake. For well-compacted dams, this analogy may not be quite so appropriate and the major movements may take place simultaneous with the strong shaking. However, the theory used in converting laboratory test data to field predictions assumes no difference whether the movements occur during or immediately after the shaking. More data and comparisons are required for the behavior of well compacted dams during earthquakes to see how well the theory and field experience agrees.

In the writer's opinion a far more significant aspect is the fact that in its present form the finite element program used to compute the post-earthquake deformations makes use of small strain theory with a smooth distribution of strains across each element, and continuity of deformations from one element to the next. In other words, the program can not handle excessively large deformations, or any type of break-up or local failure and concentration of movement along some previously undefined zone of sliding.

Some improvements could be made. The small strain limitation could be greatly relaxed by making progressive deformation calculations at the end of successive time intervals during the strong shaking. The nodal point positions could then be adjusted along with a change in material properties to be compatible with the permanent deformations which developed up to the end of that time step, and this process repeated until the end of shaking. This would still not allow for a break-up or shearing action as observed in the field with some of the dams. The writer feels that this refinement to a step by step analysis would not significantly improve the accuracy unless it was reasonably certain that the dam would not crack or shear significantly.

A method of analysis which can first predict the time of formation and location of a crack or shear zone, and then follow the shearing sliding or flowing type of deformations after the cracks have formed would appear to be well into the future, requiring major advances both with regard to knowledge of material properties as well as new developments in analytical formulations.

(iii) Shear Stress Distribution on Horizontal Planes - Like the finite element equilibrium method from which this displacement method was derived, the significant effect of the earthquake is assumed to be in causing cyclic shear stress on horizontal planes. Other components of the cyclic stress are ignored, and the soil deformation properties are based on laboratory tests which attempt to simulate only this cyclic stress effect. More work is required both analytically and experimentally to investigate the validity of the assumptions inherent in this method. For example, it is not yet completely established that for embankments the horizontal component of shear stress is the most significant, and little work has been done to date to investigate the significance of other components.

(iv) <u>2-D Versus 1-D Seismic Response Calculations</u> - Most previous seismic stability analyses have used the results of a 1-D (horizontal base acceleration) response analysis to calculate the distribution of seismic shear stresses. This study also mainly used the 1-D method especially for the first calculations. The results of one comparative study using both 1-D and 2-D acceleration input indicated that the 2-D method computed shear stresses about 13 percent greater than the 1-D method. On this basis the seismic stresses for the early 1-D calculations were increased by 13 percent for use in the permanent deformation analyses. More work is required to determine the effect of the vertical component of acceleration on the seismic shear stresses and permanent deformations.

(v) <u>Input Base Accelerations</u> - Mention has already been made of the use of 2-D versus 1-D input base accelerations. Little attention has been given thus far to the nature of the vertical component of the accelerations. Serious use of the vertical component must also imply serious considerations of the basic data to be assured that it is as realistic as the horizontal component.

Data presented by Housner (28) Duke, et al. (22) or Seed and his colleagues (29) of maximum recorded acceleration versus distance invariably show a wide scatter. Even data for rock accelerations, for the same earthquake show the same scatter. Thus, a selection of a base motion for purposes of analysis must recognize a considerable amount of uncertainty as reflected by the wide scatter in the recorded accelerations from strong earthquakes. This was partially taken into account in the foregoing analysis, which showed that beyond a certain value of acceleration, the calculated permanent deformation appeared to be quite sensitive to increases in base acceleration. By taking base acceleration values within the range of scatter of the recorded data, it was shown that permanent deformations could be calculated which was reasonably close to the observed movements (large flow and shear movements excluded).

Reliable knowledge of the input earthquake motion appears to be the single most important factor in any seismic stability analysis. The seismic stresses and the resulting permanent deformations are significantly sensitive to the input motion, even within the range of scatter of the recorded data for a particular case. Furthermore, to this writer, it does not seem likely that future recorded data will soon narrow the range of uncertainty in the expected maximum base accelerations for a particular site. Therefore, it is suggested that for design purposes of important structures such as earth dams in populated areas, the upper limit of possible ground accelerations must be used to define the input motion.

(vi) Soil Properties - Computer Storage of Lab Test Data - To store the soil test data in the computer for calculating the soil properties corresponding to the stresses at each element, it was necessary to make some simplifying assumptions as to the variation with stress conditions. Plotting the data to double log scales lead to approximate straight lines in many cases, which were easy to describe analytically. Unfortunately, small variations in the position of data points on a log-log plot may lead to a large numerical variation when the best fit line is extrapolated to a new condition beyond the data. Further work would appear to be in order in checking and improving the method of formulating the lab data for storage in the computer.

(vii) Soil Properties - Stiff and Partially Saturated Soils - The laboratory test data used for these analyses was taken from previous studies of the same dams. The previous studies had concentrated on evaluating the known weaker soils to see if they could have liquefied or developed large strain potentials due to the particular earthquake. The results of some tests on the clay core for the Upper San Fernando Dam became available toward the end of these studies, but no test data for other clays has been obtained. Furthermore, there is no test data for the stiff compacted soils of the type used in the more recently placed zones of the dams studied, and there was no data from any tests on any partially saturated soils above the water table. Data for these soils required in the computer analyses were obtained by extrapolations from the known test data as described in Appendix I.

This is a rather weak point in the analyses. The elements must remain continuous. Therefore, a strong outer shell of elements can severly limit the calculated deformations of the dam, even though the internal elements are composed of liquefied soil. Considerable more work is required to develop appropriate testing methods and obtain representative data for the seismic deformation behavior of partially saturated and other relatively stiff soils which make up a significant part of a typical earth dam.

Conclusions

A method has been suggested for calculating the permanent deformations induced in an earth dam embankment, embankment or cut slope due to an earthquake. The method has been used to calculate the deformations of five old earth dams which suffered various known amounts of deformations during earthquakes in the past. In all cases the direction of the calculated displacements agreed with the observed direction of the movements; vertically up or down and horizontally upstream or downstream. The calculated magnitudes of the movements were found to be sensitive to parameters for which values could not be specified exactly. At different dams these parameters included properties of strong compacted or partially saturated materials, maximum base acceleration and position of the freatic surface. However, reasonable assumptions for these parameters led to fair agreement between the calculated and the observed post-earthquake permanent deformations.

The suggested method utilizes finite element analyses which is based on small strain theory and an intact structure. At three of the dams, the embankment cracked, sheared or flowed extensively as a result of the earthquake. These types of movements beyond the point of break-up, cannot be handled by the suggested analytical method and therefore, it is not surprising that where shearing or break-up occurred, the observed final positions of particular points were larger than were calculated. However, the relative order of magnitude of the calculated movements agreed with the observed relative displacements from one dam to the next, and were large enough to suggest the possibility of cracking and break-up for the more brittle outer shell zones.

In conclusion, it must be re-emphasized that the suggested method is intended only as a step and exploration towards the final solution to the complicated problem of earthquake induced permanent deformations in earth structures. As stated above, the method is limited analytically in its present form by not being able to handle cracking, shearing or flowing movements. It is limited on a physical input basis concerning the exact base motion, especially the maximum acceleration, and by insufficient knowledge concerning the deformation behavior of stiff and brittle soils and partially saturated soil under cyclic loading as applied to the embankment problem.

Looking to the future, there are many studies which can be made to revise and improve the method. However, until such time as the input data such as knowledge of soil properties in all parts of the dam, freatic surface and base accelerations are known with considerably more precision than at present, some discrepancies must be expected between the observed and the calculated movements from case history studies. However, since only by conducting such case history studies can the reliability of any proposed analytical method be established, more such studies are encouraged.

In this regard, the five dams which were studied were all old and of inferior construction by todays' standards. Case history studies of more modern dams with stronger soil and better available input data are urgently required as a guide to extending proposed methods such as the one described herein to use in designing modern earth structures.

Acknowledgements

The writer is indebted to his many friends, students and associates for ideas and assistance gained during countless discussions on the problem of soil strength and stability of soil structures during earthquakes.

The 1-D and 2-D finite element program for seismic response analyses were kindly supplied by the Geotechnical Engineering Group, Department of Civil Engineering, University of California, Berkeley, and especially adapted for use on the UCLA IBM 360 computer by Mr. T. Udaka during the summer of 1972. The work was carried out under the auspices of grants from the National Science Foundation for studying soil behavior and soil liquefaction during earthquakes.

Grateful appreciation is expressed for this assistance.

APPENDIX I

Permanent Deformation Parameters From Cyclic Load Triaxial Tests

Illustrative Example --Dry Canyon Dam Soil. Derivation of the permanent deformation parameters from cyclic load triaxial tests is illustrated for data obtained from remolded samples of hydraulic fill from the core of the Dry Canyon Dam (16). Data pertaining to other soils are presented in summary form hereafter. A listing of the soils studied along with the general classification data and reference to the original test data is shown in Table I-1.

Figs. 3 and 4 in the main body of the text illustrate the nature of problem for which the permanent deformation soil parameters are required. Fig. 3 illustrates the recorded data from a typical triaxial test on a sample of soil, anisotropically consolidated and cyclicly loaded undrained to simulate the pre-earthquake and earthquake stress conditions at a particular element of soil within an embankment. The recorded accumulative strains (*) for each cycle are conveniently studied after replotting as shown on Fig. 4. The results of four tests are shown together in the same figure to illustrate the general effect of different cyclic stress levels.

The instrument used to record the axial deformations shown on Fig. 3 was set to record large strains, but was not sensitive to small deformations. However, it is a simple matter to set the instrument to a higher sensitivity, and thus record the small strains under low cyclic stresses. The results of a series of such tests in which both small and large strains were recorded simultaneously on two different instruments are presented on Fig. I-1 and Fig. I-2. It is noted that the general shape of the curves are similar for both small and large strains, the only difference being the scale used for plotting the data.

(*) In this study cyclic strains are defined as follows: For $K_c = 1.0$ $\mathcal{E}_1 = \frac{1}{2}$ peak to peak strain amplitude; For K_c 1.0 $\mathcal{E}_1$ = compressive strain amplitude.

Table I-1

Classification Data For Soils Studied

Soil Description	D_{50} mm	C_u	D_r	LL	PI	Ref.
Dry Canyon Dam. Hydraulic Fill silty sand. Recompacted for laboratory testing.	0.10	150	50			
Sacramento River Sand. Uniformly graded clean fine quartz sand.	0.2	1.4	38 60 78 100			
Sheffield Dam. Clayey silty sand 40 to 60% >0.02 mm. Sandy samples were non-plastic silty samples.			35 to 40	— 24	— 4	
Upper San Fernando Dam:						
<u>Alluvium</u> Gravelly and coarse to med. silty sand.	0.15 to 1.5	5 to 20				
<u>Hydraulic Fill Shell</u> Coarse to fine silty sand.	0.07 to 0.14	5 to 10				
<u>Hydraulic Fill Core</u> Silty clay.	0.007 to 0.02			40 to 52	18 to 30	
Lower San Fernando Dam:						
<u>Alluvium</u> Silty sand.	0.02 to 1.0	5 to 15		—	—	
<u>Hydraulic Fill Shell</u> Coarse to fine silty sand.	0.04 to 1.0	5 to 10		—	—	
<u>Hydraulic Fill Core</u> Silty clay (no Cyclic Load tests on clay).				40 to 70	20 to 40	

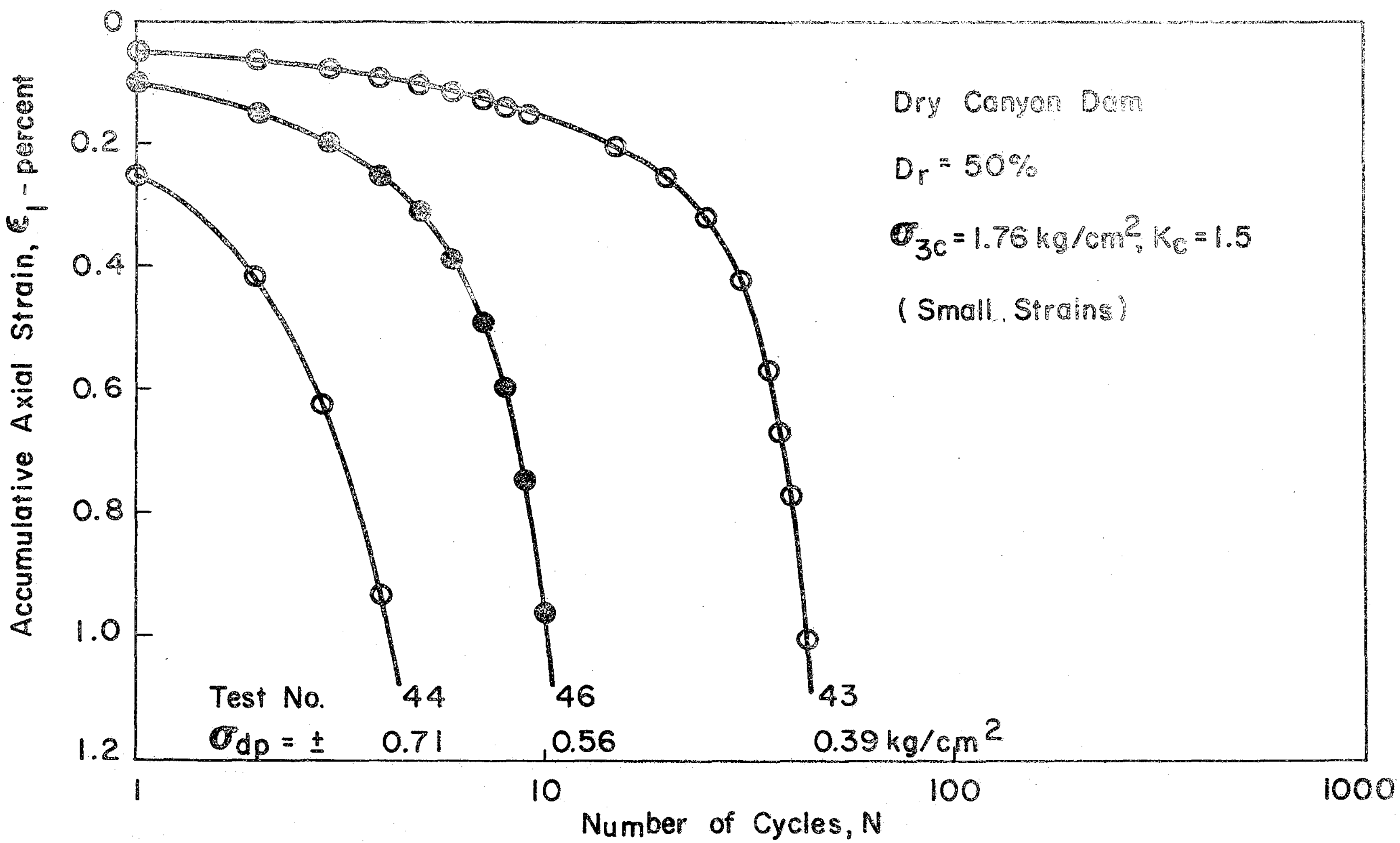

FIG. I-1. PULSATING LOADING TEST RESULTS FOR SMALL STRAINS.

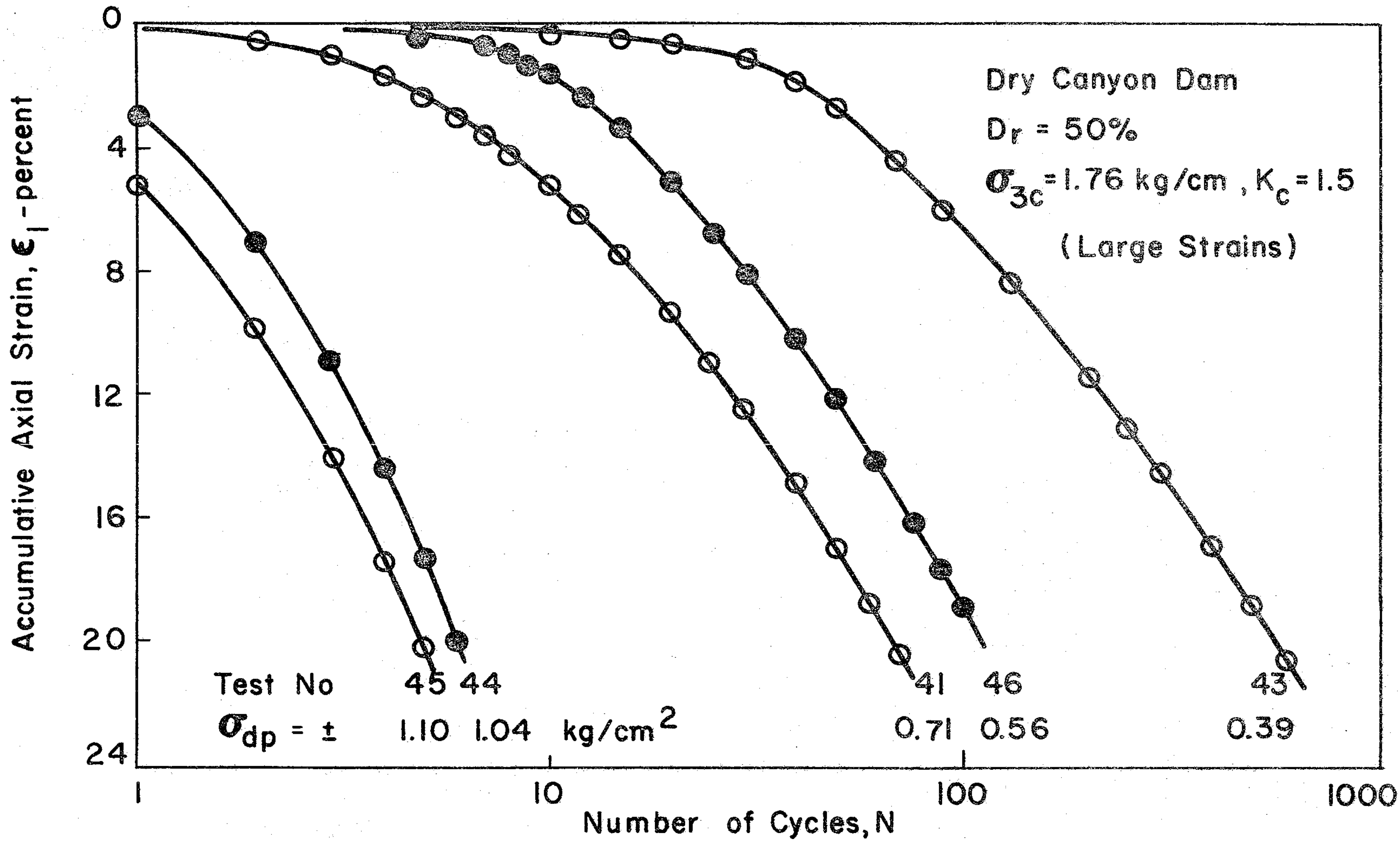

FIG. I-2. PULSATING LOADING TEST RESULTS FOR LARGE STRAIN.

From these two sets of data it is a straight forward matter to obtain a cross plot as shown on Fig. I-3 which presents the cyclic stress conditions required to produce any amount of strain. This figure is similar to Fig. 4 in the main text, and in fact was derived from the same basic data.

Although it has been found convenient to use semi-log paper to plot the data for visual presentation, because the data points do not generally form straight lines, this form of presentation is not particularly useful in formulating parameters for storage in a computer. It has been found, however, that curves such as shown on Fig. I-3 will form straight lines on log-log paper. Thus the data of Fig. I-3 is shown replotted to double log scales on Fig. I-4a.

Any one of the data lines on Fig. I-4 can be expressed by an intercept C_1 and a slope S_1 according to the following equation:

$$\sigma_{dp} = C_1 \left(\frac{N}{10}\right)^{S_1} \qquad \text{(I-1)}$$

Because most of the test data, and the eventual extrapolation to the field will be associated with N in the range about 5 - 30, it was felt appropriate to select the intercept C_1 at 10 cycles so as to minimize errors involved in extrapolating to other N values in the solution of realistic earthquake problems. The intercept C_1 has the same dimensions as σ_{dp}.

Examination of the several lines on Fig. I-4 indicate that they all have approximately the same slope S_1. This has been found to be approximately true for all other sets of data examined. In fact, as will be shown later on, the same value of S_1 appears to be approximately valid for all data pertaining to one soil at one density, and not just to a particular consolidation condition as shown on Fig. I-4. Thus the slope S_1 becomes a

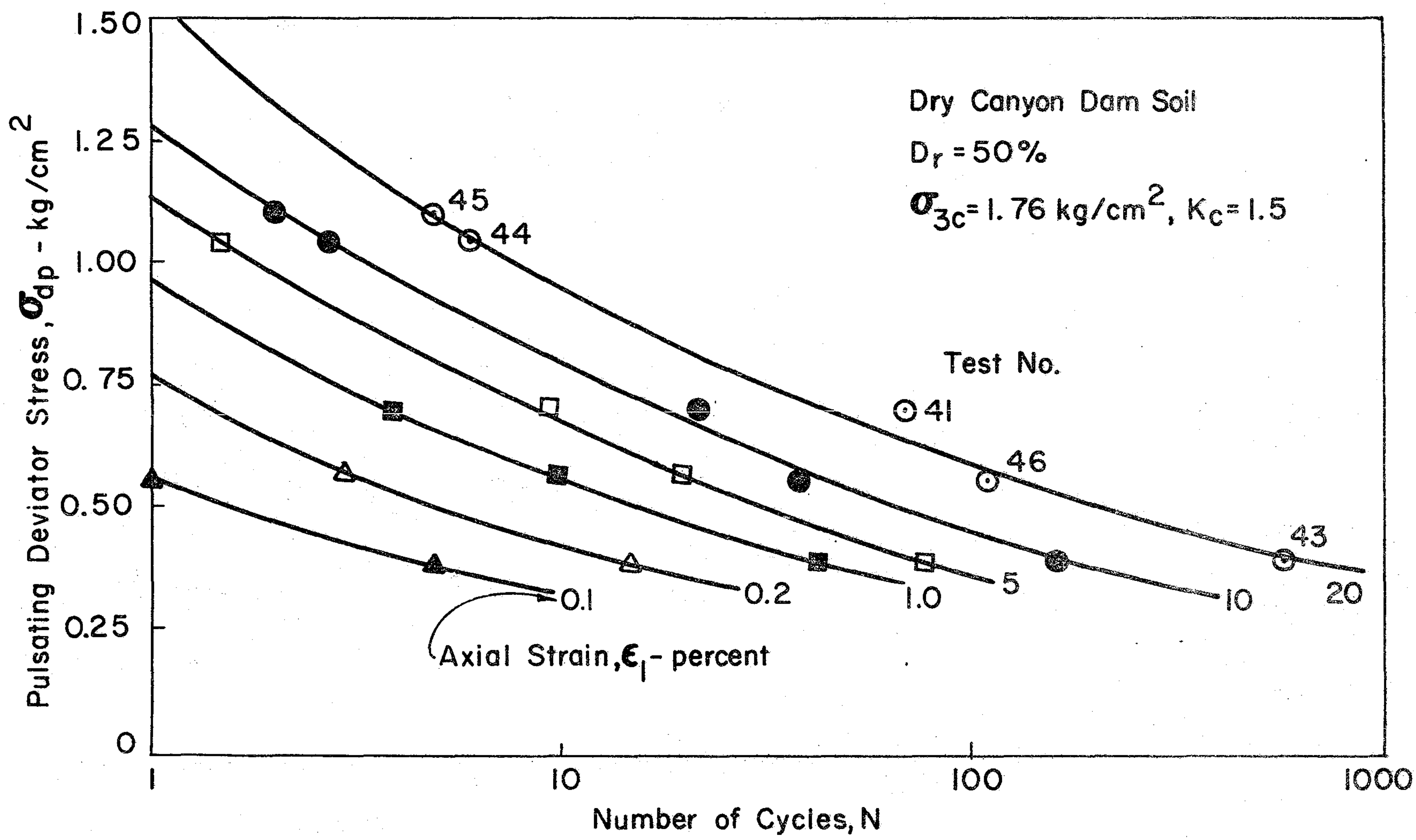

FIG. I-3. SUMMARY OF ONE SERIES OF PULSATING LOADING TESTS.

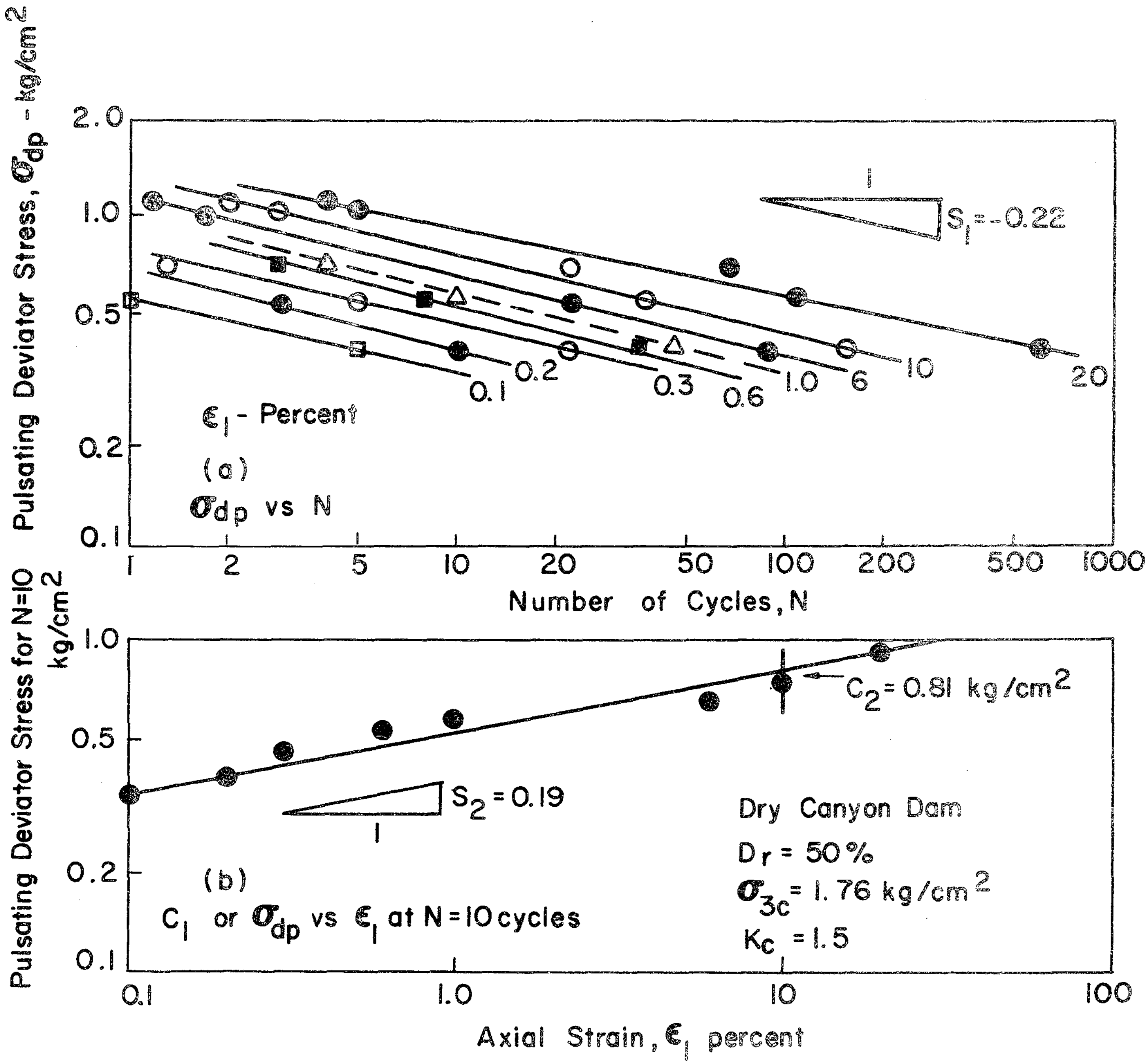

FIG. I-4. PULSATING LOAD TESTS RESULTS TO LOG-LOG SCALE.

key parameter in the computer storage of the permanent deformation test data. It is a dimensionless parameter.

It is now necessary to find a way of relating the parameter C_1 to the initial consolidation stress conditions, so that data of the form shown by Fig. I-4 or I-3, or Fig. 4 in the main text can be reproduced at will in the computer for any element in the embankment. Therefore, the next step is to plot the intercept C_1 versus the percent axial strain ε_1 as shown on Fig. I-4b. Plotted to double log scales, this data also approximates a straight line defined by the equation:

$$C_1 = C_2 \left(\frac{\varepsilon_1}{10} \right)^{S_2} \tag{I-2}$$

where S_1 is the slope and C_1 is the intercept at ε_1 = 10 percent axial strain. The 10 percent value was selected for these studies because it was felt that many of the calculations would involve strains of about this magnitude. It would be a simple matter to use another intercept, and for design purposes with modern dams where only low strains are to be expected, an intercept of say 1 percent may be more appropriate.

Laboratory test data for other series of tests on samples of this same soil consolidated to different stress conditions were also plotted as shown on Fig. I-3 and I-4, and the corresponding parameters S_1, C_1, and S_2 were determined. These are summarized in Table I-2.

Examining the data on Table I-2, as well as similar data from other soils, the following trends were observed:

(i) The values of S_1 appeared to have no defined trend with respect to consolidation pressure, but with a few exceptional excursions they appeared to be similar for all cases. Thus, for these studies S_1 was taken as the average of all values obtained.

Table I-2

Permanent Strain Parameters

Dry Canyon Dam Recompacted Hydraulic Fill $D_r \approx 50$ percent

K_c	σ_{3c} Kg/cm^2	S_1 Test	S_1 Ave	c_2 Kg/cm^2	S_2 Test	S_2 Ave	c_3 Kg/cm^2	S_3	c_4 Kg/cm^2	S_4	c_5	S_5	c_6	S_6
1.0	1.34	-0.17		0.60	0.06	0.55	0.0	0.42						
1.0	1.75	-0.23		0.73	0.05									
1.5	1.76	-0.22	-0.22	0.81	0.19	0.19	0.0	0.45	0.0	0.0	0.42	0.06	0.03	0.27
2.0	1.34	-0.30		0.61	0.31	0.33	0.0	0.48						
2.0	1.76	-0.21		0.85	0.35									

(ii) The values of C_2 appeared to vary systematically with consolidation pressure as will be described hereafter.

(iii) The values of S_2 appeared to be almost independent of K_c, but to vary with σ_{3c} as described hereafter.

To formulate the values of C_2 and S_2 in terms of consolidation pressure, the data were plotted as follows. Values of C_2 for all cases are plotted on Fig. I-5. For each K_c condition the value of C_2 can be represented by the equation:

$$C_2 = C_3 + S_3 \cdot \sigma_{3c} \qquad \text{(I-3)}$$

The data in Fig. I-5 indicate that the intercept $C_3 = 0$ for all cases, but for other soils and other conditions this is not always the case.

The variation of the three parameters C_3, S_3 and S_2, with the consolidation stress ratio K_c is shown on Fig. I-6. The general case of C_3 versus K_c is shown on Fig. I-6a, according to the equation:

$$C_3 = C_4 + S_4(K_c - 1) \qquad \text{(I-4)}$$

The variations of S_3 and S_2 with K_c are shown on Figs. I-6b and I-6c respectively, according to the equations:

$$S_3 = C_5 + S_5(K_c - 1) \qquad \text{(I-5)}$$

$$S_2 = C_6 + S_6(K_c - 1) \qquad \text{(I-6)}$$

Thus the permanent deformation data for all anisotropic stress conditions for this soil at one density are represented by seven different empirical parameters: S_1, C_4, S_4, C_5, S_5, C_6, S_6. When these are used in Eqs. I-1 through I-6, it is possible to compute the permanent axial strain ε_1 at any element defined by the initial consolidation stresses σ_{3c} or σ_{3c} and K_c or α, and subjected to a known pulsating deviator stress σ_{dp} for a known number of cycles N. As described in the main text, knowing ε_1, the corresponding value of pseudo pulsating Young's modulus

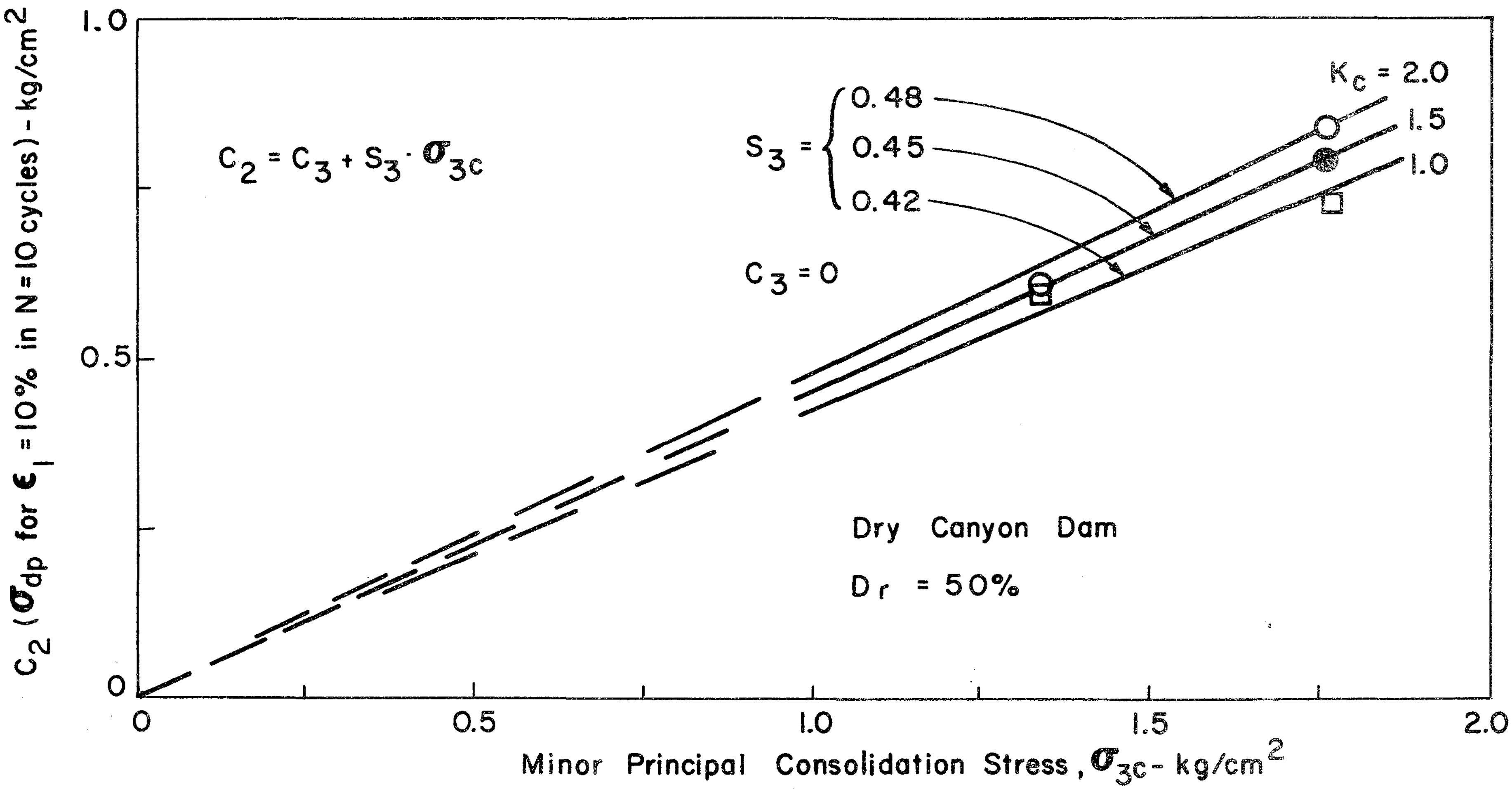

FIG. I-5. PULSATING DEVIATOR STRESS TO CAUSE 10 PERCENT STRAIN IN 10 CYCLES.

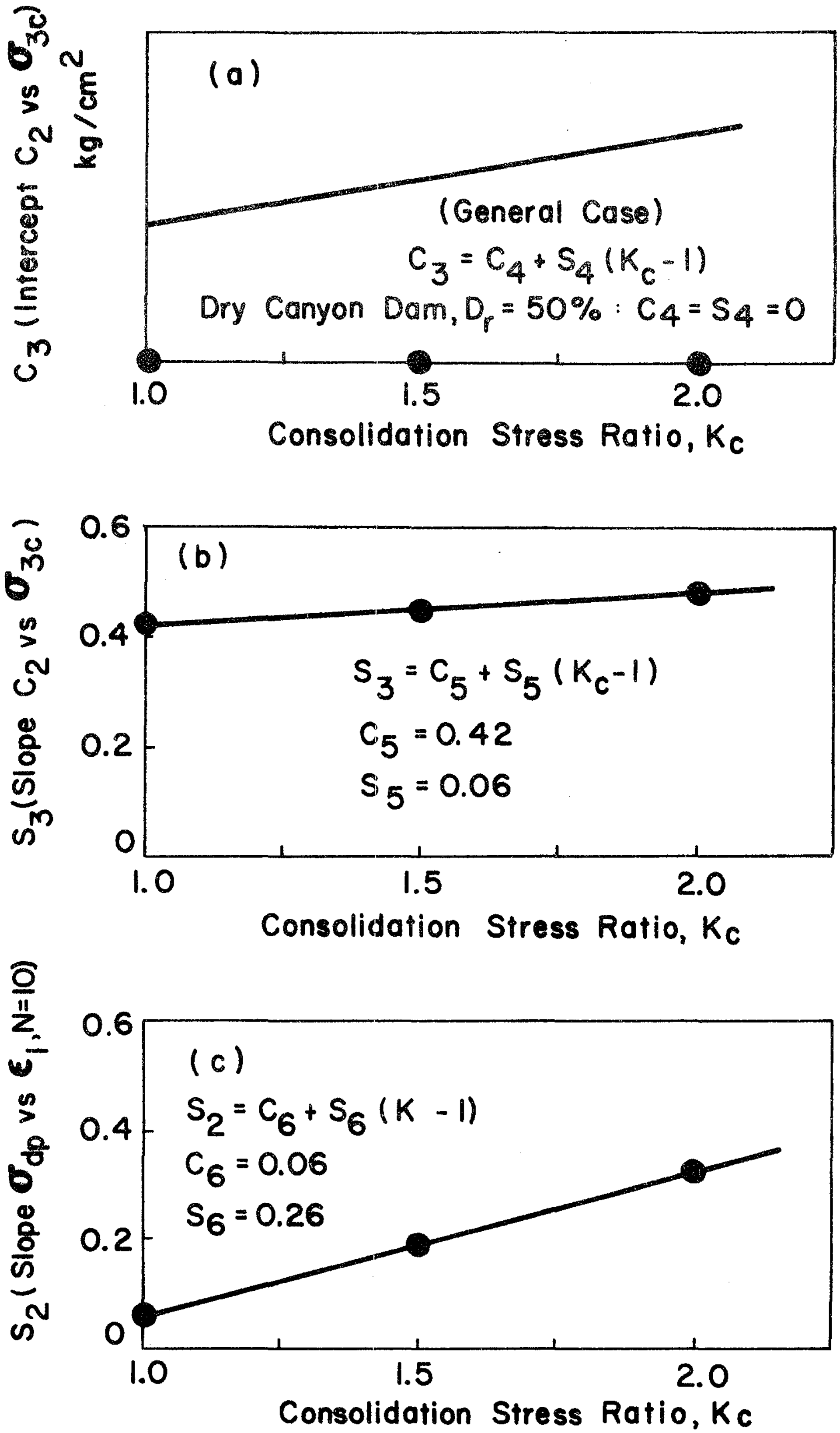

FIG. I-6. COMPILATION OF PULSATING LOADING DATA, DRY CANYON DAM SOIL, $D_r \approx 50\%$

E_p is computed from Eq. I-7.

$$E_p = \frac{\sigma_{dp}}{\varepsilon_1} \qquad \text{(I-7)}$$

and used in the finite element program in combination with the assumed initial values.

Calculation of ε_1 is conveniently done after some rearrangement of the foregoing equations. Substitution of C_1 from Eq. I-2 into Eq. I-1 and rearranging leads to:

$$\varepsilon_1 = 10\left(\frac{N}{10}\right)^{-\frac{S_1}{S_2}} \left(\frac{\sigma_{dp}}{C_2}\right)^{\frac{1}{S_2}}$$

where ε_1 is the <u>percent</u> axial strain after N cycles of a uniform pulsating deviator stress σ_{dp}. The values of S_1, S_2 and C_2 are obtained from the laboratory test data by way of the equations described above.

Data From Other Soils

Following the same procedures described above, cyclic load triaxial test data from other soils was similarly analyzed. Table I-3 summarized the data measured from undisturbed samples of soil from three zones of the Upper San Fernando Dam; the alluvium foundation, the silty sandy hydraulic fill shell, and the hydraulic fill clay core. Data from similar undisturbed samples taken from the Lower San Fernando Dam are presented on Table I-4. Unfortunately, the available data from the previous study of the Sheffield Dam was not sufficient to determine the parameters for that soil.

The data from the Dry Canyon and the two San Fernando Dams were each obtained at a limited number of relative densities. In order to provide a better basis for extrapolating to a broader range of relative densities,

Table I-3

Permanent Strain Parameters
Upper San Fernando Dam

Soil	D_r %	σ_{3c} Kg/cm^2	K_c	S_1 Test	S_1 Ave	C_2 Kg/cm^2	S_2 Test	S_2 Ave	C_3 Kg/cm^2	S_3	C_4 Kg/cm^2	S_4	C_5	S_5	C_6	S_6
Alluvium Foundation	65	1.0	1.0	-0.2	-0.2	1.02	0.173	0.173	0.49	0.52	0.52	0.05	0.52	0.45	0.17	0.0
Hydraulic Fill Silty Sand Shell	55	1.05	1.0	-0.266	-0.18	0.76	0.20		0.48	0.24	0.47	0.02	0.21	0.42	0.18	0.02
		2.16	1.0	-0.214		1.00	0.187									
		1.05	1.5	-0.195		0.91	0.194		0.48	0.39						
		2.16	1.5	-0.133		1.35	0.160									
		2.16	1.5	-0.133		1.33	0.145									
		1.05	2.0	-0.147		1.25	0.184		0.50	0.70						
		2.16	2.0	-0.23		2.02	0.28									
Hydraulic Fill Clay Core	Say 55 as per sand	1.0	1.0	-0.131		0.76	0.122	0.121	0.15	0.60	0.15	0.10	0.60	0.30	0.12	0.024
		2.0	1.0	-0.187		1.38	0.180									
		1.0	1.5	-0.102		0.95	0.088	0.133	0.20	0.75						
		2.0	1.5	-0.25		1.70	0.180									

Table I-4

Permanent Strain Parameters

Lower San Fernando Dam

Soil	D_r %	3c Kg/cm^2	K_c	S_1 Test	S_1 Ave	C_2 Kg/cm^2	S_2 Test	S_2 Ave	C_3 Kg/cm^2	S_3	C_4 Kg/cm^2	S_4	C_5	S_5	C_6	S_6
Alluvium Foundation	67	1.05	1.0	-0.135	-0.135	1.43	0.14	0.14	0.56	0.80	0.56	0.20	0.80	0.70	0.18	0.0
Hydraulic Fill		1.05	1.0	-0.16		0.85	0.120		0.43	0.36						
Silty Sand	55	3.16	1.0	-0.12		1.02	0.145									
Shell		1.05	1.5	-0.20	-0.15	2.05	0.254		0.54	0.70	0.44	0.17	0.35	0.63	0.15	0.0
		3.16	1.5	-0.184		2.75	0.177									
		1.05	2.0	-0.136		1.70	0.157		0.60	1.00						
		2.10	2.0	-0.087		2.70	0.123									

data from previous tests on Sacramento River sand were also analyzed. These data are presented on Table I-5, and cover a range of relative density from 38 to 100 percent.

A summary of the key parameters for all soils studied is presented in Table I-6. Unfortunately, no data was available for partly saturated soils, or for well compacted soils other than the clean uniformly grated Sacramento River sand.

Each of the separate parameters from the compilation of data in Table I-6 has been plotted versus relative density on Figs. I-7 through I-10. This compilation summary illustrates what is known of the variation of the permanent deformation parameters with density. So far as the data extends, there appears to be a consistent pattern both in sense and magnitude of the values for the different soils. Some parameters appear to increase, some decrease, and some remain approximately constant as the relative density increases.

Using the data and trends as guides, parameters for the Sheffield and Hebgen Dam soils were estimated, as well as for the soils in zones of the other dams for which data was not available. Data for the partially saturated soils above the water table were obtained by extrapolations from Figs. I-7 through I-10 assuming the soil behaved as a very dense material.

The permanent deformation parameters used for the various zones in the five dams studied are listed in Tables I-7 through I-11.

Table I-5 Permanent Strain Parameters, Sacramento River Sand

D_r	σ_{3c}	K_c	S_1		C_2	S_2		C_3	S_3	C_4	S_4	C_5	S_5	C_6	S_6
%	Kg/cm^2		Test	Ave	Kg/cm^2	Test	Ave	Kg/cm^2		Kg/cm^2					
38	1.0	1.0	-0.16		0.44	0.04	0.04								
	5.0	1.0			2.10			0.0	0.4						
	15.0	1.0		-0.13	5.90					0.0	0.5	0.4	0.36	0.04	0.20
	5.0	2.0	-0.11		4.5	0.16	0.25	0.5	0.76						
	15.0	2.0			8.6	0.33									
60	1.0	1.0			0.7										
	5.0	1.0			3.0			0.4	0.45						
	15.0	1.0			7.8										
78	1.0	1.0	-0.19		1.0	0.19	0.24	0.45	0.9						
	5.0	1.0			5.0	0.29									
	15.0	1.0		-0.19	11.0					0.4	0.7	0.9	0.38	0.24	0.04
	5.0	2.0			7.6	0.29	0.26	1.2	1.25						
	15.0	2.0			13.2	0.23									
100	1.0	1.0	-0.24		2.4	0.8	0.8								
	5.0	1.0			10.0			1.5	1.65						
	15.0	1.0		-0.24	18.5					1.5	7.6	1.65	0.34	0.80	-0.46
	5.0	2.0			16.6	0.38	0.32	9.0	1.9						
	15.0	2.0			25.0	0.27									

Table I-6

Compilation of Test Data on Permanent Strain

Parameters For Various Soils

Parameter	D_r	S_1	C_4	S_4	C_5	S_5	C_6	S_6
Units	%	-	Kg/cm^2	Kg/cm^2	-	-	-	-
Dry Canyon Dam Recomp. Hyd. Fill	50	-0.22	0.0	0.0	0.42	0.06	0.05	0.25
Sacramento River Sand	38	-0.13	0.0	0.5	0.4	0.36	0.04	0.20
	78	-0.19	0.4	0.7	0.9	0.38	0.24	0.04
	100	-0.24	1.5	7.6	1.65	0.34	0.80	-0.46
Upper S.F. Alluvium	65	-0.20	0.52	0.05	0.52	0.45	0.17	0.0
Upper S.F. Silty Sand	55	-0.18	0.47	0.02	0.21	0.42	0.18	0.02
Upper S.F. Clay	55?	-0.168	0.15	0.10	0.60	0.30	0.12	0.024
Lower S.F. Alluvium	67	-0.135	0.56	0.20	0.80	0.70	0.18	0.0
Lower S.F. Silty Sand	55	-0.15	0.44	0.17	0.35	0.63	0.15	0.0

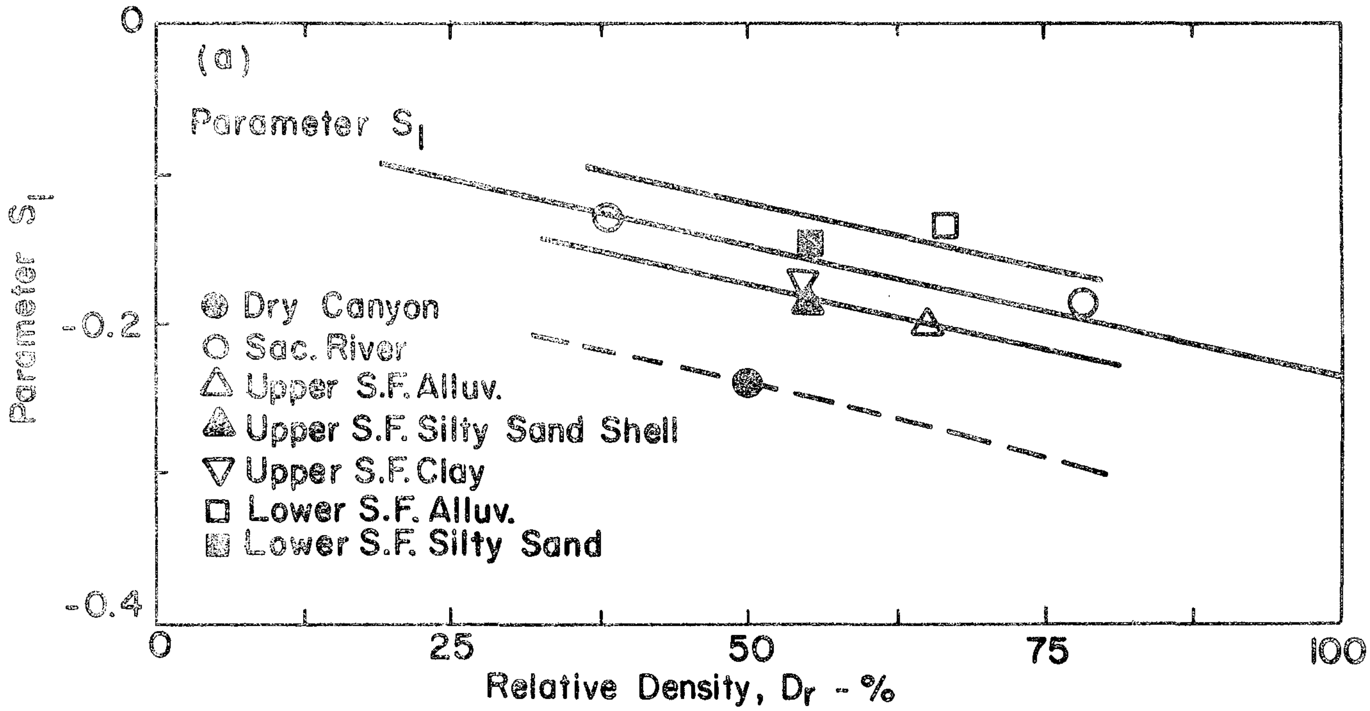

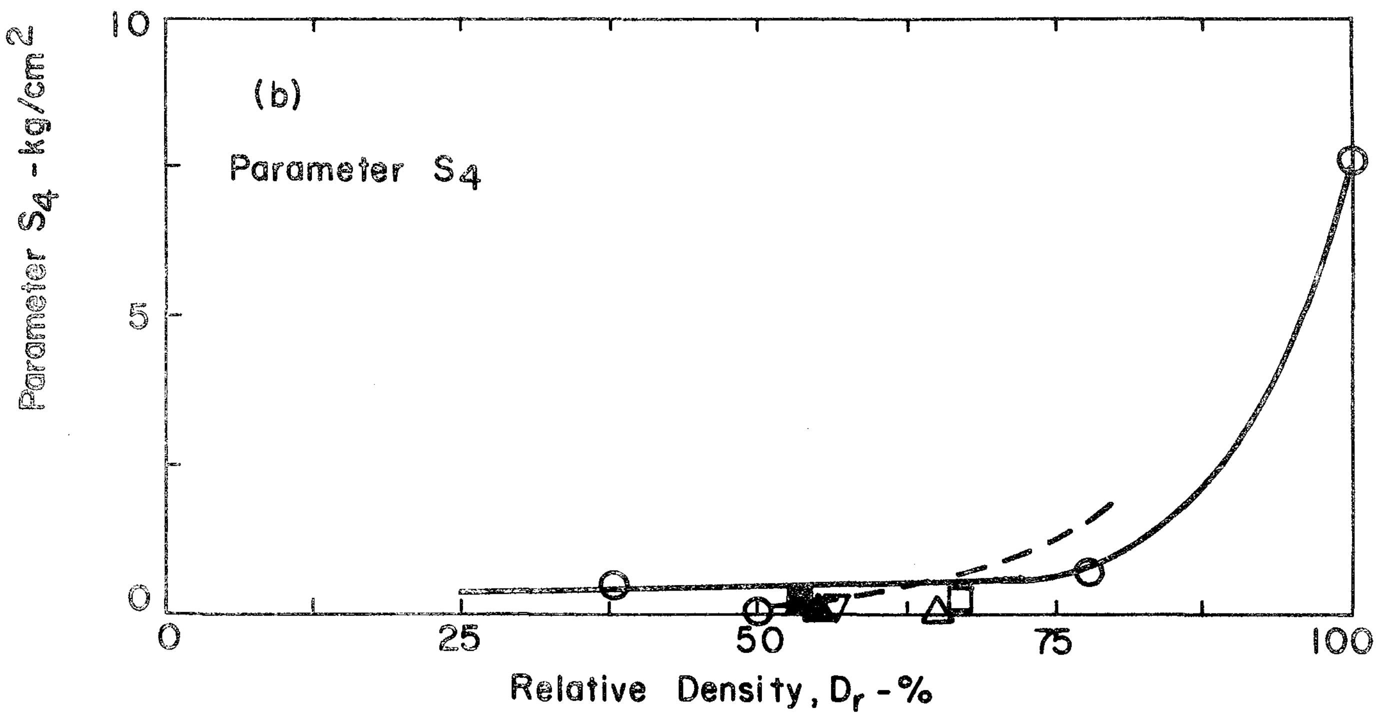

FIG. I-7. COMPILATION OF PERMANENT STRAIN PARAMETERS FROM VARIOUS SOILS (1 OF 4)

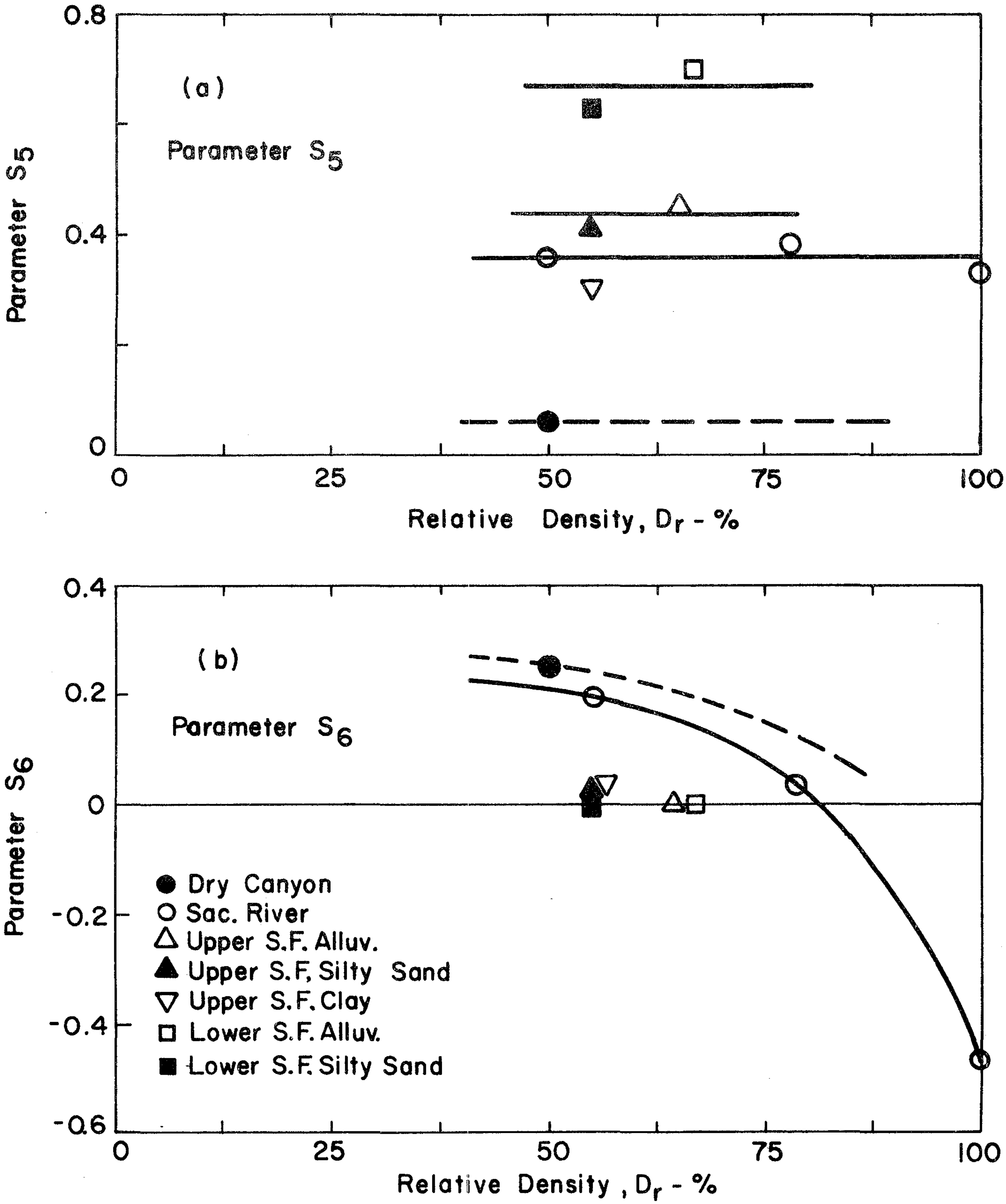

FIG. I-8. COMPILATION OF PERMANENT STRAIN PARAMETERS FOR VARIOUS SOILS (2 OF 4)

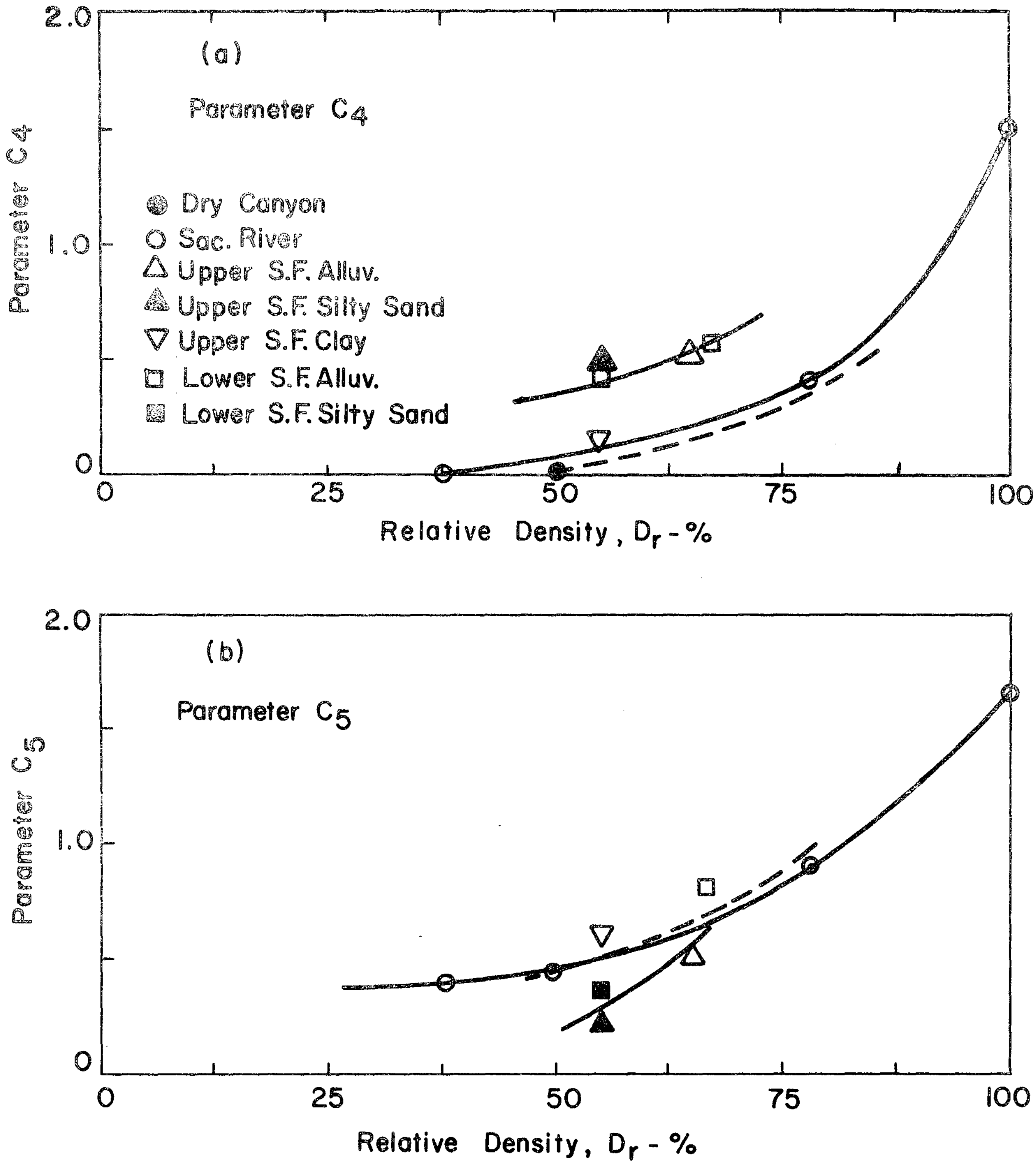

FIG. I-9. COMPILATION OF PERMANENT STRAIN PARAMETERS FOR VARIOUS SOILS (3 OF 4).

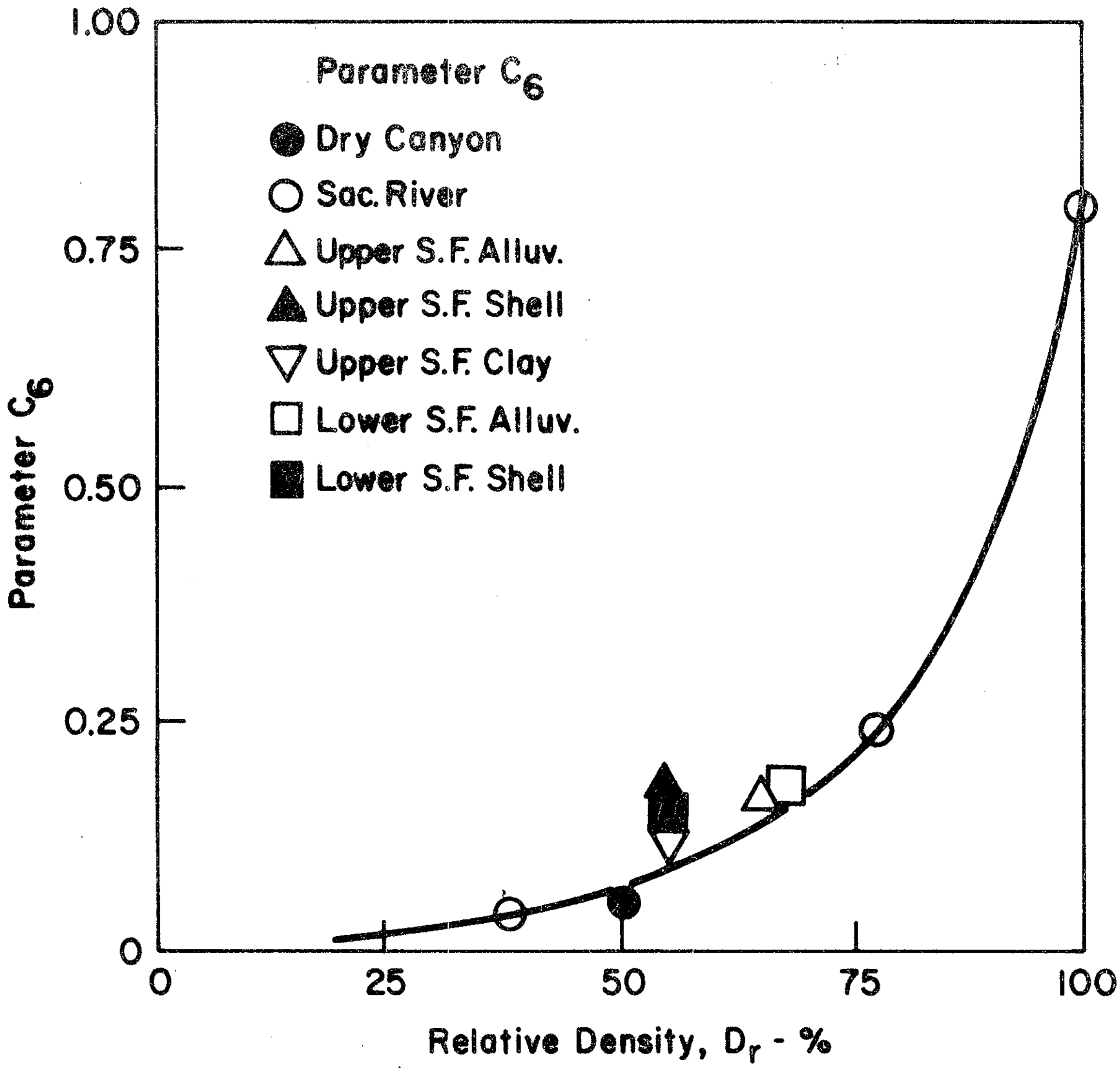

Fig. I-10 Compilation of Permanent Strain Parameters For Various Soils (4 of 4)

Table I-7 Summary of Soil Property Data Used In Permanent Deformation Analyses Dry Canyon Dam

	Parameter	Mat.	Classification D_r	γ_m	γ_b	Pre Earthquake γ_{used}	E	ν	Post Earthquake Permanent Strain S_1	C_4	S_4	C_3	S_5	C_6	S_6	C_{r_1}	ϕ
	Units		%	lb/ft^3	lb/ft^3	$tons/ft^3$	$tons/ft^2$	-	-	$tons/ft^2$	$tons/ft^2$	-	-	-	-	-	deg.
Below Water Table	Alluvium Foundation	1	77	131.0	108.	.035	800	0.3	-0.28	0.30	1.80	0.95	0.06	0.20	0.16	0.65	38.
	Wagon Hauled Shell	2	62	125.0	99.	.031	570	0.3	-0.26	0.10	0.50	0.60	0.06	0.10	0.22	0.60	33.
	Wagon Roll Core	3	63	127.1	102.	.033	600	0.3	-0.27	0.20	0.72	0.70	0.06	0.15	0.19	0.62	36.
	Hyd. Fill Core	4	47	120.5	89.	.029	500	0.3	-0.26	0.00	0.00	0.42	0.06	0.05	0.26	0.55	30.
Above Water Table	Wagon Hauled Shell	5	62	124.5	98.	.060	570	0.3	-0.30	1.0	3.0	1.0	0.06	0.6	-0.02	0.9	40.
	Wagon Roll Core	6	68	126.5	102.	.061	600	0.3	-0.30	1.0	3.0	1.0	0.06	0.6	-0.05	0.9	40.
	Compacted Berm	7	80	133.0	111.	.065	700	0.3	-0.30	1.0	3.0	1.0	0.06	0.6	-0.06	0.9	40.

Table I-8 Summary of Soil Property Data Used In Permanent Deformation Analyses Sheffield Dam

	Classification				Pre Earthquake			Post Earthquake Permanent Strain								
Parameter	Mat.	D_r	γ_m	γ_b	γ_{used}	E	ν	S_1	C_u	S_u	C_5	S_5	C_6	S_6	C_{r_1}	ϕ
Units		%	lb/ft^3	lb/ft^3	$tons/ft^3$	$tons/ft^2$	-	-	$tons/ft^2$	$tons/ft^2$	-	-	-	-	-	deg.
Fill, Above wt.	1	40	107	-	.053	200.	0.35	-0.19	0.25	0.00	0.75	0.30	0.18	0.10	0.65	35.
Fill, Below wt.	2	40	120	58	.029	200.	0.35	-0.15	0.05	0.05	0.30	0.28	0.08	0.15	0.55	35.
Foundation, Below wt.	3	40	120	58	.029	200.	0.35	-0.15	0.05	0.05	0.30	0.28	0.08	0.15	0.55	35.

Table I-9 Summary of Soil Property Used In Permanent Deformation Analyses Upper San Fernando Dam

		Classification				Pre Earthquake			Post Earthquake Permanent Strain								
	Parameter	Mat.	D_r	γ_m	γ_b	γ_{used}	E	ν	S_1	C_4	S_4	C_5	S_5	C_6	S_6	C_{r_1}	ϕ
	Units		%	lb/ft^3	lb/ft^3	$tons/ft^2$	$tons/ft^2$	-	-	$tons/ft^2$	$tons/ft^2$	-	-	-	-	-	deg
Below Water Table	Compacted Cap	1	80?	132	70	0.035	500.	0.35	-0.22	0.80	1.00	0.80	0.55	0.30	-0.10	0.70	39.
	Hyd. Fill Sand Shell	2	55	123	61	0.031	500.	0.35	-0.18	0.47	0.02	0.21	0.42	0.18	0.02	0.55	37.
	Hyd. Fill Clay Core	3	55	123	61	0.031	500.	0.35	-0.168	0.15	0.10	0.60	0.30	0.12	0.02	0.55	35.
	Upper Alluvium	4	65	131	69	0.0345	600.	0.35	-0.20	0.52	0.05	0.52	0.45	0.17	0.0	0.65	37.
	Lower Alluvium	5	80	134	72	0.036	700.	0.35	-0.24	0.90	1.00	0.90	0.50	0.40	-0.10	0.70	40.
Above Water Table	Compacted Cap	6	80?	129	-	0.0645	500.	0.35	-0.3	1.0	3.0	1.0	0.5	0.6	-0.1	0.9	40.
	Hyd. Fill Sand Shell	7	55	129	-	0.0645	500.	0.35	-0.3	1.0	3.0	1.0	0.5	0.6	-0.1	0.9	40.
	Hyd. Fill Clay Core	8	55	129	-	0.0645	500.	0.35	-0.3	1.0	3.0	1.0	0.5	0.6	-0.1	0.9	40.
	Upper Alluvium	9	65	132	-	0.066	630.	0.35	-0.3	1.0	3.0	1.0	0.5	0.6	-0.1	0.9	40.

Table I-10 Summary of Soil Property Data Used In Permanent Deformation Analyses Lower San Fernando Dam

	Parameter	Classification				Pre Earthquake			Post Earthquake Permanent Strain								
		Mat.	D_r	γ_m	γ_b	γ_{used}	E	ν	S_1	C_4	S_4	C_5	S_5	C_6	S_6	C_{r_1}	ϕ
	Units		%	lb/ft^3	lb/ft^3	tons/ft^3	tons/ft^2	-	-	tons/ft^2	tons/ft^2	-	-	-	-	-	deg.
Below Water Table	Alluvium	1	67	134	72	0.036	700.	0.35	-0.14	0.56	0.20	0.80	0.70	0.18	0.0	0.70	38.
	Hyd. Fill Sand Shell	2	55	124	62	0.031	500.	0.30	-0.15	0.44	0.17	0.35	0.63	0.15	0.0	0.55	37.
	Hyd. Fill Clay Core	3	55	124	62	0.031	500.	0.30	-0.13	0.15	0.20	0.70	0.60	0.10	0.0	0.55	37.
	Ground Shale	4	70?	132	66	0.033	550.	0.30	-0.15	0.60	0.23	0.50	0.08	0.18	0.0	0.65	37.
	Compacted Cap	5	80?	132	70	0.035	600.	0.33	-0.18	0.80	1.0	1.0	1.0	0.25	-0.04	0.70	40.
Above Water Table	Compacted Cap	6	80	130	-	0.065	600.	0.33	-0.3	1.0	3.0	1.0	1.0	0.6	-0.05	0.9	40.
	Ground Shale	7	70	130	-	0.065	500.	0.30	-0.3	1.0	3.0	1.0	1.0	0.6	-0.02	0.9	40.
	Hyd. Fill Sand Shell	8	55	134	-	0.067	500.	0.30	-0.3	1.0	3.0	1.0	1.0	0.6	0.0	0.9	37.
	Compacted Berm	9	85?	138	-	0.069	700.	0.30	-0.3	1.0	3.0	1.0	1.0	0.6	-0.06	0.9	40.

Table I-11 Summary of Soil Parameters Used in Permanent Deformation Analyses, Hebgen Dam

	Classification				Pre-Earthquake			Post Earthquake								
Parameter	Mat.	D_r	γ_m	b	γ_{used}	E	ν	S_1	C_4	S_4	C_5	S_5	C_6	S_6	C_{r1}	ϕ
Units		%	lb/ft^3	lb/ft^3	T/ft^3	T/ft^3	-	-	T/ft^3	T/ft^3	-	-	-	-	-	deg.
Earthfill upstream saturated	1	55	130	68	0.034	500.	0.35	-0.15	0.10	0.20	0.5	0.4	0.10	0.10	0.58	35.
Loose Rock Downstream (assumed saturated from seepage through abutments)	2	75	135	73	0.037	750.	0.35	-0.17	0.2	0.40	0.6	0.4	0.15	0.8	0.62	35.
Rock and Earthfill Downstream Assume partly saturated	3	65	130	-	0.065	500.	0.35	-0.2	2.0	1.0	2.0	0.5	1.0	-0.2	0.9	35
Concrete Core	4	-	150	-	0.034	500.	0.2	Same as Material 1								

Notes:

Materials 1 and 2; data obtained by interpolation from average data for saturated soil at D_r shown.

Material 3; data obtained by interpolation from average data for saturated soil at D_r = 100%.

Material 4, Concrete Core; to avoid stiff core holding up adjacent soil, core material taken as saturated soil.

APPENDIX II

Correlation Factors, Triaxial To Field For Anisotropic Consolidation

As mentioned in the main body of the text, the pulsating loading triaxial test cannot reproduce all of the essential conditions of the cyclic loading of an element of soil in the field. The cyclic simple shear test is conceptually superior to the triaxial test in this regard, but because of equipment limitations it cannot exactly reproduce the field stress conditions either. Thus, if pulsating triaxial tests are used in the laboratory, it is necessary to apply correlation factors to the data before it can be applied to field calculations. These factors are of two parts; correlation between triaxial and simple shear results, and correlations to the simple shear data to account for the practical limitations of this equipment to reproduce the field stress conditions throughout a sample.

Seed and Peacock (20) have discussed these correlation factors in detail for the field case of sand soils and level ground surface where the shear stress on the horizontal, potential failure plane, prior to the earthquake is zero. This corresponds to consolidation stress ratios as follows:

Field or simple shear $\qquad \alpha = \dfrac{\tau_c}{\sigma_{nc}} = 0$

Triaxial simulation of field conditions $\qquad K_c = \dfrac{\sigma_{1c}}{\sigma_{3c}} = 1.0$

For this case, Seed and Peacock have lumped together the two types of correlation factors into a single equation to convert pulsating loading laboratory triaxial strengths into field pulsating loading strengths as follows:

$$\left(\frac{\tau_p}{\sigma_{nc}}\right)_{field} = C_r\left(\frac{\sigma_{dp}}{2\,\sigma_{3c}}\right)_{lab\ triax} \qquad \text{(II-1)}$$

The values of τ_p or $\sigma_{dp/2}$ represent the uniform pulsating shear stress required to cause failure of an element or sample in the same number of cycles. The normal stresses σ_{nc} or σ_{3c} represent the effective overburden consolidation stress in the field and the effective isotropic consolidation stress in the laboratory. The factor C_r is a correlation factor; Seed and Peacock have evaluated C_r on a semi-theoretical, semi-empirical basis for liquefaction of saturated sands. They suggest values of C_r with relative density as shown on Table II-1.

Table II-1

C_r Values Suggested by Seed and Peacock for $K_c = 1.0$, $\alpha = 0.0$

D_r - percent	C_r
40	0.55
60	0.60
70	0.65
80	0.68
90	0.73

Beyond this information there is little available data on which to select, correlation factors for soils such as compacted clays, partially saturated soils, or any soils under sloping surfaces which are consolidated anisotropically to stress ratios $\alpha \not\approx 0.0$ or $K_c \not\approx 1.0$. Thiers and Seed (40) have presented data which show that for San Francisco Bay mud the cyclic simple shear strength is approximately the same as the cyclic triaxial strength.

Seed et al. (6) have presented data for both cyclic simple shear and triaxial tests on a silty sand consolidated to similar isotropic and slightly anisotropic stress conditions. A summary of the pulsating loading strength data from these tests is shown on Fig. II-1. The triaxial data were for K_c = 1.0 and the simple shear data were for α = 0.0. The difference in pulsating shear stress required to cause failure is similar to that reported from the comprehensive study by Peacock and Seed (32) on a clean medium sand.

Finn et al. (31,32) have since shown that the simple shear apparatus can be improved to remove some limitations, for example, stress concentrations at the boundaries, and these improvements lead to higher simple shear strengths. In a later study, Seed and Peacock (20) used an improved simple shear apparatus and also found that higher strengths were obtained, which lead in part to the selection of the C_r values shown above.

Returning back to data from the early Sheffield Dam study, some tests were also performed on anisotropically consolidated simple shear and triaxial test specimens using comparable consolidation stress ratios of K_c = 1.2 for triaxial tests and α = 0.09 for simple shear tests. At this anisotropic consolidation stress condition the normal stress on the potential failure plane σ_{fc}, was 8 percent greater than the minor principal stress σ_{3c}.

Results of a series of tests at one value of normal stress for each of the two types of tests are shown on Fig. II-2. Again the triaxial tests gave higher strengths than the simple shear tests. Evaluating these and other data for 10 cycles from tests at different normal consolidation stresses, but the same stress ratios, leads to the pulsating loading strengths shown on Fig. II-3. Although the triaxial strengths are greater than the simple shear strengths, the difference is not as great as on Fig. II-1 for isotropic consolidation conditions.

In the original Sheffield Dam study (6), and in subsequent seismic stability analyses of dams, the comparison of strength to stress under

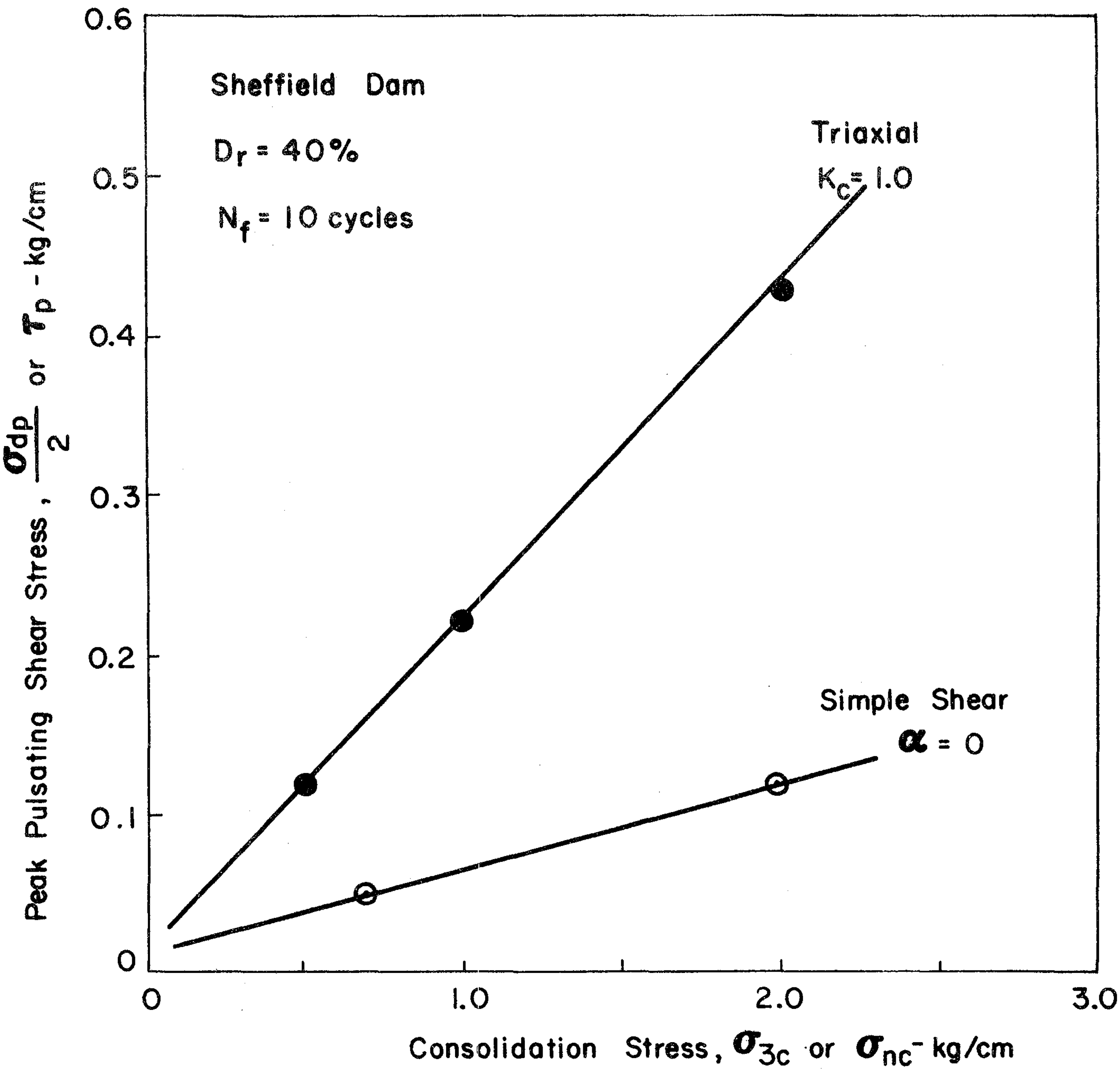

FIG. II-1. COMPARISON OF CYCLIC TRIAXIAL AND CYCLIC SIMPLE SHEAR TESTS $K_c=1.0$, $\alpha=0$

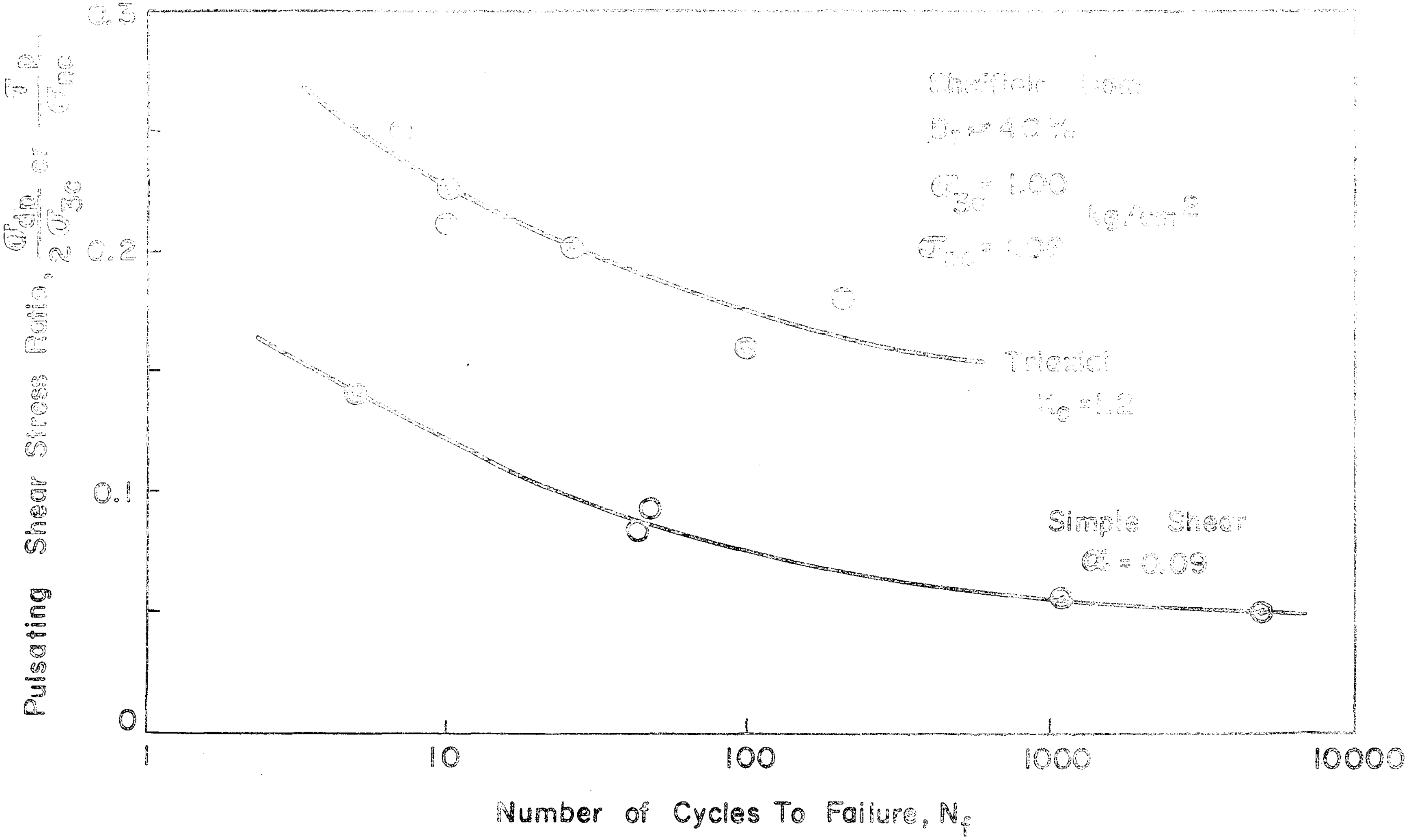

FIG. II-2. COMPARISON OF PULSATING SHEAR STRESS CAUSING FAILURE IN TRIAXIAL AND DIRECT SHEAR TESTS.

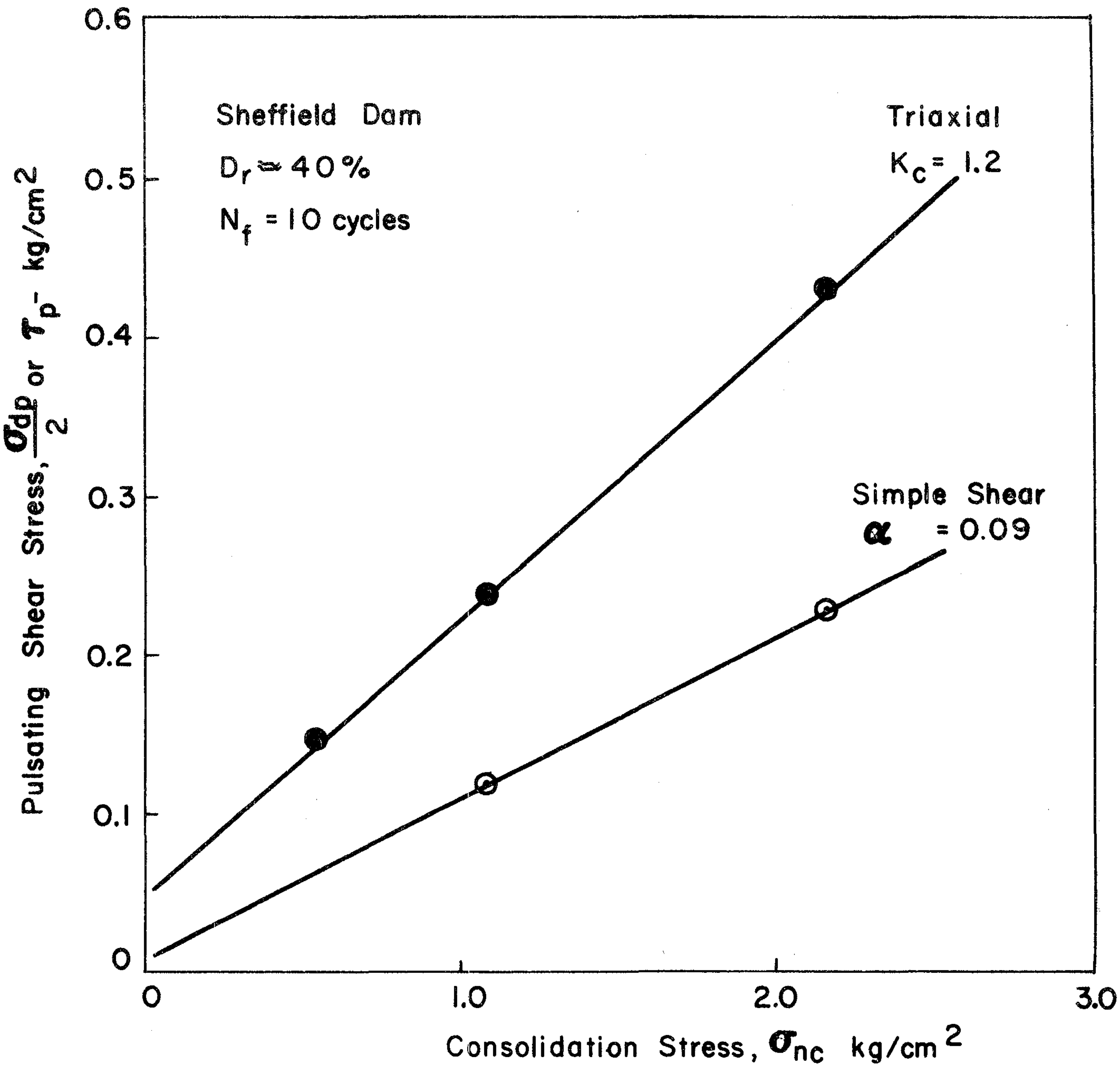

FIG. II-3. COMPARISON OF PULSATING SHEAR STRESS CAUSING FAILURE USING TRIAXIAL AND SIMPLE SHEAR TESTS.

pulsating loading conditions has been made on the basis of the maximum total stress defined as:

$$\text{total stress} = \text{static stress} + \text{pulsating stress} \qquad \text{(II-2)}$$

For field or simple shear conditions this is:

$$\tau_{max} = \tau_{c} + \tau_{p} \qquad \text{(II-3)}$$

and for triaxial test conditions this is:

$$\sigma_{d\,max} = \sigma_{dc} + \sigma_{dp} \qquad \text{(II-4)}$$

For isotropic consolidation $\tau_c = \sigma_{dp} = 0$, and $\tau_{max} = \tau_p$ or $\sigma_{d\,max} = \sigma_{dp}$. For anisotropic consolidation conditions τ_c and σ_{dp} are both greater than zero.

In the Sheffield Dam study it was noted that on this basis the difference between triaxial and simple shear strengths decreased with increasing degree of anisotropic consolidation. The data were limited to $K_c = 1.0$, $\alpha = 0.0$ and $K_c = 1.2$, $\alpha = 0.09$ conditions. But from the trends indicated from this data, it appeared that for $K_c = 1.5$, $\alpha = 0.19$ the triaxial and the simple shear strengths would be approximately the same. This has been used in subsequent seismic stability analyses following the equilibrium method (7).

The permanent deformation method duscussed in this report separates the static from the pulsating stresses throughout the analyses. The earthquake induced permanent deformation parameters are direct functions of the pulsating stress and the corresponding accumulative strain resulting only from this pulsating load. Thus the data from the previous Sheffield Dam study shown on Fig. II-3 refers only to the pulsating stress σ_{dp} or τ_p, and not to the maximum stress as defined above. However, as indicated by comparison of Figs. II-1 and II-3, the higher anisotropic stress conditions leads to less difference between triaxial and simple shear results.

It must be recalled that the data on Fig. II-1 and Fig. II-3 were all obtained by the early tests on the same unimproved simple shear apparatus from which Seed and Peacock developed their C_r factors for $K_c = 1.0$ conditions. The data on Figs. II-1 and II-3 contain no correction for any equipment limitations involved and thus whatever limitations applied to the $K_c = 1.0$ data should also apply to the $K_c > 1.0$ data as well.

A summary of this information is presented on Fig. II-4 showing the correlation ratio C_r as a function of K_c. The lower curve is defined by data from Figs. II-1 and II-3 for three different confining pressures. The data are consistent and show an increase in C_r with increasing K_c. The upper curve passes through the point C_r 0.55 for $K_c = 1.0$ as defined by Seed and Peacock (20) for the relative density of this loose soil. The curve then slopes linearly up to a maximum of $C_r = 1.0$ at $K_c = 1.5$ which is consistent with the C_r values used for the previous equilibrium stability analyses using total stresses. The slope of this line is not inconsistent with the slope of the lower line derived from pulsating stresses only. If the intercept at $K_c = 1$ were moved up to C_r 0.55 to account for limitations in laboratory equipment, then it is not inconsistent that the data points at $K_c = 1.2$ should also be moved up to the vicinity of the upper curve, also to account for equipment limitations.

Unfortunately, this appears to be the only available comparable data between triaxial and simple shear pulsating loading tests on anisotropically consolidated samples. Therefore, on the basis of the indications from this data, the analyses described in this report used a C_r correlation factor which varied with relative density and with K_c ratio as follows:

For $K_c = 1.0$: C_r versus relative density as given by Seed and Peacock (20) and summarized on Table II-1.

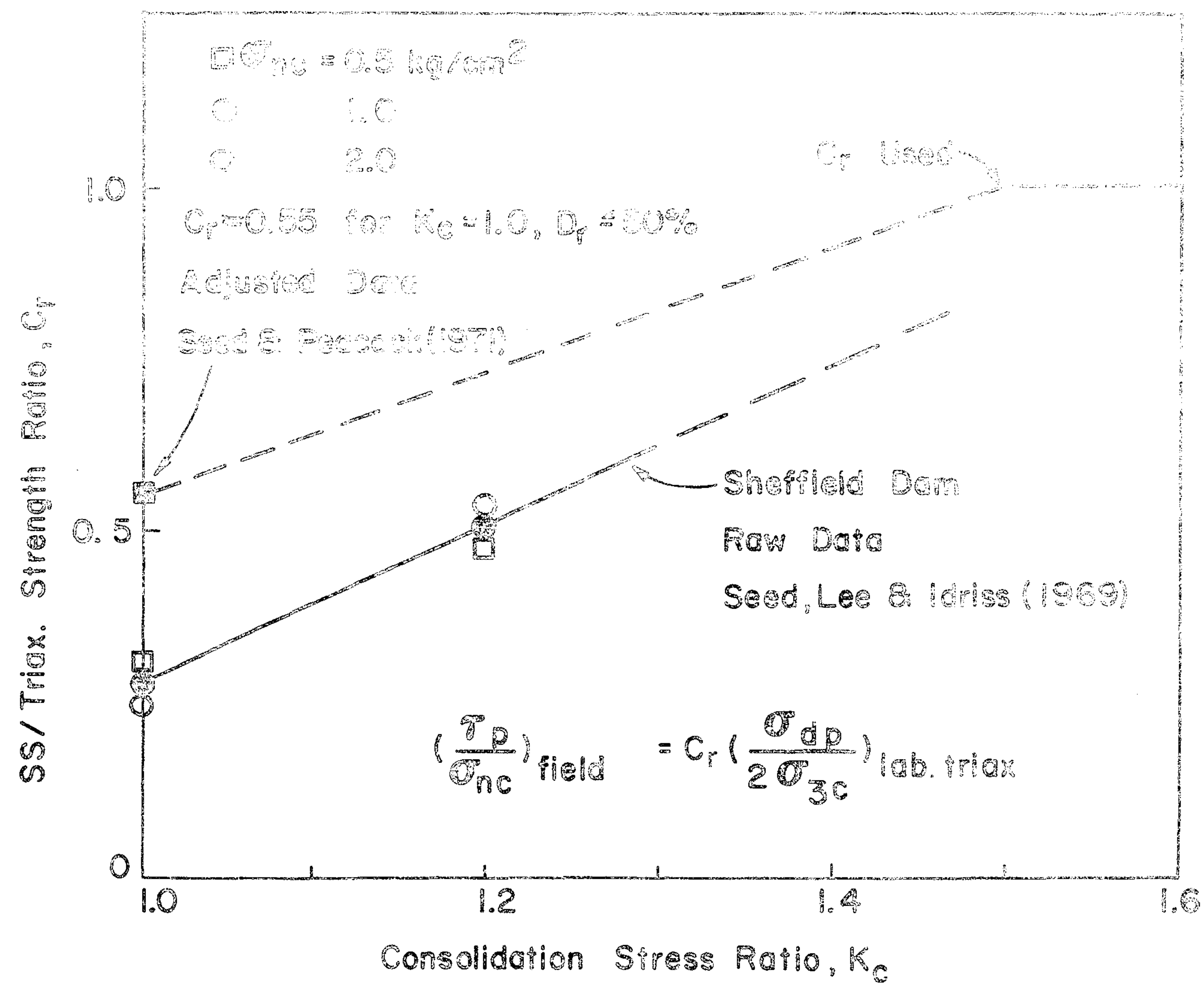

FIG. II-4. CORRECTION FROM PULSATING TRIAXIAL TEST TO PULSATING FIELD CONDITIONS.

For $K_c = 1.5$: $C_r = 1.0$.

For intermediate K_c ratios: a linear extrapolation between $K_c = 1.0$ and $K_c = 1.5$.

Because of the limited data available especially for $K_c > 1.0$, for clays and for stiff or strong soils, and because C_r has a strong influence on the final results, it will be important to obtain more data in future studies.

APPENDIX III

Number of Equivalent Cycles

The time history of pulsating shear stress induced in any element of soil in a real earthquake is highly random. Ideally, laboratory tests should be so conducted to reproduce this same random stress-time history for each sample simulating every significant element in the field in order to approximate similar stress paths for field and laboratory conditions. Unfortunately, this is not practical for several reasons:

i. Equipment for producing a specified random stress-time history on a sample is not readily available in most laboratories.

ii. Each earthquake is different, and for design purposes there is no way of knowing in advance what will be the shape of the stress-time history produced by the most critical future earthquake. Even for the same maximum peak acceleration, the form of the time history will likely be different from one earthquake to the next.

iii. Variations in dimensions and properties of the structure and of the assumed input motion will likely vary during successive stages of the design. Each change will probably result in a different stress-time history for the many key elements, and it would be impractical to repeat the entire laboratory testing program for each of these changes.

iv. The type of non-linear seismic response analysis uses strain dependent modulus and damping factors based on an equivalent linear representation of a single hysteretic stress-strain loop for each iteration of a complete time history. Thus the use of an equivalent system of uniform cycles is consistent for both the stress-strain and the strength formulations of the problem.

For these pragmatic reasons, pulsating loading tests have always been run using a time history of uniform stress pulses. The number of pulses of a particular cyclic stress required to cause failure in terms of a certain prescribed deformation is noted for each test. A family of three to four cyclic loading tests on similar samples defines the pulsating loading strength of the soil for any number of uniform cyclic stresses. To apply these data to the field it is necessary to convert the actual random stress time history into an equivalent number of uniform cycles, N_{eq} of an average cyclic stress intensity τ_{av}, as illustrated schematically on Fig. III-1.

The conversion from random to uniform cyclic stresses is made on the basis that either effect produces the same response in the sample. In other words, the random stress-time history shown on Fig. III-1a would cause the same amount of strain in a soil sample as would the uniform stress-time history of Fig. III-1b. On this basis, the two effects are equivalent.

This concept of τ_{av} and N_{eq} has been used for all previous seismic stability analyses cited herein. A detailed description of the method used to calculate the τ_{av} - N_{eq} relationships has also been given by Lee and Chan (21), and the results of many calculations have also been presented. However, for convenient reference, the method will be briefly summarized in this Appendix, and a few summary comments added.

In addition to defining the concept of τ_{av} - N_{eq} as stated above, the calculations also assume that the soil response depends only on the magnitude of the many stress pulses which it receives, and not on the order in which they come. Thus the total effect of a random distribution of cyclic stresses can be calculated by calculating the effect of each cycle taken separately, and then adding all the effects together.

At present, this is only an assumption, which requires further experimental verification. Ishihara and Yasuda (13) have recently published the results of a series of cyclic loading tests on loose saturated sand from Niigata, Japan using a stress-time history proportional to the accelerogram recorded at that city during the destructive earthquake of 1964. The record is peculiar in that it consists of a long time history of low level motion ending with one large asymmetric cycle which is 60 percent greater on one

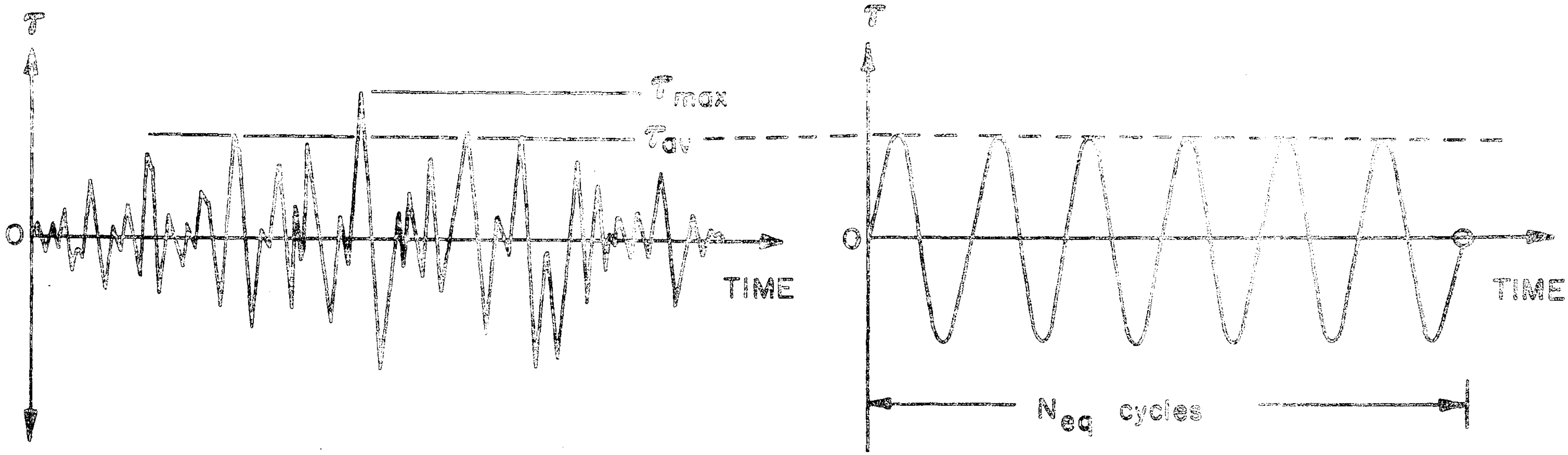

(a) Computed Actual Response

(b) Equivalent Response

FIG. III-1 CONCEPT OF EQUIVALENT NUMBER OF UNIFORM CYCLES.

direction than the other. They found that the liquefaction response of samples was somewhat dependent on whether the largest stress cycle was applied in extension or compression of a pulsating loading triaxial test. Further studies of the effect of random versus uniform intensity cyclic loading are being planned at UCLA, but for the present it is assumed that the response of the soil is not significantly affected by the order in which the random stresses are applied.

On the basis of these assumptions, the following method is used to calculate the uniform stress, $\tau_{av} - N_{eq}$ equivalence from any given random cyclic stress-time history.

Referring to Fig. III-1a, the first step is to select some arbitrary value τ_{av} less than τ_{max}. It is convenient to express this as a ratio:

$$R = \frac{\tau_{av}}{\tau_{max}} \qquad \text{(III-1)}$$

and to use the same ratio for every element of soil within the structure. Convenient values for R range from about 0,65 to 0.85. As described here and in the main text, the choice of R has no significant effect on the final results and thus the selection can be made on an arbitrary basis.

The second step is to note the number of cycles N_{ref} of intensity τ_{av} required to cause failure. This is done by reference to a plot of cyclic loading strength of the appropriate soil consolidated to the appropriate stresses representative of field conditions. This is illustrated on Fig. III-2.

The third step is to divide the range of stresses $0 \pm \tau_{max}$ up into a few increments of stress $\Delta\tau_i$, and note the mean stress level τ_i at each of these increments. Generally, four to six increments are sufficient, and they need not be of the same magnitude.

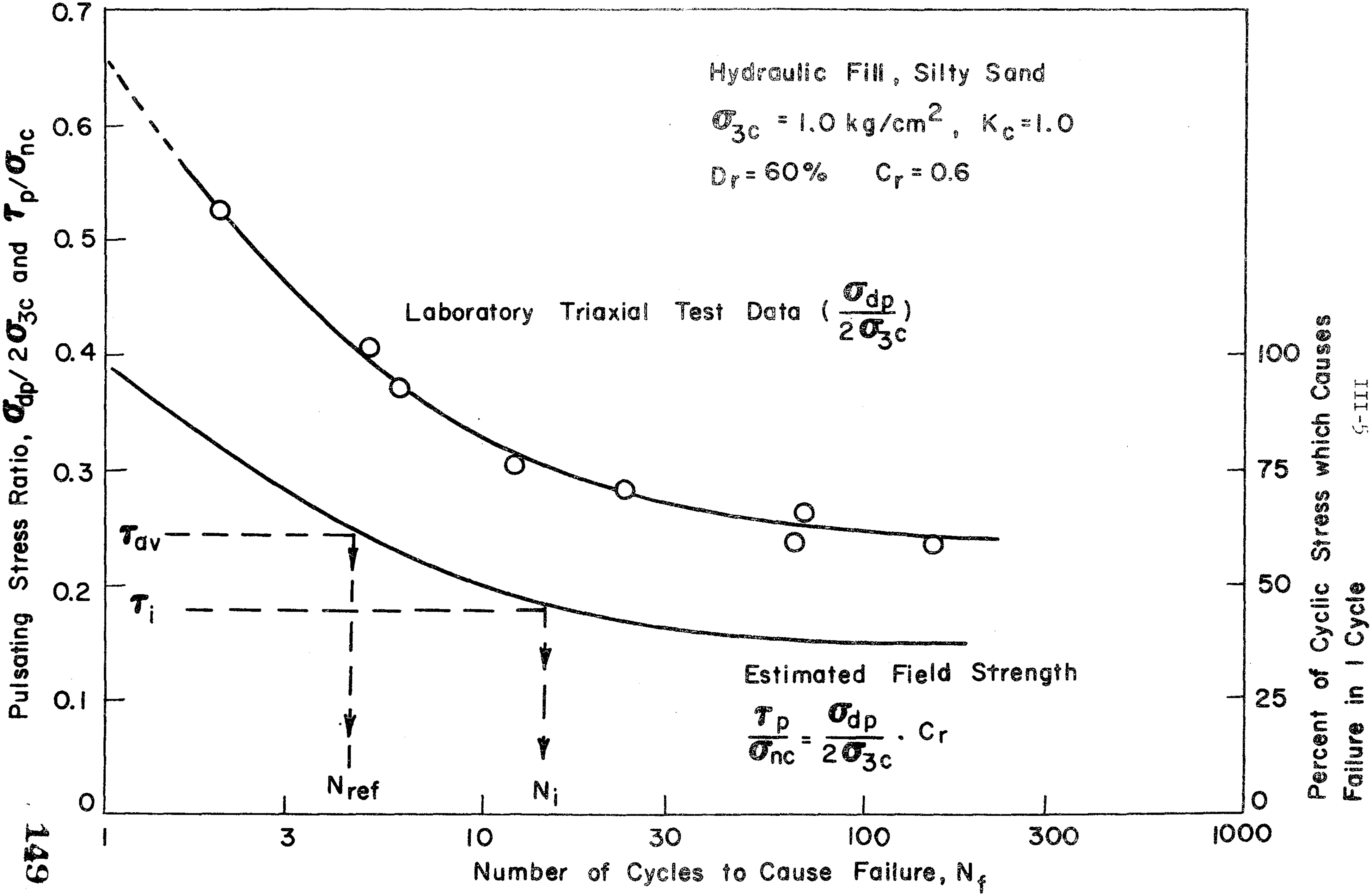

FIG. III-2 PULSATING LOADING STRENGTH OF A TYPICAL SOIL.

The fourth step is to count the number of cyclic peaks N_{ci} which fall within each increment. Note that one positive and one negative peak are required to define one complete cycle, so the count is made of both. For each increment the value of N_{ci} corresponding to the mean stress τ_i is tabulated for future reference.

The fifth step is to determine the effect of applying a series of uniform stress cycles τ_i to a soil. This is done for each separate stress increment as indicated on Fig. III-2 by noting the number of uniform cycles of stress N_i, of intensity τ_i required to cause "failure".

It is noted that N_i cycles of τ_i are equivalent to N_{ref} cycles of τ_{av}, in that either combination will cause "failure" of the sample in the sense that the term failure is used. Thus it follows that:

$$1 \text{ cycle of } \tau_i = \frac{1}{N_i} \cdot N_{ref} \text{ cycles of } \tau_{av} \tag{III-2}$$

and

$$\Delta N_{eq_i} = N_{ci} \text{ cycles of } \tau_i = \frac{N_{ci}}{N_i} \cdot N_{ref} \text{ cycles of } \tau_{av} \tag{III-3}$$

Applying Eq. III-3 for all $\pm$ increments and summing leads to:

$$N_{eq} = \sum_i \Delta N_{eq_i} \tag{III-4}$$

Where N_{eq} is the number of uniform cycles of stress intensity $\pm \tau_{av}$ that has an equivalent effect on the soil to the entire random time history stresses.

Selection of a different initial value of τ_{av} would lead to a different corresponding value of N_{eq}, but the basic equivalence would remain the same. Thus it is a simple matter after the first calculations have been made to adjust the τ_{av} - N_{eq} values if desired, until one of them is a convenient or whole number.

It follows from the foregoing discussion that the τ_{av} - N_{eq} relation is not only a function of the input earthquake, but it also depends on the characteristics of the soil in the dam or foundation being shaken. Different cyclic load strength curves from the typical data shown on Fig. III-2 would lead to a different τ_{av} - N_{eq} relation.

Lee and Chan (21) collected a large number of cyclic load data from a variety of soils, to study the range of variation from soil to soil. For comparison purposes it was found convenient to plot the data on a dimensionless strength basis by extrapolating the curve back to N = 1 cycles and expressing every other strength value as a percentage of the cyclic load strength at N = 1. This is also illustrated on Fig. III-2. The mean, and the ± 75% limits of the data compiled at that time are shown in Fig. III-3a. This data does not include the results of tests from the San Fernando Dams, because they were not available at that time.

The limit curves shown on Fig. III-3a to a semi-log scale are closely defined by straight lines on log-log paper as shown on Fig. III-3b. The slope of these lines has the same physical meaning as the slope S_1 of the permanent deformation parameters described in Appendix I. Reference to the summary list of data for the soils involved in this study show that the values of S_1 are within the range of limits shown on Fig. III-3b.

To study the effect of the earthquake on the τ_{av} - N_{eq} relations, Lee and Chan (21) analyzed the records for a large number of strong motion records. They found that approximately the same τ_{av} - N_{eq} results were obtained from using the accelerogram directly as from using the stress history computed at some location within a soil mass being shaken by the

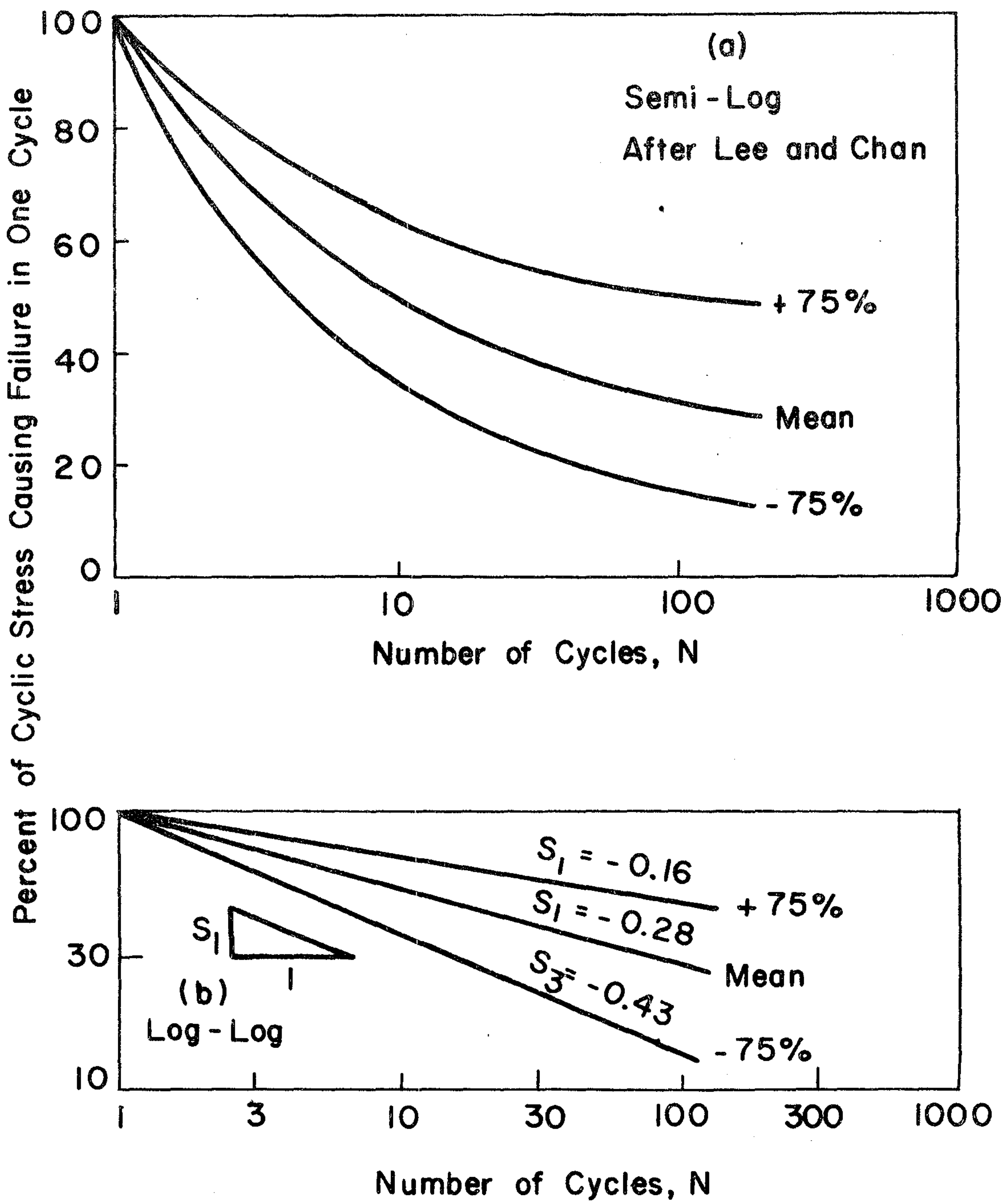

FIG. III-3 COMPILATION OF MANY CYCLIC LOAD TESTS ON SOILS MEAN AND ± 75% RANGE OF DATA accelerogram. Furthermore, they found that the τ_{av} - N_{eq} relations were approximately independent of the locations within the soil where the stress histories were calculated. However, they found that for any one earthquake, or for earthquakes of the same magnitude, there was a wide scatter in the computed τ_{av} - N_{eq} results. Attempts to reduce the scatter by correlating with soil type or epicenter distance were not successful.

Nevertheless, from the data which was obtained it was possible to define general trends of increasing N_{eq} with earthquake magnitude for each value of R selected. These trends are shown by single lines on Fig. III-4 for three different values; R = 0.65, 0.75 and 0.85. It must be emphasized, however, that the single lines shown on Fig. III-4 represent only the major trend of fairly widely scattered data. For any one earthquake magnitude any one R value, the extreme range of N_{eq} might be as much as +100% or -70% of the value indicated by the curve.

These relations refer to the mean of the soil strength data shown on Fig. III-3. Surprisingly, because of the wide scatter in the data, the major trend curves shown on Fig. III-4 apply almost equally as well to the soil strength data for the ± limits as for the mean curve on Fig. III-3.

In conclusion, from the foregoing discussion, and especially from the results of the previous study by Lee and Chan (21), the concept behind representing the actual random stress history with an equivalent number of cycles appears to be sound, although lacking in direct experimental confirmation. However, because of the apparent random variability of recorded earthquake motions, any selected combination of τ_{av} and N_{eq} for design purposes must be considered to be somewhat approximate. Fortunately,

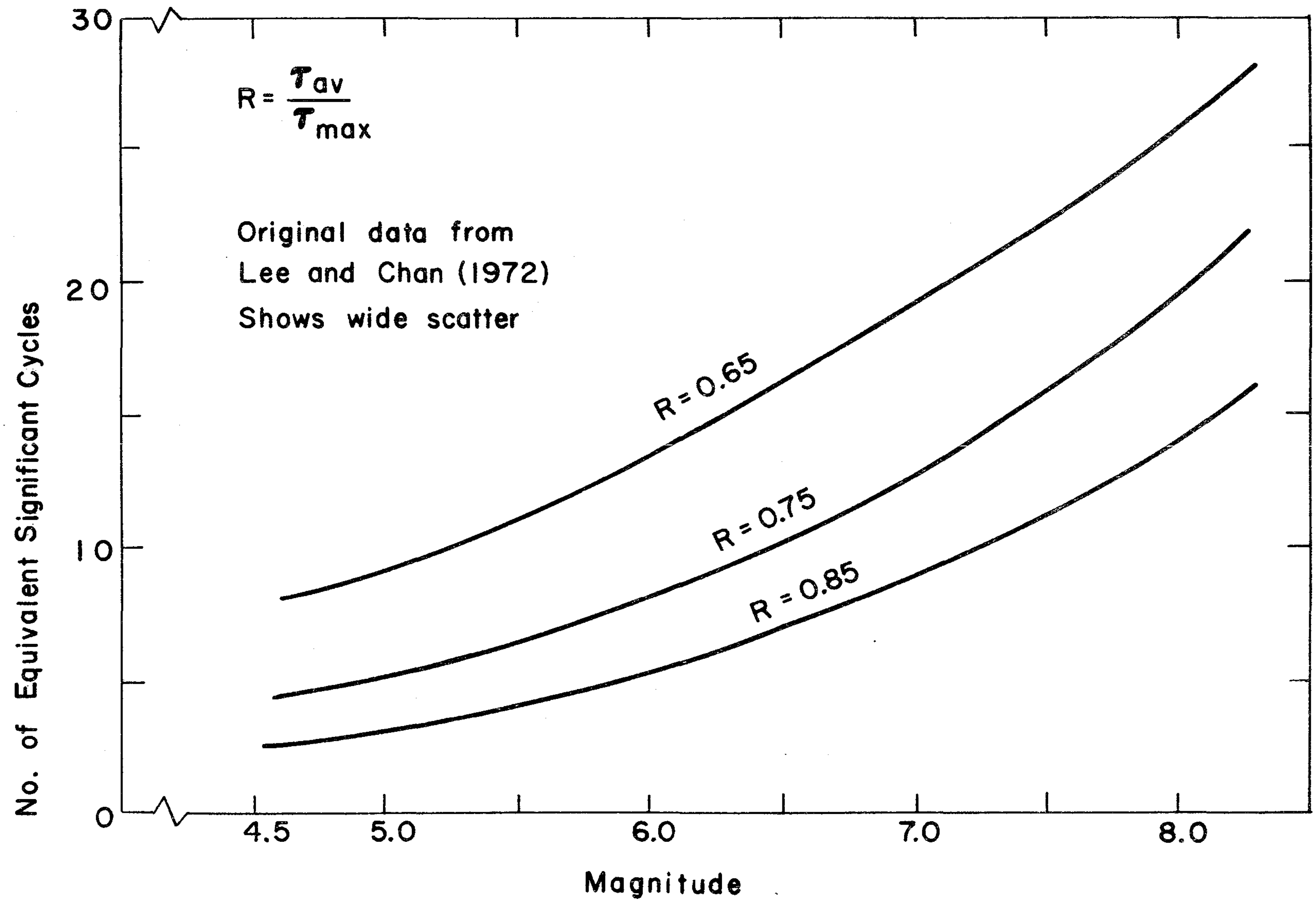

Number of Equivalent Significant Uniform Cycles

FIG, III-4 AVERAGE OF N_{eq} - R VARIATIONS WITH MAGNITUDE as discussed in the main body of the text, the final calculated permanent deformations are not strongly dependent on the number of equivalent cycles selected, so that some uncertainty in N_{eq} does not invalidate the results of calculations based thereon.

APPENDIX IV

Distribution of Maximum Recorded Accelerations

The main text of this report illustrates that the calculated permanent deformations are quite sensitive to the maximum response analysis. The purpose of this appendix is to illustrate the nature of variability that must be considered in assigning a maximum acceleration for an assumed input base motion used in the seismic response analysis.

In previous studies, Housner (28) and Seed, Idriss and Kiefer (29), have separately presented correlations between maximum acceleration on firm ground and on rock, based on the recorded data available at those times. These recorded data showed considerable scatter, but there were few records from the same earthquake, especially at similar close epicentral distances, to illustrate the variability in accelerations from just a single event.

The San Fernando earthquake of February 9, 1971 provided a wealth of such information. Schnabel and Seed (23) have used the recorded motions on rock from this earthquake to revise the previous Seed, Idriss and Kiefer (29) recommendations of maximum accelerations in rock. Duke, et al. (22) have studied all of the recorded maximum accelerations from some 95 sites where the strong motion recorders were located at ground level. Data from this report are replotted in Figs. IV-1 through IV-6 of this appendix along with the upper and lower limits given by Schnabel and Seed (23) for accelerations in rock for this magnitude of earthquake. Duke, et al. (22), also studied seismoscope records from an even greater number of sites, but these data are not included herein.

In an attempt to sort out the possible effect of different ground conditions, Duke, et al. (22) classified each of the recording sites according to the type of ground conditions as follows:

1. Igneous or metamorphic rock
2. Sedimentary rock
3. Shallow alluvium (20 to 60 ft)
4. Deep alluvium (greater than 60 ft)

They further categorized the data in terms of the distance of the recording station from the "energy center". This energy center was defined as the center of gravity of the released energy of the earthquake based on interpretation of data on aftershock locations, and on inferred subsurface fault breakage. This inferred energy center was approximately 3 km southwest of the instrumental epicenter of the main shock. Thus the epicenter distances and energy center distances to the recording stations are the same for most practical purposes.

The maximum of the two recorded horizontal components of acceleration, and the maximum recorded vertical acceleration for each recorded ground motion of the San Fernando earthquake are presented on Fig. IV-1 and Fig. IV-4, classified according to the ground conditions. The extremely high recorded accelerations at the Pacoima Dam were deliberately not plotted because of questions as to whether they represented the general level of acceleration in the area, or whether they were due to some very unusual local conditions. Reference to these four figures illustrates that the vertical accelerations are generally less than the horizontal accelerations, and that even within zones of similar ground conditions there is considerable scatter.

Referring to the figures in sequence indicated that there are progressively more data for the soft sites than for the hard sites, and as the number of data points increase, so does the amount of scatter. Unfortunately there are only a few recordings on igneous or metamorphic rock, and it is only

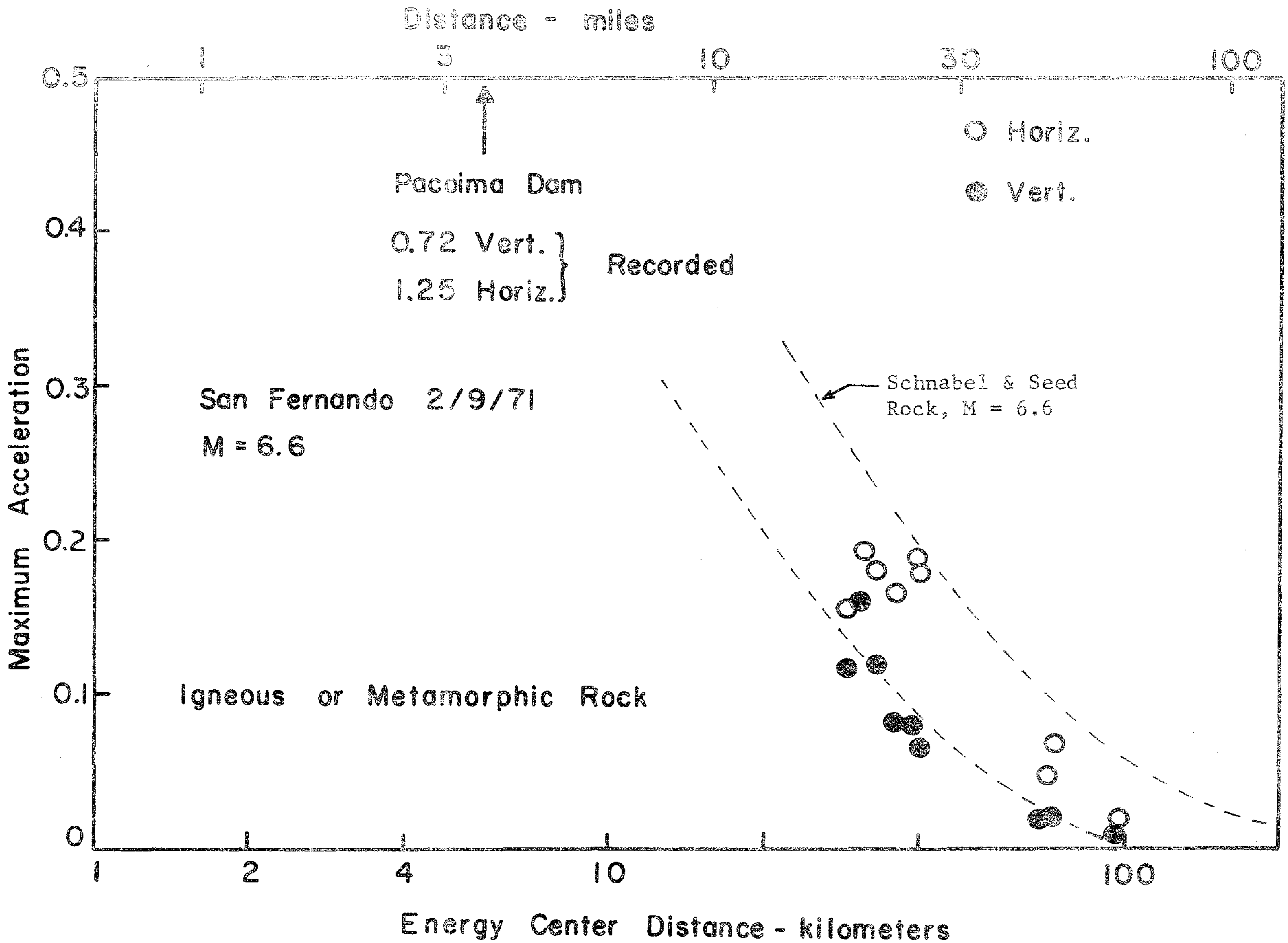

FIG. IV-1 PEAK RECORDED ACCELERATIONS, SAN FERNANDO EARTHQUAKE (1 OF 4)

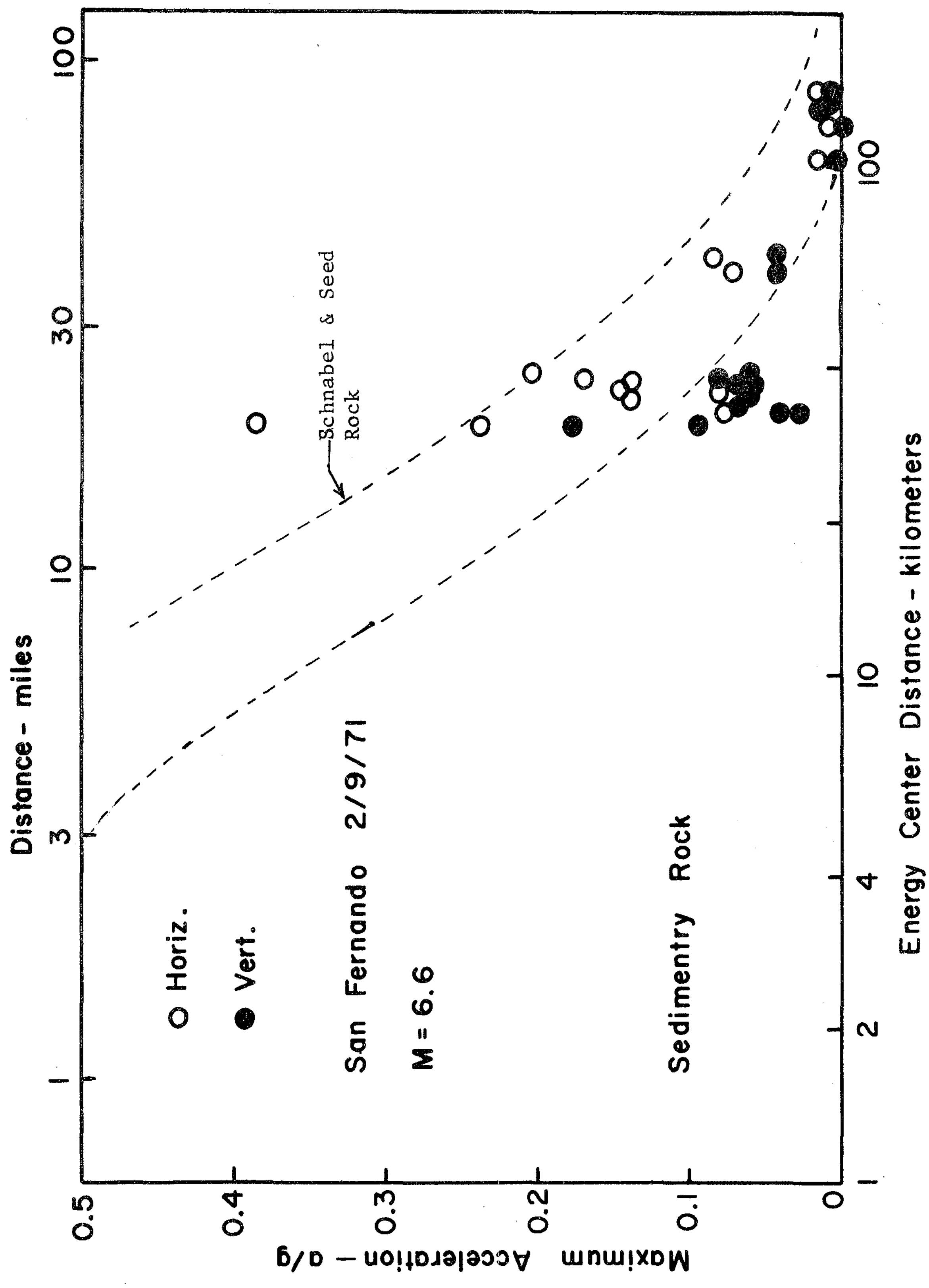

FIG. IV-2 PEAK RECORDED ACCELERATIONS, SAN FERNANDO EARTHQUAKE (2 OF 4)

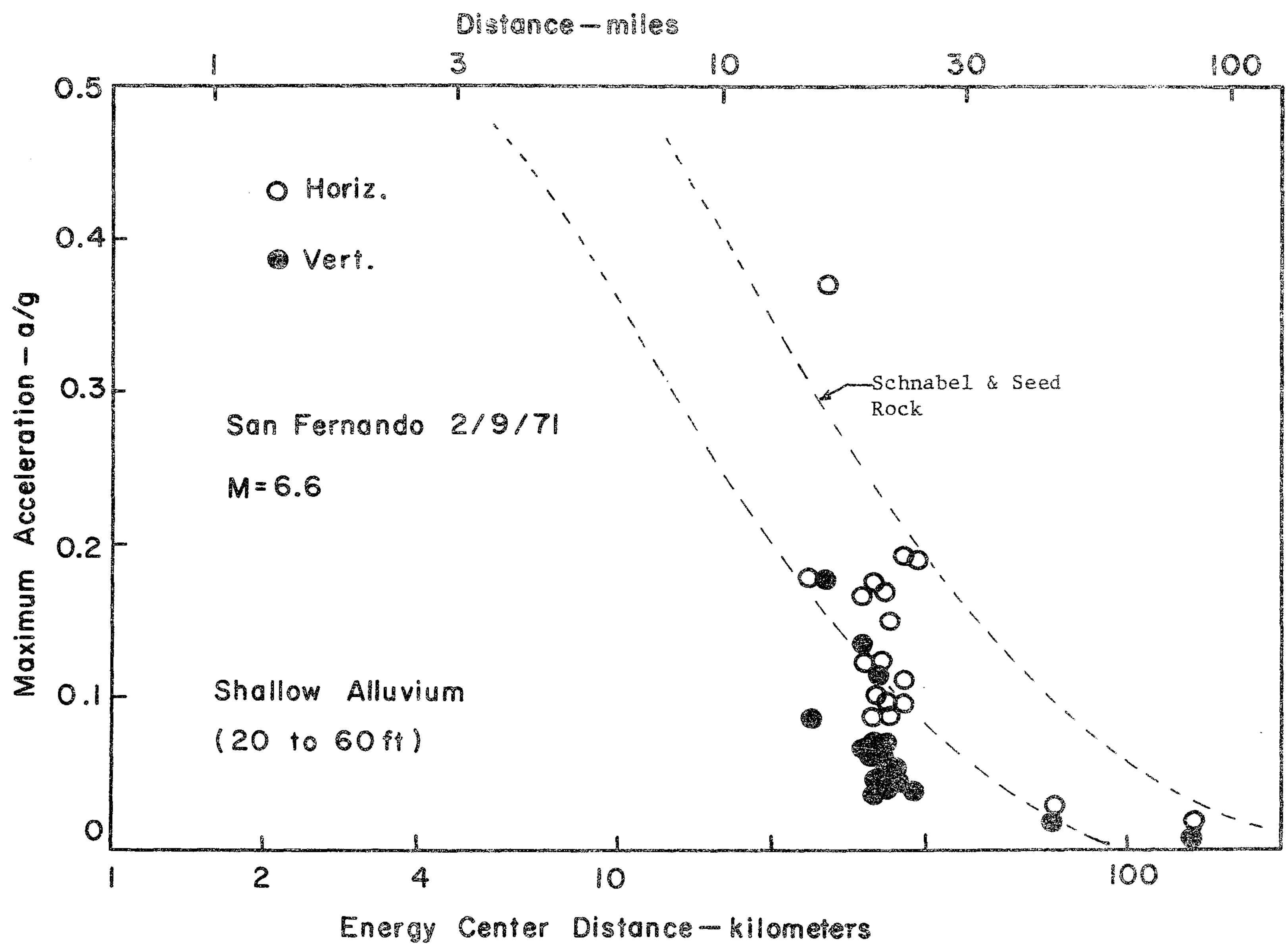

FIG. IV-3. PEAK RECORDED ACCELERATIONS, SAN FERNANDO EARTHQUAKE (3 OF 4)

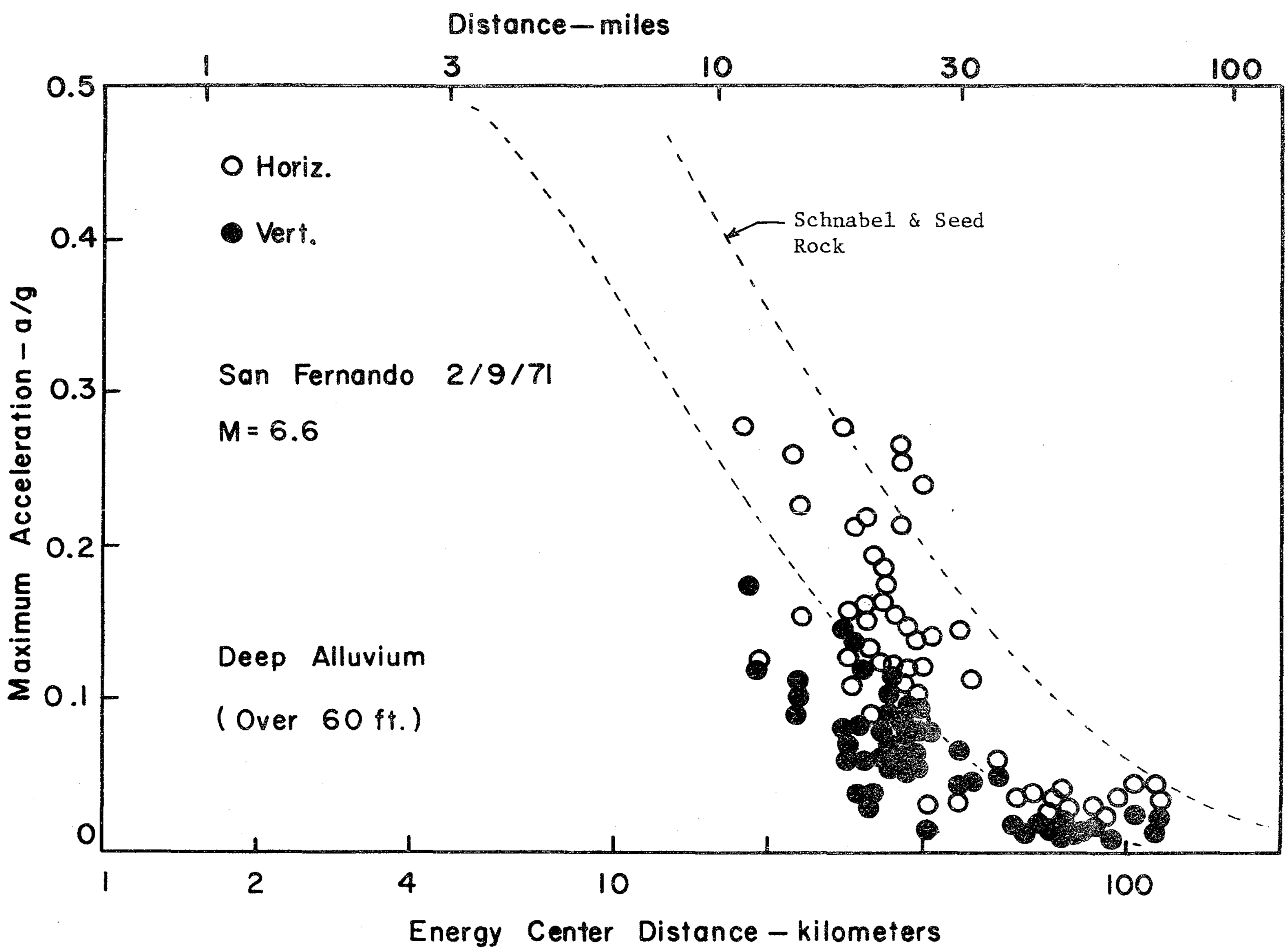

FIG. IV-4. PEAK RECORDED ACCELERATIONS, SAN FERNANDO EARTHQUAKE (4 OF 4) speculation as to whether more data on this type of ground would lead to more scatter or not. The data presented by Schnabel and Seed (23) for recordings on rock sites for this and other earthquakes also shows considerable scatter as indicated by the dashed lines on Figs. IV-1 to IV-4, for earthquakes of $M \approx 6.6$.

To compare the effect of ground conditions directly, the maximum horizontal component of acceleration from the sites on igneous rock, and on deep alluvium have been plotted together on Fig. IV-5. The data from the rock sites fall more or less in the middle of the data from the deep alluvium sites. Data from the other two types of sites also fall within this same range. Thus without further studies, it would appear that there is no clearly defined difference between maximum accelerations on rock and on soil, at least from this earthquake.

Another interesting comparison is the maximum horizontal components of acceleration in two perpendicular directions. The data for the deep alluvium sites is shown on Fig. IV-6. The solid dots show the largest acceleration of the two horizontal components and the open dot shows the maximum peak of the other horizontal component. Again it is noted that there is a wide scatter indicating that at some sites there is considerable difference in maximum acceleration depending on the direction of motion. While it is probably conservative to choose the larger of the two components, the great difference at some sites suggests that the largest component may not always be in the most critical direction with respect to the particular dam being considered.

Of course, maximum acceleration is only one of the several characteristics of strong motion earthquake records. Frequency content, duration, number of cycles and general arrangement of the cycles are all important (29), and have not been considered in this brief discussion. Nevertheless, as

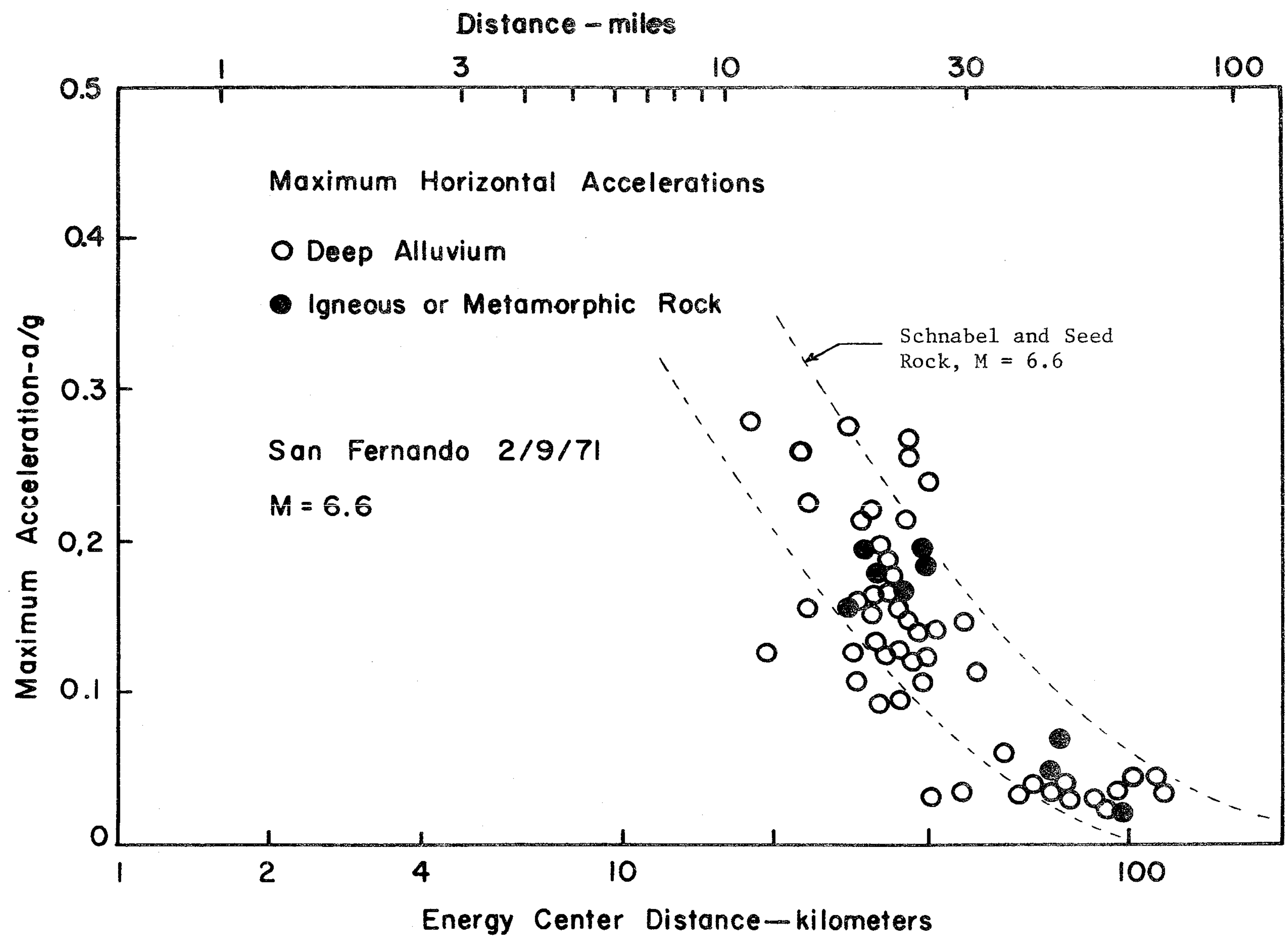

FIG. IV-5. COMPARISON OF PEAK RECORDED ACCELERATION ON ROCK AND ON DEEP ALLUVIUM.

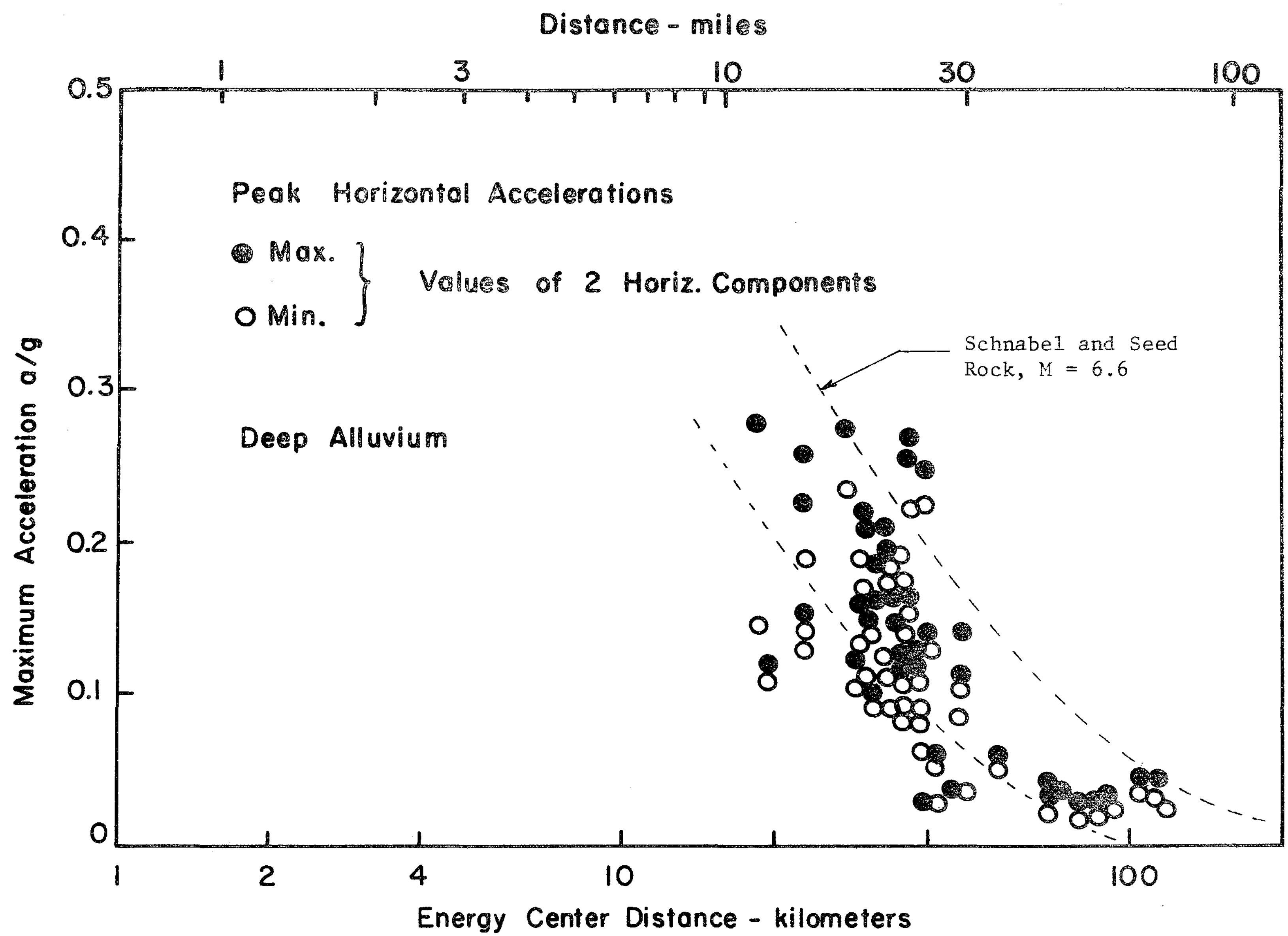

FIG. IV-6. COMPARISON OF PEAK HORIZONTAL ACCELERATIONS FROM TWO COMPONENTS OF EACH STATION.

illustrated in the main body of the report, maximum acceleration is an important factor in determining the seismic stresses developed in an earth embankment. The wide range of scatter in the data from this one earthquake suggests that caution must be exercised in any conclusions based on case history studies of the behavior of structures during other earthquakes when an important input parameter is the maximum base acceleration. For most case histories, the base acceleration must be estimated from one or two, or often no actual recorded motions for that earthquake. According to the recorded data from the San Fernando earthquake, the actual maximum base acceleration at any particular epicentral distance may range over fairly wide limits. The factors which govern this variation are not as yet sufficiently well understood to provide a high degree of confidence in any single value that might be selected for calculation purposes.

APPENDIX V

Alternative Deductive Reasoning For Eq. 13

When the first draft of this report was circulated, several persons expressed confusion concerning Eq. 13. As a result the following alternative description was developed, attempting to describe a model intended by this equation. This model is physically illustrated in Fig. V-1 for the case of a single element or a sample of soil. The total deformations throughout the entire life history up to and after the end of an earthquake are idealized in two separate stages: initial deformations before the earthquake u_i and the deformation during the seismic disturbance u_p.

The spring and dashpot simulations shown in the model are simply figurative and used to illustrate a mechanism for separating the pre-earthquake, earthquake and final post earthquake behavior of an element and a soil sample. The dashpot damping λ is high so that deformations within element A can only occur during a long period of sustained static loading. The spring stiffness K_i remains constant throughout all stages. The stiffness K_p is comparatively large before the earthquake, but as the earthquake continues K_p decreases progressively.

At any time the total stiffness of the soil is made up of two stiffnesses,

$$K_{ip} = \frac{1}{\frac{1}{K_i} + \frac{1}{K_i}} \qquad \text{(V-1)}$$

The static, pre-earthquake gravity load on the sample or element is represented by F_g. The initial displacement corresponding to this load is u_i. Because of the relative stiffnesses of the two springs before the earthquake, for the initial gravity loading $K_p >> K_i$, so that K_{ip} K_i. Thus the initial displacement is made up almost entirely of compression in Element A.

The pulsating loading induced by the earthquake, or the simulation of this loading in a laboratory cyclic load test is shown by $\pm f_p(t)$. This is a

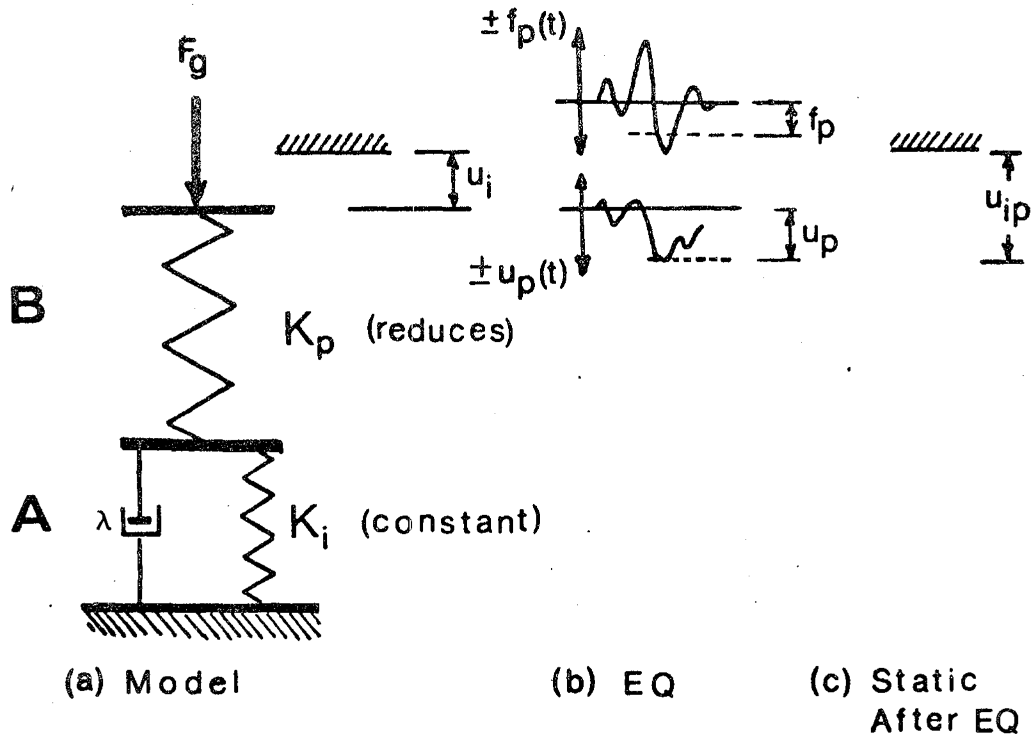

Fig. V-1 Analogy for Seismic Induced Permanent Deformations transient pulsating force which is superimposed on the constant static gravity force F_g for a short period of time only. The corresponding deformations during this cyclic loading period are indicated by $\pm u_p$ (t). They are due entirely to the spring in Element B. The equivalent average cyclic force is denoted by f_p, and the maximum accumulative displacement after any elapsed time is denoted by U_p. Because K_p decreases progressively as the earthquake continues, the values of u_p (t) are not necessarily symmetric and are not constant with time. Since it is the permanent and not the cyclic deformation which is of interest in this study, the value of U_p used in the subsequent calculations is taken as the maximum accumulative displacement at the end of the earthquake, or at any other intermediate time that may be desired.

Note that in the laboratory test the sample is free to deform unrestrained whereas the corresponding element of soil in the field must deform within the limitations of the constraints of other elements and boundaries. Thus the field deformation of any particular element may be different from the value of u_p measured in a cyclic triaxial test, even though the element stiffness will have the potential to develop this displacement, if it were free of constraints.

A pseudo secant spring constant for Element B may be used to define the accumulative deformation u_p by comparing it with the causitive loads. One definition for such a pseudo spring constant might be:

$$K_{p1} = \frac{F_g + f_p}{u_p} \qquad \text{(V-2)}$$

whereas another definition might be:

$$K_{p2} = \frac{f_p}{u_p} \qquad \text{(V-3)}$$

Either equation could be used to define u_p knowing the other terms. The numerical values of K_{p1} and K_{p2} are different because of the way in which the gravity force F_g is included. If Eq. V-2 is used, F_g must be included as part of the applied force. If Eq. V-3 is used, the effect of F_g is present, but unseen, since the value of K_{p2} must be obtained by cyclic testing with a constant value of F_g also applied. For the purposes of this study, the concept of Eq. V-3 was used in defining a pseudo spring constant K_p, for the permanent deformation calculations.

Actually in this study, solid finite elements are used instead of simple springs. However the same analogy applies if pseudo modulus values are used to define the stiffness matrices corresponding to the single spring stiffnesses illustrated in Fig. V-1. Thus a pseudo value for the initial nodal point deformations *<u>Ui</u> in the dam before the earthquake are defined by a linear elastic gravity-turn-on analysis with element stiffnesses formed from an appropriate static secant modulus Ei.

To define the softening during pulsating loading, a pseudo secant modulus is calculated from the results of cyclic loading laboratory tests on samples anisotropically consolidated to the appropriate field static gravity stresses.

$$Ep = \frac{\sigma dp}{\varepsilon p} \qquad \text{(V-4)}$$

Thus, for example, if the cyclic loading data in Fig. 5 corresponds to tests performed to simulate conditions at a particular element in the field, and the design earthquake is represented by Neq = 8 uniform cycles of stress $\sigma_{dp} = 0.55$ kg/cm^2; the corresponding accumulative axial strain in the laboratory specimen would be $\varepsilon_p = 0.7$ percent. From these data the pseudo modulus is calculated; Ep = 0.55/0.007 = 78 kg/cm^2.

Having defined Ei and Ep, an overall secant modulus is defined by

$$Eip = \frac{1}{\frac{1}{E_i} + \frac{1}{E_p}} \qquad \text{(V-5)}$$

which is Eq. 13 on page 28 of the main text.

Using element stiffnesses defined in terms of Eip along with the static gravity loads in a gravity-turn-on analysis will lead to total displacements at each nodal point $\underline{Uip}$ from the beginning of construction to the end of the earthquake. Finally by subtracting the calculated pseudo initial displacements from the total displacements, the net displacements due only to the earthquake are obtained:

$$\underline{Up} = \underline{Uip} - \underline{Ui} \qquad (V\text{-}6)$$

APPENDIX VI - REFERENCES

1. Seed, H. Bolton and Whitman, Robert V., "Design of Earth Retaining Structures for Dynamic Loads", Proceedings 1970 Specialty Conference on Lateral Stresses, ASCE, Cornell University, June 1970, pp. 103-147.

2. Taylor, D. W., "Fundamentals of Soil Mechanics", Wiley 1948, pp. 452-453.

3. Terzaghi, Karl, "Mechanism of Landslides", Applications of Geology to Engineering Practice, (Berkey Volume), Geological Society of America, 1950, p. 89.

4. Oddi, M. M. and Humphreys, J. D., "Correspondence on Slope Stability During Earthquakes", Geotechnique, vol. 11, no. 4, December 1961, pp. 354-356.

5. Seed, H. Bolton, "Earthquake Resistant Design of Earth Dams", Canadian Geotechnical Journal, vol. 4, no. 1, 1967, pp. 1-27.

6. Seed, H. Bolton, Lee, K. L., and Idriss, I. M., "An Analysis of the Sheffield Dam Failure", Journal of the Soil Mechanics and Foundations Division, ASCE, vol. 95, no. SM-6, November 1969, pp. 1453-1490.

7. Seed, H. B., Lee, K. L., Idriss, I. M., and Makdisi, F., "A Study of the Performance of the Two San Fernando Dams During the February 9, 1971 San Fernando Earthquake", Report to be published by the Earthquake Engineering Research Center, 1973.

8. Ambraseys, N. N., "On the Seismic Behavior of Earth Dams", Proceedings 2nd World Conference on Earthquake Engineering, Tokyo, Japan, vol. II, 1961, pp. 13-41.

9. Seed, H. Bolton, "A Method of Earthquake Resistant Design of Earth Dams", Journal of the Soil Mechanics and Foundations Division, ASCE, vol. 92, no. SM-1, January 1966, pp. 13-41.

10. Seed, H. Bolton and Martin, Geoffrey R., "The Seismic Coefficient In Earth Dam Design", Journal of the Soil Mechanics and Foundations Division, ASCE, vol. 92, no. SM-3, May 1966, pp. 25-58.

11. Lowe, J. and Karafiath, L., "Stability of Earth Dams Upon Drawdown", Proceedings 1st Pan American Conference on Soil Mechanics and Foundation Engineering, vol. II, Mexico City, 1960, pp. 537-560.

12. Seed, H. Bolton and Lee, Kenneth L., "Liquefaction of Saturated Sands During Cyclic Loading Conditions", Journal of the Soil Mechanics and Foundations Division, ASCE, vol. 92, no. SM-6, November 1966, pp. 105-134.

13. Lee, Kenneth L. and Seed, H. Bolton, "Cyclic Stress Conditions Causing Liquefaction of Sands", Journal of the Soil Mechanics and Foundations Division, ASCE, vol. 93, no. SM-1, January 1967, pp. 47-70.

14. Seed, H. Bolton and Lee, Kenneth L., "Pore Water Pressures in Earth Slopes Under Seismic Loading Conditions", Proceedings 4th World Conference on Earthquake Engineering, Santiago, Chile, January 1969.

15. Lee, Kenneth L. and Seed, H. Bolton, "Dynamic Strength of Anisotropically Consolidated Sand", Journal of the Soil Mechanics and Foundations Division, ASCE, vol. 93, no. SM-5, September 1967, pp. 169-190.

16. Lee, Kenneth L. and Walters, Henry G., "Earthquake Induced Cracking of Dry Canyon Dam", paper presented at the ASCE National Meeting, October 1972, Houston, Texas, prepring no. 1794.

17. Lee, Kenneth L. and Walters, Henry G., "Earthquake Induced Cracking of Dry Canyon Dam", Proceedings 5th World Conference on Earthquake Engineering, Rome, Italy, 1973.

18. Newmark, N. M., "Effects of Earthquakes on Dams and Embankments", Geotechnique, vol. 15, no. 2, June 1965, pp. 139-173.

19. Seed, H. Bolton and Goodman, R. E., "Displacements of Slopes in Cohesionless Materials During Earthquakes", Journal of the Soil Mechanics and Foundations Division, ASCE, vol. 92, no. SM-2, March 1966, pp. 125-146.

20. Seed, H. Bolton and Peacock, W. H., "Test Procedures for Measuring Soil Liquefaction Under Cyclic Loading", Journal of the Soil Mechanics and Foundations Division, ASCE, vol. 97, no. SM-8, August 1971, pp. 1099-1119.

21. Lee, K. L. and Chan, K., "Number of Equivalent Significant Cycles in Strong Motion Earthquakes", Proceedings Microzonation Conference, Seattle, vol. II, 1972, pp. 609-627.

22. Duke, C. M., et al., "Effects of Site Classification and Distance on Instrumental Indices in the San Fernando Earthquake", Report No. UCLA-ENG-7247, June 1972.

23. Schnabel, P. B. and Seed, H. B., "Accelerations in Rock for Earthquakes in the Western United States", Report No. EERC-72-2, University of California, Berkeley, July 1972. Also published in the Bulletin of the Seismological Society of America, vol. 63, no. 2, April 1973, pp. 501-516.

24. Kulhawy, F. H., Duncan, J. M. and Seed, H. B., "Finite Element Analysis of Stresses and Movements In Embankments During Construction", Geotechnical Engineering Report TE69-4, Department of Civil Engineering, University of California, Berkeley, 1969.

25. Clough, R. W. and Woodward, R. J., "Analysis of Embankment Stresses and Deformations", Journal of the Soil Mechanics and Foundations Division, ASCE, vol. 93, no. SM-4, July 1967, pp. 529-549.

26. Nunn, Herbert, "Municipal Problems of Santa Barbara", Bulletin, Seismological Society of America, vol. 15, no. 4, December, 1925, pp. 308-319.

27. Scott, Ronald F., "The Calculation of Horizontal Accelerations From Seismoscope Records", Bulletin of the Seismological Society of America Conference, vol. 63, no. 5, October, 1973, pp. 1637-1661.

28. Housner, G. W., "Engineering Estimates of Ground Shaking and Maximum Earthquake Magnitude", Proceedings 4th World Conference on Earthquake Engineering, Session AI, 1969, pp. 1-13.

29. Seed, H. B., Idriss, I. M. and Kiefer, F. W., "Characteristics of Rock Motion During Earthquakes", Journal of the Soil Mechanics and Foundations Division, ASCE, vol. 95, no. SM-5, September 1969, pp. 1199-1218.

30. Finn, W. D. L., Pickering, D. J. and Bransby, P. L., "Sand Liquefaction in Triaxial and Simple Shear Tests", Journal of the Soil Mechanics and Foundations Division, ASCE, vol. 97, no. SM-4, April, 1971, pp. 639-659.

31. Finn, W. D. L., "Liquefaction of Sands", Proceedings Microzonation Conference, University of Washington, Seattle, October-November, 1972, vol. I, pp. 87-111.

32. Peacock, W. H. and Seed, H. Bolton, "Sand Liquefaction Under Cyclic Loading Simple Shear Conditions", Journal of the Soil Mechanics and Foundations Division, ASCE, vol. 94, no. SM-3, May, 1968, pp. 689-708.

33. Ishihara, K. and Yasuda, S., "Sand Liquefaction Due to Irregular Excitation Soils and Foundations", vol. 12, no. 4, December, 1972, pp. 65-77.

34. Ghaboussi, J., Wilson, E. L. and Isenberg, J., "Finite Element for Rock Joints and Interfaces", Journal of the Soil Mechanics and Foundations Division, ASCE, vol. 99, no. SM-10, October, 1973, pp. 833-848.

35. Lee, Kenneth L. and Albaisa, Aurelio, "Earthquake Induced Settlements in Saturated Sands", Journal of the Geotechnical Engineering Division, ASCE, vol. GT1, no. 4, April 1974.

36. Silver, M. L. and Seed, H. Bolton, "Volume Changes in Sands During Cyclic Loading", Journal of the Soil Mechanics and Foundations Division, ASCE, vol. 97, no. SM-9, September, 1971, pp. 1171-1182.

37. Seed, H. Bolton, "Stability of Earth and Rockfill Dams During Earthquake Embankment Dam Engineering", Casagrande Volume, Edited by Hirschfeld and Paulos, Wiley, 1973, pp. 239-269.

38. Steinbrugge, K. V. and Cloud, W. K., "Epicentral Intensities and Damage in Hebgen Lake, Montana Earthquake of August 17, 1959", Bulletin of the Seismological Society of America, vol. 52, no. 2, April 1962, pp. 181-239.

39. Sherard, J. L., et al., "Earth and Earth Rock Dams", Wiley, 1963, pp. 164-170.

40. Thiers, G. R. and Seed, H. B., "Strength and Stress-Strain Characteristics of Clays Subjected to Seismic Loading Conditions", ASTM STP 450, 1969, pp. 3-56.